An Investigation of a Heterogeneous Aminohydroxylation Catalyst

By

Mohamed Islam Fadlalla

Submitted in fulfilment of the academic requirements for the degree of

Master of Science in the

School of Chemistry,

University of KwaZulu-Natal,

Durban,

South Africa

December 2010

As the candidate's supervisors we have approved this dissertation for submission.

Signed: _____ Name:_____ Date:_____

Signed: _____ Name:_____ Date:_____

Abstract

Os-Zn-Al hydrotalcite-like compounds (HTlc's) were synthesised by the co-precipitation method and characterised using different techniques (powder XRD, ICP-OES, FT-IR spectroscopy, BET-surface area measurements, SEM and SEM-EDS, cryo-TEM, ^{27}Al SS-NMR and TGA-DSC). The hydrotalcite-like catalyst was used to heterogenise the aminohydroxylation reaction. Among the three solvents investigated (toluene, MeCN/water (1:1 v/v) and t-BuOH/water (1:1 v/v)) in the aminohydroxylation reaction, toluene showed the slowest reaction rate, MeCN/water (1:1 v/v) and t-BuOH/water (1:1 v/v) demonstrated fast reaction rates comparable to each other. The reaction temperature was only significant when toluene was used as the solvent system (reaction time (100% depletion of starting material) and temperature are inversley proportional). The catalyst HTlc structure demonstrated a significant effect in terms of the reaction time and isolated yield of the β-amino alcohols. Under the same testing conditions a heat treated catalyst (non-HTlc) showed a shorter reaction time, a reduction in the isolated yield of β-amino alcohols with a rise in diol formation. All the different classes of olefins (aliphatic, aromatic, and functionalised) that were tested, gave 99.99% depletion of starting material. However, due to the same purification difficulties encountered in the homogeneous amino hydroxylation (AA) reaction, the isolated yield of β-amino alcohols achieved here, ranged from 13 to 35 %, with the highest yield (35%) obtained when methylcinnamate was used as the olefin. Characterisation of the spent catalyst showed that HTlc structure is maintained, but crystallinity was lost (the material becomes polycrystalline) after the reaction. The leaching test showed that 4.5% and 5.5% of Os leached from the catalyst to the reaction solution when MeCN/water (1:1 v/v) and *t*-BuOH /water (1:1 v/v) were used as the solvent system, respectively. The leached form of Os was determined to be inactive, indicating that this system is truly heterogeneous. The recycling study (three cycles) indicated that the catalyst can be recycled, but with a decrease in the reaction rate (which could be due to structure defects and loss of crystallinity), and with no significant difference in the isolated yield of the amino-alcohol.

The crystal structure of three β-amino alcohols are also reported. The crystal structure of the β-amino alcohol of cyclohexene, methylcinnamte and *t*-butylcrotonate were needle-like triclinic, $p\bar{1}$, needle-like monoclinic, p_{21}/c and cubic-like triclinic, p-1, respectively.

Preface

The experimental work described in this dissertation was carried out in the School of Chemistry, University of KwaZulu-Natal, Westville Campus, Durban, from January 2010 to November 2010, under the supervision of Prof. H. B. Friedrich and G. E. M. Maguire.

These studies represent original work by the author and have not otherwise been submitted in any form or degree or diploma to any tertiary institution. Where use has been made of the work of others it is duly acknowledged in the text.

_____

Mohamed Islam Fadlalla

B. Sc (Honours) (UKZN-Westville Campus)

DECLARATION - PLAGIARISM

I, _____ declare that

1. The research reported in this thesis, except where otherwise indicated is my original research.
2. This thesis has not been submitted for any degree or examination at any other university.
3. This thesis does not contain other persons' data, pictures, graphs or other information, unless specifically acknowledged as being sourced from other person.
4. This thesis does not contain other persons' writing, unless specifically acknowledged as being sourced from other researchers. Where other written sources have been quoted, then:
    a. Their words have been re-written but the general information attributed to them has been referenced.
    b. Where their exact words have been used, then their writing has been placed in italics and inside quotation marks, and referenced.
5. This thesis does not contain text, graphics or tables copied and pasted from the Internet, unless specifically acknowledged, and the source being detailed in the thesis and in the References sections.

Signed: _____

Conference Contributions and Publications

Part of the work discussed in this dissertation has been presented as a poster presentation in the following conference:

CATSA Conference 2010, Bloemfontein, poster presentation, *Investigation into heterogeneous aminohydroxylation reaction using hydrotalcite-like catalyst.* M. I. Fadlalla, G. E. M. Maguire, H. B. Friedrich.

Publications

1) M. I. Fadlalla. H. B. Friedrich. G. E. M. Maguire. M. D. Bala*, Acta. Cryst.,* **E66** (2010) o463.
2) M. I. Fadlalla. H. B. Friedrich. G. E. M. Maguire. B. Omondi, *Acta. Cryst*., **E66** (2010) o3279.
3) M. I. Fadlalla. H. B. Friedrich. G. E. M. Maguire. B. Omondi, *Acta. Cryst.*, **E67** (2011) o648.

I (M. I. Fadlalla) carried out all the experimental work that lead to these publications, except the crystal data collection and solving of the structures.

Acknowledgments

I want to first and foremost thank Allah for his blessings and guidance. I extend my gratitude to Mintek and THRIP for the financial support. Furthermore, I extend my heart-felt gratitude and appreciation to both of my supervisors Prof H. B. Friedrich and Dr. G. E. M. Maguire for their support, guidance, supervision and encouragement.

In addition, I thank the following people: Dr. B. O. Owaga (University of Johannesburg) and Dr. M. Fernandes (University of Witwatersrand) for obtaining the crystal data and solving of the structures. Mrs. J. Naidoo, for her efficient handling of all financial matters. Mr. G. Moodley, for ensuring availability of chemicals and consumables. Mrs. A. Naidoo for all her assistance with instrumental analysis. Mr. D. Jagjivan for his assistance with all NMR related enquiries. Members of the electron microscopy unit of the University of KwaZulu-Natal (Westville campus) for their assistance with cryo-TEM, SEM and SEM-EDS analysis. Furthermore, I would like to thank Ms. T. Chetty and Mr. V. Dasireddy for their help with thermal gravimetric analysis and powder X-ray diffraction analysis, respectively. I also take the opportunity to thank the members of the catalysis research group for their input during the group meetings.

Furthermore, I greatly thank Ms. D. Naicker for proof reading this manuscript, her input and her friendship. I deeply acknowledge Dr. L. Pillay for her help with the ICP-OES analysis and Dr. M. Bala for proof reading the part of this manuscript dealing with crystal structures. I express my sincere thanks to Mr. S. Kumarchakka for his assistance with the NMR elucidation of the different compounds. I thank the following people: Mr. N.M. Pillay, Ms. V. Duki, Ms. L. Komarsamy, Mr. E. Kadwa and Ms. A. Singh for their friendship and support.

Lastly, my gratitude knows no boundaries to my mother (Mrs. H. Karar), my aunt (Mrs. E. Karar) and my siblings: Omer, Dina, Razan and Yassin, for their care, patience and encouragement.

List of figures

List of tables

List of schemes

Abbreviations

AA	=	amino alcohol or amino hydroxylation
ATR	=	attenuated total reflection
BET	=	Brunauer-Emmet-Teller (surface area characterisation technique)
t-BuOH	=	*tert*-butanol
DHQ-PHAL	=	hydroquinine 1,4-phthalazinediyl diether
EDS	=	energy dispersive spectroscopy
ESR	=	electron spin resonance
EXAFS	=	extended x-ray absorption fine structure spectroscopy
FT-IR	=	Fourier transform-infrared
g	=	gram
GC	=	gas chromatography
HPLC	=	high performance liquid chromatography
HPLC-MS	=	high performance liquid chromatography-mass spectroscopy
HT	=	hydrotalcite
HTlc	=	hydrotalcite-like compound
HTlc's	=	hydrotalcite-like compounds
HTlca's	=	hydrotalcite-like catalyst
HRTEM	=	high resolution transmission electron microscopy
ICP-OES	=	inductively coupled plasma-optical emission spectroscopy
L	=	liter
LC-MS	=	liquid chromatography-mass spectroscopy
LC-MSD	=	liquid chromatography-mass spectroscopy detector
LDH	=	layered double hydroxide

MeCN	=	acetonitrile
mmol	=	millimolar
mol	=	molar
mL	=	millilitre (10^{-3} liter)
NMR	=	nuclear magnetic resonance
PEG	=	polyethylene glycol
ppm	=	part per million
SEM	=	scanning electron microscopy
TEM	=	transmission electron microscopy
TGA-DSC	=	thermal gravimetric analysis-differential scanning calorimetry
TeoCNNaCl	=	2-trimethylsilylethyl-*N*-chloro-*N*- sodiocarbamate
TsO	=	*p*-toluensulfooxide
UV-vis	=	ultra violet-visible
XRD	=	X-ray diffraction
$(QN)_2PHAL$	=	1,4-bis(9-*O*-quininyl)phthalazine
Å	=	Ångstrom (10^{-10} meter)
µL	=	microliter (10^{-6} liter)

Contents

Chapter One

Introduction

1.1 Catalysis

One of the most accepted definitions of a catalyst is, "a substance that increases the rate at which a chemical system approaches equilibrium, without being consumed in the process".[1] A catalyst operates by lowering the activation energy of the reaction by providing a new mechanistic path for the molecules to react (Fig. 1.1).[1,2] The adsorption of the reactants is an energetically favoured process, this is shown by the reduction in the potential energy for the adsorption step. The reaction step requires energy but significantly less than in the absence of the catalyst. The product desorption from the surface of the catalyst also requires energy, however, once again less than that for the reaction (Fig. 1.1).[2]

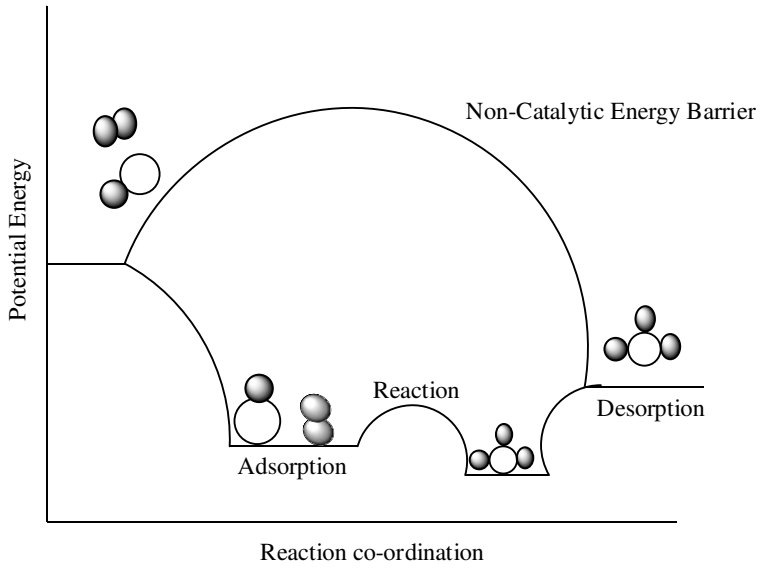

Fig. 1.1: The action of a catalyst.[2]

Catalysis is of significant importance in our lives, in terms of production of chemicals and energy sources. In the chemical industry 75% of all chemicals produced require the use of

a catalyst.[3] Many organic intermediates that are required in the production of synthetic fibers, plastics, dyes and pharmaceuticals are produced with the aid of a catalyst. Catalysts are also used in the petrochemistry industry for crude oil processing, refining, purification and chemical transformation.[3] In recent years green house gases production (especially CO_2) has risen due to automobiles, power stations and industrial plants exhaust. Therefore, to reduce the gas emission from these sources, catalysts are employed. Catalysis can be divided into three broad groups:

i) Enzyme catalysis, (e.g. body metabolism)[4]

ii) Homogeneous catalysis, (e.g. hydroformylation and drug synthesis)[4]

iii) Heterogeneous catalysis (e.g. hydrocarbon chain cracking and oil refining).[4]

In this dissertation only homogeneous and heterogeneous catalysis will be discussed.

1.2 Homogeneous *vs* heterogenous catalysis

In homogeneous catalysis both reactants and catalyst are in the same phase with no observable boundaries. In heterogeneous catalysis the reaction takes place in different phases (catalyst usually in the solid phase, while reactant(s) is (are) in the liquid or gas phase).[5,6] Both (homogeneous and heteroogenous) forms of catalysis have advantages over each other (Table 1.1). The main advantages of homogeneous catalysis are high selectivity and efficiency. These are attributed to the high degree of dispersion enabling all metal atoms to be catalytically active.[7] Because the reactants can approach the catalytic center from any direction without blocking neighboring catalytically active sites, less metal loading is required in homogeneous catalysis. Another advantage is the availability of methods and techniques that can be used to determine the mechanisms of the reactions.[5,7,8,9] In heterogeneous catalysis, only the surface atoms are catalytically active and are available to carry out the reaction. However, heterogeneous catalysis presents a high level of ease in the separation of the product from the catalyst. This advantage is of great importance in large scale production and when toxic transition metals (e.g. Os) are utilized.[1,5]

Table 1.1: Comparison between homogeneous and heterogeneous catalysis.[7]

Properties	Homogeneous catalyst	Heterogeneous catalyst
Active centers	All atoms are active	Only surface atoms are active
Concentration	Low	High
Selectivity	High	Lower
Diffusion problems	Practically absent	Present (mass-transfer-controlled reaction)
Reaction condition(s)	Mild (50-200 ^{o}C)	Severe (often > 250 ^{o}C)
Applicability	Limited	Wide
Activity loss	Irreversible reaction with the products (cluster formation); poisoning	Sintering of metal crystallites; poisoning
Structure/ stoichiometry	Defined	Undefined
Modification possibility	High	Low
Thermal stability	Low	High
Catalyst separation	Laborious	Simple
Catalyst recycling	Possible	Unnecessary
Cost of catalyst losses	High	Low

1.3 Oxidative catalysis

Oxidation can be defined as the gain of an oxygen atom, loss of electron(s) or loss of hydrogen.[10] Transition metals are effective candidates for catalyzing these reactions due to their many oxidation states.[5] Oxidation catalysis can be used in the synthesis of several agrochemicals and high value fine chemicals, production of high tonnage commodities (synthesis of the required intermediates) and pharmaceutical chemicals.[11] Osmium is suitable, among other transition metals, in oxidation reactions due to the different oxidation states (-2 to +8) it can encompass.[5] Asymmetric aminohydroxylation, along

with asymmetric dihydroxylation, are the most reported homogeneous oxidative catalysis reactions where osmium is used as the active species, in the production of β amino-alcohols and diols respectively.[12-14]

1.4 Aminohydroxylation

Vicinal amino alcohol(s) (β-amino alcohol) are a common structural component in many naturally occurring compounds, examples of biologically active compounds are presented in Table 1.2.[15] They function as starting materials in the synthesis of biologically active compounds. β-amino alcohols are classified into three general groups, based on the type of molecule that contains them, these include:[15,16]

i) Naturally occurring compounds.
ii) Synthetic pharmacologically active molecules.
iii) Chiral ligands.[16]

Currently, there are several homogeneous synthetic routes that lead to the production of β-amino alcohols. These routes are divided into four main groups:

i) Addition of the two heteroatoms (oxygen and nitrogen) to a molecule that does not contain either of them.
ii) Addition of one of the two heteroatoms to a molecule that already contains the other heteroatom.
iii) Forming a bond between two molecules, in which each contains one of, but not the same, heteroatom.
iv) Manipulation of functional groups in a molecule that already contains both the heteroatoms.[16]

Table 1.2: Biologically active molecules containing β-amino alcohols.[15]

Name	**Structure**	**Activity**
Acranile	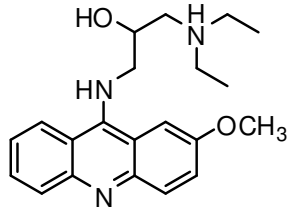	Antiprotozoal
Albuterol	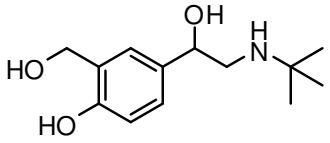	Bronchodialator
Ethambutol	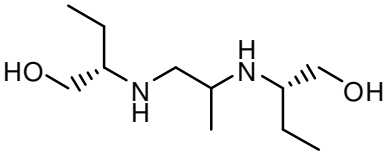	Tuberculostatic
Metaraminol	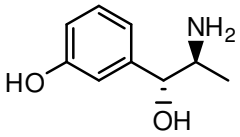	Sympathomimetic
Oxilofrine	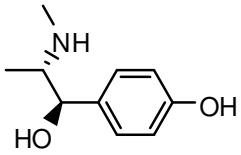	Sympathomimetic
Prenalterol	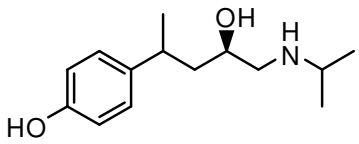	Cardiotonic

One of the simplest routes to protected β-amino alcohol is a reaction that was first reported in 1996.[14] This is the Sharpless asymmetric aminohydroxylation (AA) reaction. This reaction falls under group (i) (addition of both heteroatoms). Protected β-amino alcohols

can be produced by this single step, using a wide range of simple and functionalised olefins, with modest to high enantioselectivity, regioselectivity and yield.[13] Scheme 1.1 shows the Sharpless (AA) reaction. This example includes an Os complex as the catalyst, hydroquinine 1,4-phthalazinediyl diether ($(DHQ)_2PHAL$) as a chiral ligand for the control of the enantioselectivity and a nitrogen source.[13]

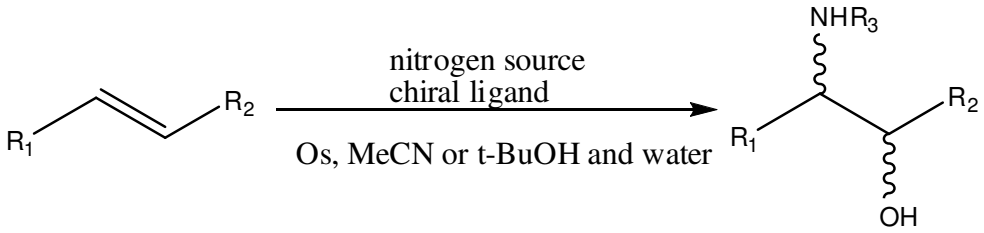

Scheme 1.1: The Sharpless asymmetric aminohydroxylation reaction.

The Sharpless (AA) reaction can be carried out using six-different methods that are currently available.[13] The only significant difference between these approaches is the nitrogen source.

1.4.1 Nitrogen sources for the aminohydroxylation reaction

The different nitrogen sources that can be used in the aminohydroxylation reaction can be classified into three main groups, which are: sulfonamides, carbamates and amides.[17] It is noteworthy that the nitrogen source influences the regioselectivity, enantioselectivity and the rate of the conversion to the β-amino alcohol.[12-14] From the sulfonamide group, chloramine-M and chloramine-T have been primarily studied (Fig. 1.2a and b respectively). Chloramine-M shows comparable activity (yield %) with chloramine-T. However, in terms of the reaction rate chloramines-M demonstrates the ligand accelerated catalysis phenomenon (the catalyst activity (reaction rate) increases when chloramine-M is used in the presence of a chiral ligand). On the other hand, chloramine-T demonstrates the

ligand decelerated catalysis phenomenon (catalyst activity (reaction rate) decreases when chloramine-T is used in the presence of a chiral ligand). The behavior of chloramine-M is believed to be due to the smaller substituent on the sulfur atom. The main advantage of chloramine-M over chloramine-T is that the by-product (methane sulfonamide) can be removed by a simple aqueous wash,[15,18] whilst the removal of the by-product of chloramine-T (*p*-toluene sulfonamide) requires tedious purification methods.[15]

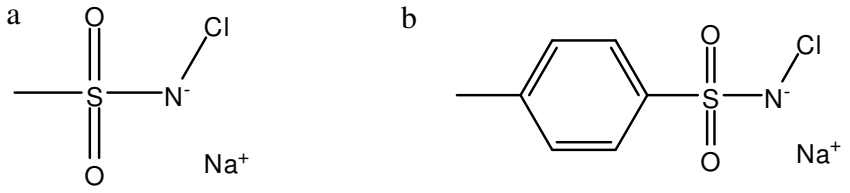

Fig. 1.2: Structure of Chloramine-M (a) and Chloramine-T (b).

Ethyl carbamates are the predominantly used nitrogen source that belong to the carbamates group. [15] Carbamates offer two main advantages over chloramine-T.[15] These include: the ease of deprotection to obtain the free amine and improvement in the rate of the reaction, enantio and regioselectivity.[15,19,20.]

The mostly utilized nitrogen-source of the amide group is from N-bromoacetamide. It is advantageous in that only a stoichiometric amount is required, hence the isolation and purification of the product is greatly simplified.[15,21] Table 1.3 shows the effect of the nitrogen source on the yield of the obtained β-amino alcohol.

Table 1.3: Effect of the different nitrogen sources on the isolated yield of the β-amino alcohols.

Substrate	Chloramine-T	Chloramine-M	TeoCNNaCl	N-bromoacetamide
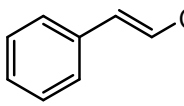	64% [15]	65% [18]	70% [19]	81% [20]
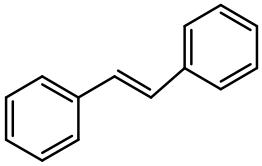	52% [15]	71% [18]	92% [19]	50% [20]
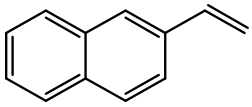	-	-	70% [19]	-
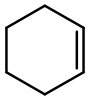	59% [21]	49% [18]	51% [19]	-

1.4.2 Mechanism of the aminohydroxylation reaction

The mechanistic proposals for aminohydroxylation have been based on the dihydroxylation reaction mechanism. The mechanism (Scheme 1.2) divided into two pathways (the 3+2 and the 2+2 pathway), are proposed on the basis of the electronic argument to account for the preference of nitrogen addition to the β-carbon of the alkenes. The key intermediate is the imidotrioxoosmium(VIII) **4** (pushes the reaction in the aminohydroxylation direction rather than the dihydroxylation reaction direction), which adds to the ligand forming **8**, then **8** with syn-stereospecificity adds to the alkene to form the azaglycolate **5** (3+2 pathway). The formation of **4** can take place following one of two pathways. In the (2+2) pathway cycloaddition of the alkene to the imidotrioxoosmium **4** to form the osmaazetidine **6**, this is followed by the coordination of the ligand to the

osmaazetidine species to form **7**. The ligand affects the enantio- and the regioselectivity of the reaction, influencing the equilibrium position, favoring the formation of species **7**, which gives the osmium azaglycolate **5** through 1,2-migration of the carbon-osmium bond.[14,15]

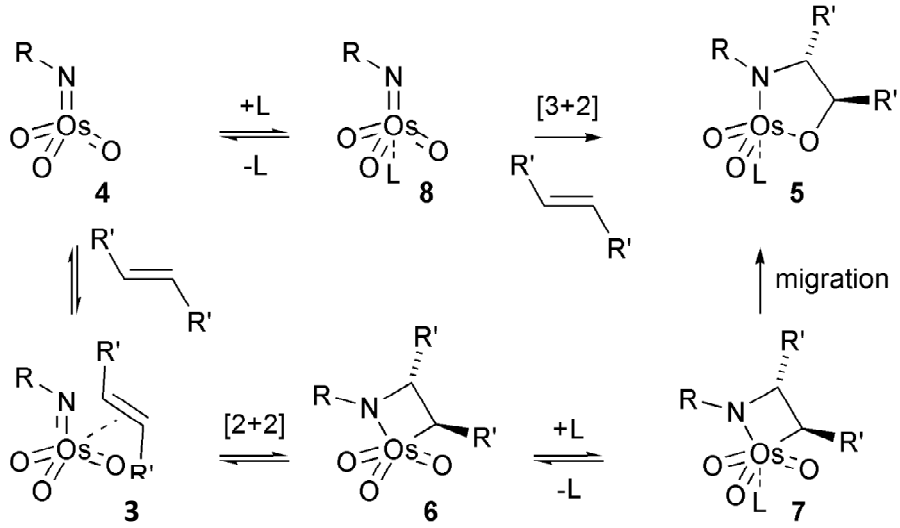

Scheme 1.2: The two proposed mechanisms ([2+2] and [3+2]) for the asymmetric aminohydroxylation reaction.[14]- *Reproduced by permission of the Royal Society of Chemistry.*

Regardless of the mode of the addition of the ligand, the ligand influences the enantio- and regioselectivity and increases the rate of the reaction. To explain the effect of the ligand, another mechanistic scheme is proposed (Scheme 1.3). This reaction mechanism consists of two cycles (a primary and a secondary cycle). In the primary cycle, the ligand mediates the addition of the alkene to the imidotrioxoosmium(VIII) **4** to form the azaglycolate **5**. Then the azaglycolate species will be re-oxidised by the nitrogen source to give **9**. The β-aminoalcohol is formed when **9** undergoes hydrolysis, this path results in high selectively. However, **9** can add another alkene to form **10**, and release the β-aminoalcohol after undergoing hydrolysis. This process results in low selectivity. Hence, to favour the primary cycle, the reaction should be carried out in a aqueous solvent system.[12,14]

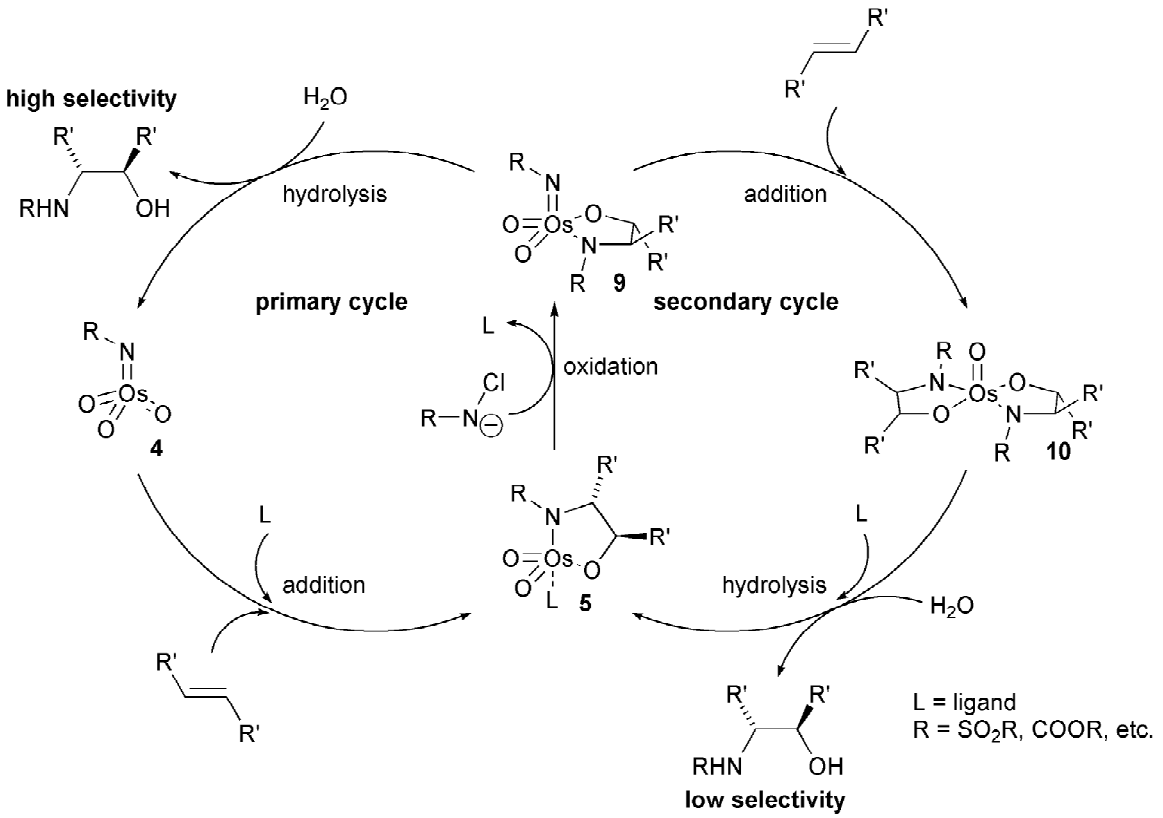

Scheme 1.3: The primary and secondary cycle mechanistic proposal for the catalytic Sharpless asymmetric aminohydroxylation.[12]-*Reproduced by permission of the Royal Society of Chemistry.*

1.5 Heterogenisation of the AA reaction

The homogeneous asymmetric aminohydroxylation reaction uses both Os and a Cinchona alkaloid ligand. The metal and the chiral ligand are the expensive components of the reaction. There have been a few attempts at heterogenising the asymmetric aminohydroxylation reaction to allow the re-use of these components. The asymmetric aminohydroxylation reaction, with its great scope and efficiency, is not used on an industrial scale. One attempt was by supporting the 1,4-bis(9-O-quininyl)phthalazine ($(QN)_2PHAL$) ligand on silica gel (Fig. 1.3).[22] The results obtained with this approach showed percentage yields of β-amino alcohols ranging from 30 to 81% (based on the

olefin nature) and *ee* values ranging from 88 to >99 %. However, this system resulted in Os leaching and osmium addition was required to restore the original activity.[22]

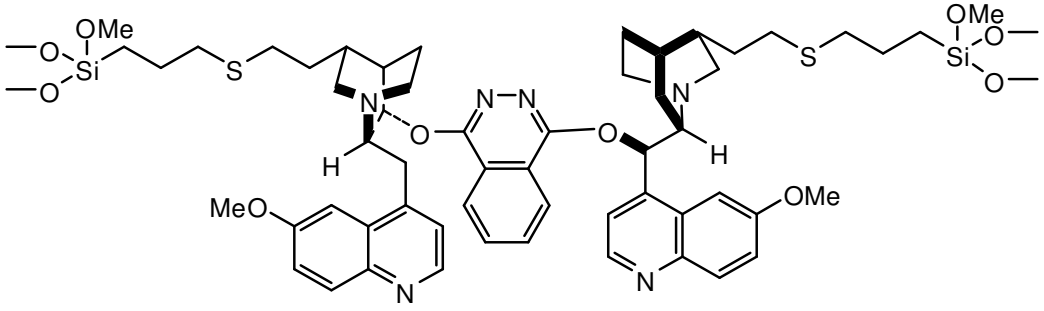

Fig. 1.3: Structure of the $(QN)_2PHAL$ ligand on silica gel.[22]

A different approach was to support the $(QN)_2PHAL$ on a polymer (Fig. 1. 4), which resulted in percentage conversions to β-amino alcohols ranging from 73 to 98% and *ee*'*s* ranging from 83 to 87%. However, upon recycling of the catalyst the percentage conversion reduced to 58% and the *ee* value to 81%.[23] Unlike the silica supported catalyst, the catalyst activity was not restored by further addition of Os.

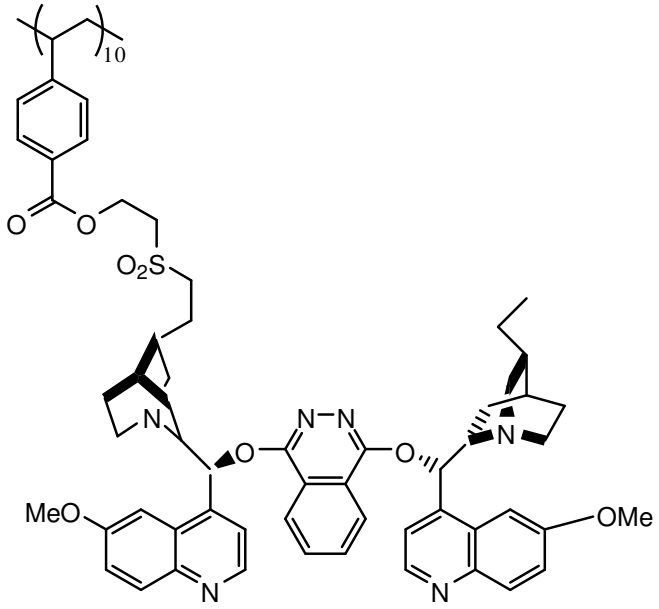

Fig. 1.4: Structure of $(QN)_2PHAL$ supported on a polymer.

Another approach was to immobilize Os on macroporous resins (Scheme 1.4). This approach resulted in yields of β-amino alcohols ranging from 39 to 90% (based on the nature of the olefins) and *ee* values ranging from 84 to >99%. However, this method cannot be considered heterogeneous. The Os species leaves the resin upon being oxidized by the oxidant and carries out the reaction in a homogeneous manner, upon consumption of the olefin, the Os species re-bind to the vinyl-groups in the resin. This approach also resulted in Os leaching, since not all the Os species re-bind to the resin.[24]

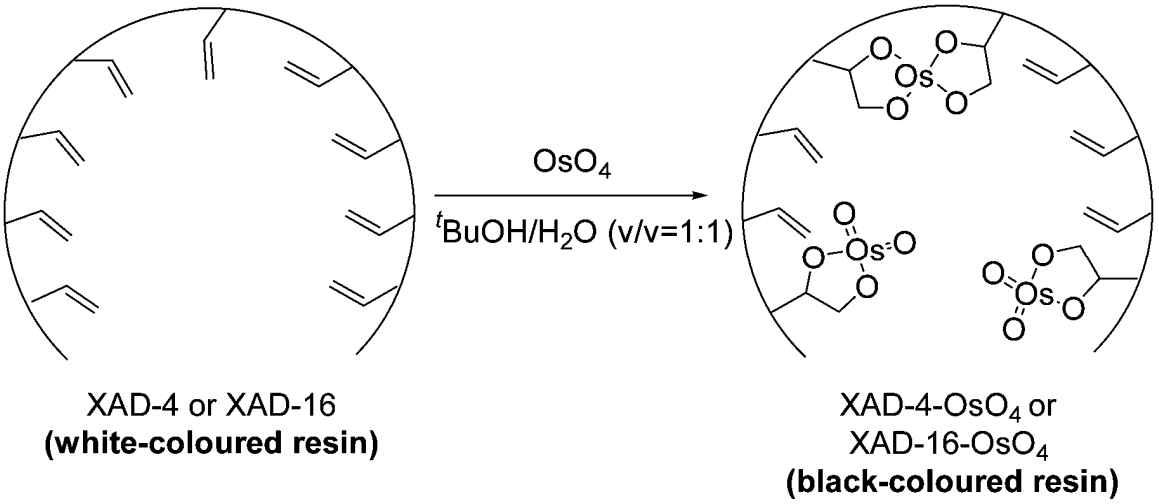

Scheme 1.4: The reaction for osmylating a macroporous resin.[24]-*Reproduced by permission of the Royal Society of Chemistry.*

Another unique approach was taken by supporting the two molecules of (DHQ-PHAL) on soluble polyethylene glycol (PEG). This method provides two catalytic sites to carry out the reaction (Fig. 1.5). The percentage yield of β-amino alcohols obtained range from 45 to 93% (based on the nature of the olefin) and *ee* values range from 74 to 99%.[25] The recyclability study showed that no significant loss of catalytic activity was observed upon recycling, unlike the other techniques.[22-24] However, the reaction time increases with an increase in the recycle number. Furthermore, the reaction took place in a single phase and cannot be considered truly heterogeneous.[25]

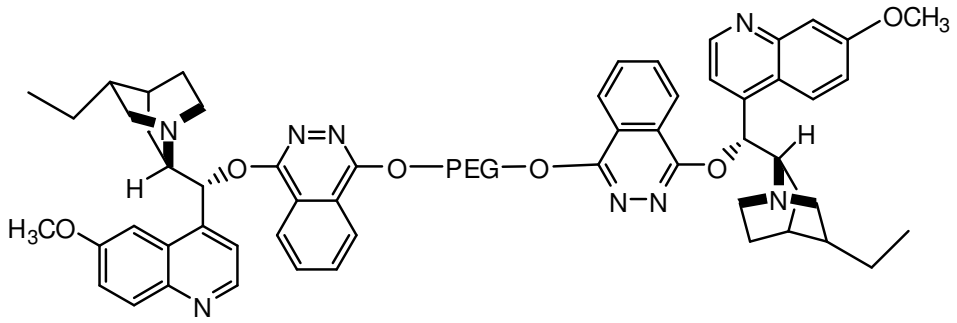

Fig. 1.5: Structural representation of soluble (DHQ-PHAL) on a PEG.[25]

The last approach to heterogenizing this reaction is one that is closely related to that taken in this study, but with a fundamental difference. It involves supporting OsO_4 on layered double hydroxide (LDH). The use of this approach resulted in yields of β-amino alcohols ranging from 45 to 55% and *ee* values ranging from 40 to 78%. However, high levels of Os leaching were observed. The authors suggested that could be due to the high polarizing effect of chloramine-T, as the nitrogen source.[26]

The studies mentioned previously have two facts in common, Os leaching and the excellent to acceptable *ee's* attained. Furthermore, two techniques[23,24] were not truly heterogeneous in approach but gave effortless separation. Therefore, the main problem is not heterogenizing the ligand but rather heterogenizing the Os. This study is focused on heterogenizing Os, rather than the chiral ligand, thus dealing with the aminohydroxylation reaction instead of the asymmetric aminohydroxylation.

1.6 References

1) G. C. Bond, *Heterogenous Catalysis:principles and applications*, 1974, Oxford University Press.

2) http://www.spaceflight.esa.int/impress/text/education/catalysis/index.html access date 29/8/2010.

3) www.nacatsoc.org/who.asp. access date 29/8/2010.

4) J. T. Richardson, *Principle of catalyst development*, (1989) Plenum Press, New York.

5) D. Shriver, P. Atkins, *Inorganic chemistry*, 3rd edition, (1999) Oxford University Press.

6) G. C. Bond, *Principle of catalysis*, the Chemical Society, (1972), London.

7) J. Hagen, *Industrial Catalysis: A practical approach,* 2nd edition (2006), Wiley-VCH. Weinheim.

8) P. G. Jessop, T. Ikariya, R. Noyori, *Chem. Rev.,* **99** (1999) 475.

9) W. R. Barnhart, B. Bosnich, *Organometallics*, **14** (1995) 4343.

10) P. Y. Bruice, *Organic Chemistry*, 4th edition (2004), Pearson Education, New York.

11) D. Hughes, Y Xu, P. Jenkins, P. McMorn, P. Landon, D. Enache, A. Carley, G. Attard, G. Hutchings, F. King, E. Hugh, P. Johnston, K. Griffin, C. Kiely. *Nature*, **437** (2005) 1132.

12) S. Bergmeier, *Tetrahedron*, **56** (2000) 2561.

13) O. Reiser, *Angew. Chem. Int. Ed. Engl.,* **35** (1996) 1308.

14) J. Bodkin, M. McLeod, *J. Chem. Soc., Perkin Trans*. 1 (2002) 2733.

15) B. B. Lohray, P. S. Thombare, V. Bhushan, *PINSA*, **68 A** (2002) 391.

16) S. Bergmeier, *Tetrahedron*, **56** (2000) 2561.

17) J. A. Bodkin, M. D. McLeod, *J. Chem. Soc., Perkin Trans. 1*, (2002) 2733.

18) J. Rudolph, P. C. Sennhenn, C. P. Vlaar, K. B. Sharpless, *Angew. Chem. Int. Ed. Engl.*, **35** (1996) 2810.

19) K. L. Reddy, K.R. Dress, K. B. Sharpless*, Tetrhedron Lett.*, **39** (1998) 3667.

20) G. Li, H. H. Angert, K. B. Sharpless, *Angew. Chem. Int. Ed. Engl.*, **35** (1996) 2813.

21) M. Bruncko, G. Schlingloff, K. B. Sharpless, *Angew. Chem. Int. Ed. Engl.,* **36** (1997) 1483.

22) C. E. Song, C. R. Oh, S. W. Lee, S. Lee, L. Canali, D. C. Sherrington, *Chem. Commun.*, (1998) 2435.

23) A. Mandoli. D. Pini, A. Agostini, P. Salvadori, *Tetrahedron Asymmetry*, **11** (2000) 4039.

24) C. H. Jo, S. Han, J. W. Yang, E. J. Roh, U. Shin, C. E. Song, *Chem. Commun.*, (2003) 1312.

25) X. Yang, H. Liu, M. Xu, G. Lin, *Tetrahedron Asymmetry*, **15** (2004) 1915.

26) B. M. Choudary, N. S. Chowdari, K. Jyothi, M. L. Kantam, *J. Mol. Catal. A*, **196** (2003) 151.

Chapter Two

Introduction to hydrotalcite and hydrotalcite-like compounds

2.1 Hydrotalcite (HT) and hydrotalcite-like compounds (HTlc)

In our daily life minerals are utilized for different purposes, for example as a source of energy (coal). Clays have been among the most utilised minerals for centuries.[1] Clays are used to produce many man-made products, such as ceramics,[1,2] pottery, paper coatings and drilling muds.[2] In chemistry, clays are used as catalyst supports, or as catalysts themselves. The use of clays also has many important applications in the pharmaceutical industry.[2]

Clays can be divided into two main groups, based on the net charge of the layers that constitute the structure. These are cationic and anionic clays.[1] Cationic clays are widely formed in nature, consisting of negatively charged alumino-silicate layers. The negatively charged alumino-silicate layers are balanced by cations present in the interlayer spacing between these sheets.[1,2] Based on the structure, cationic clays can be divided into two groups; the 1:1 type and the 2:1 type.[1] The 1:1 type consist of a tetrahedral sheet and a octahedral sheet. The 2:1 type consist of an octahedral sheet that is surrounded by two tetrahedral sheets.[1] Anionic clays consist of layers which are made of hydroxyl sheets (brucite-like sheets), that have a net positive charge. This positive charge is balanced by anions present in the interlayer spacing between the brucite-like sheets. Anionic clays rarely occur in nature. However, they are easily and inexpensively synthesized. Anionic clays can be described by the general formula (formula 2.1)

$$[M^{2+}_{1-x} M^{3+}_{x} (OH)_2]^{b+} [A^{n-}_{b/n}] mH_2O \qquad \text{(Formula 2.1)}$$

Where M is the metal, A is the interlayer anion.

Anionic clays can be defined and grouped by their stacking sequence, chemical composition and basal spacing.[3]

Hydrotalcite (HT) and hydrotalcite-like compounds (HTlc) are examples of anionic clays. HT and HTlc can be defined as layered positively charged brucite-like structures in which the net charge is balanced by anions in the interlayer.[1,4] It consists of hydroxyl-carbonates of aluminum and magnesium.[1,2] In nature HT exists in different forms; foliated and contorted plates and/or fibrous masses.[1,4] Hydrotalcites were discovered around 1842 in Sweden.[4] Since their discovery hydrotalcites are referred to as that or as layered double hydroxides (Fig. 2.1).[1-4] HTlc are compounds that consist of metals other than Al and Mg, but exhibit the same structure as a hydrotalcite .[4]

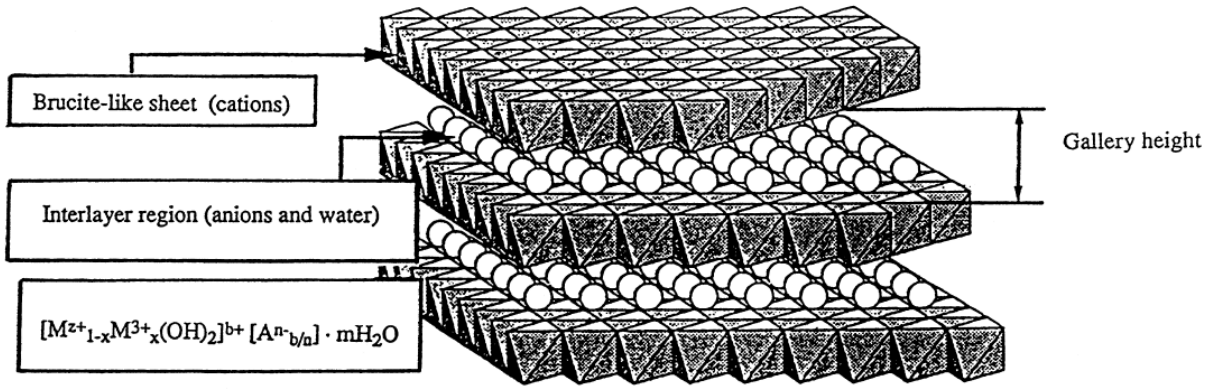

Fig. 2.1: Graphical representation of the structure of hydrotalcite compounds.[1] *Reproduced with permission from Elsevier.*

2.2 Preparation methods

The main methods for the synthesis of HTlc include precipitation, hydrothermal treatment and anionic exchange techniques. The one which is most frequently used is the precipitation approach and will be discussed in this dissertation, and the hydrothermal treatment.

2.2.1 Precipitation methods

For the preparation of HTlc with many cations (metals), the co-precipitation only occurs under supersaturated conditions. Two approaches can be followed to obtain supersaturation; the physical approach (evaporation) and chemical approach (variation of pH). In the chemical approach, it is important to obtain a pH range that is higher than or equal to the pH at which the most soluble metal hydroxides precipitate. The pH range of 8-10 is the range at which most different cations precipitate into HTlc structures.[4] This method can be divided into three different approaches; the titration method, precipitation at low supersaturation and precipitation at high supersaturation.

2.2.1.1 Titration method

This method is also known as sequential precipitation or increasing pH method.[4] Here, the acidic metal(s) (cation(s)) solution is titrated with a base solution. Base solutions that are frequently used are those of NaOH and/or $NaHCO_3$.[4] This method was used in the synthesis of the first HT, utilizing diluted solutions of Mg and Al and sodium carbonate solution.[5-7] The preparation of HTlc's containing Os has been carried out by this method.[8,9]

2.2.1.2 Precipitation at low supersaturation

The low supersaturation precipitation method, at constant pH, is the most used method in the synthesis of HTlc. This can be due to the fact that at low supersaturation, the rate of nucleation is lower than the rate of crystal growth. This results in more crystalline HTlc's.[10-12] However, to carry out the HTlc synthesis at low supersaturation, a number of conditions need to be fulfilled. These conditions are:[4]

i) Low concentration of reagents (i.e. metal solution (M(II) and M(III)) and base solution (anion).

ii) Slow addition of the two reagents.

iii) The pH must be in the range of 7-10.

iv) The temperature must be in the range of 333-353 K.

v) Washing must be done with warm water.

2.2.1.3 Precipitation at high supersaturation

The first patent dealing with the use of HTlc as a catalyst precursor used the high supersaturation technique, in the preparation of $MgAlCO_3$-HTlc, $CoMnAlCO_3$-HTlc and $CoMnMgAlCO_3$-HTlc.[13] It is noteworthy that this technique involves fast addition of the metal solution and the base solution. This results in a higher nucleation rate than crystal growth rate. As a consequence this method results in less crystalline HTlc's than those obtained using the low supersaturation approach (Section 2.2.1.2).[10,11]

2.2.1.4 Hydrothermal treatment after precipitation

The interlayer molecules that are present in HT and HTlc can be removed by calcination. The process of interlayer water removal is known as dehydration. This process usually occurs around 300 °C and does not result in the collapse of the HT or HTlc structure. The hydroxyl groups and the carbonates in the interlayer can be removed by a process known as dehydroxylation and decabonization respectively. The dehydroxylation and decabonization occur in the temperature range between 300-700 °C. The HT and HTlc structure will decompose (collapse) to the corresponding metal oxides at a temperature above 700 °C. These transitions and the product(s) obtained through them depend on:

i) The elements making up the original HTlc phase.

ii) The HTlc preparation method (aging time, temperature of precipitation).

iii) The heating atmosphere and the heating rate.

iv) Presence of impurities.

2.2.1.5 Urea hydrolysis

Urea hydrolysis is another method for preparation of HT and HTlca, for example it was used in the synthesis of a single Mg:Al (1:1) and Ni:Al (2:1) HT and HTlc. The use of urea hydrolysis provides an advantage over the co-precipitation method in that little washing is required, unlike in the co-precipitation method, where extensive washing is required to remove free alkali metals.[2] In thermally induced urea hydrolysis, temperature has an effect on the particle size, uniformity and the crystallinity level of the HT or HTlc synthesised. At lower temperatures, low nucleation rates take place leading to larger particle size HT or HTlc, while the opposite takes place at higher temperatures, leading to a more uniform and smaller particle size HT or HTlc. Furthermore, urea can be used to maintain the pH.[2] Since urea is completely soluble in water forming ammonium cyanate, pH is stabilised by forming CO_3^{-2} and CO_2 in basic and acidic media, respectively, as shown in the following chemical equations.[2]

$$NH_4^+ + H_2CO_3 \longrightarrow NH_4^+ + NCO^- \dashrightarrow (1)$$

$$NCO^- + 2H_2O \longrightarrow NH_4^+ + CO_3^{2-} \dashrightarrow (2)$$

$$NCO^- + 2H^+ + 2H_2O \longrightarrow NH_4^+ + H_2CO_3 \dashrightarrow (3)$$

2.2.1.6 Sol – gel method

In this method the desired metal salt or precursors are hydrolysed in water or an appropriate solvent (at 25 °C) to obtain a particulate sol. To obtain high dispersion of the metal, a base or acid can be added (this facilitates peptisation during hydrolysis). The main advantages of this method are; cost effectiveness and control of the particle size of the product (*i.e.* HT or HTlc) by controlling the reaction temperature and aging time. For example, large particle size HT or HTlc can be obtained by decreasing the reaction

temperature or the aging period. Furthermore, the method results in HT or HTlc with high thermal stability.[2] This method was also used in the synthesis of highly pure HT that can be used as a drug carrier.[12]

2.2.1.7 Microwave assisted synthesis

Microwave irradiation can be used in conjugation with the metal solution addition from the sol-gel method. The main advantage of microwave synthesis is the significant shortening of the reaction time and aging period. Unlike conventional methods of heating, microwave irradiation utilises non-ionising electromagnetic radiations that interact with the solution to produce uniform bulk heating.[2] On the other hand, conventional heating transfers radiation by conduction from the vessel to the solution inside the vessel. In addition, the use of microwave irradiation can enhance the kinetics of crystallisation (depending on the trivalent cation in the HTlc structure) and increase the surface area of the HTlc produced.[2]

2.3 Hydrotalcite-like compounds (HTlc)

Most HTlc have the general formula shown in Formula 2.1. In natural HTlc's the common value for x is 0.25 and a carbonate (A) value of 1. It is possible to synthesise HTlc with two or more metals and one or two different anions.[1,4]

2.3.1 The nature of M(II) and M(III)

M(II) and M(III) (divalent and trivalent metals respectively) are the metals that fill the pockets of the close packed hydroxides in the brucite-like sheet. The main criteria for M(II) and M(III) is that their ionic radii must be close to that of Mg^{2+} to form HTlc's (Table 2.1). If the metal has an ionic radius that is significantly smaller than the ionic radius of Mg^{2+} (Table 2.1), then the formation of the octahedral co-ordination in the hydroxide layer (brucite-like sheets) is inhibited due to the small ionic radius (e.g. Be^{2+}). On the other extreme, if the metal ionic radius is too large (e.g. Ca^{2+} and Ba^{2+}), it will not

form the octahedral co-ordination in the hydroxide layer (brucite-like sheet) but will form other structures. [6,21] When divalent and trivalent metals such as Cu^{2+}, Cr^{2+} and Mn^{3+} are used, compounds that are characterized by the presence of the co-operative Jahn-Teller effect are formed. In order to form HTlc's containing Cu^{2+}, another divalent metal (Table 2.1) in a ratio of Cu^{2+}/M(II) equal to or less than one must be used. This ensures that the Cu^{2+} ions in the pockets of the hydroxide layer (brucite-like sheet) will be separated from each other, taking an octahedral co-ordination.[4,9] If the ratio of the Cu^{2+}/M(II) is higher than one, the formation of Cu HTlc will not be energetically favoured, because a distorted octahedral formation will be more favourable. For trivalent cations there are two limitations.[4]

i) Stability of the cation (air stable), therefore, Ti^{3+} will not form HTlc because of their instability in air.

ii) The ionic radii of the trivalent metals must be in the range of 0.5-0.8 Å.

2.3.2 The value of x

In order to obtain HT's and HTlc's the value of x (with reference to Formula 2.1) must be in the range of $0.2 \leq x \leq 0.33$. If the value of x is out of this range then structures other than that of the HTlc will be obtained.[4]

2.3.3 The nature of the anion

The positively charged brucite-like sheets in HTlc are balanced by anions that are present in the interlayer between the hydroxide layers (brucite-like sheets). Different types of anions are used in the synthesis of HTlc.[1,4] These include:

i) Inorganic anions *e.g.* $(CO_3)^{2-}$, $(ClO_3)^{-}$, $(Fe(CN)_6)^{4-}$ and F^{-}.

ii) Heteropolyacids *e.g.* $(PMo_{12}O_{40})^{3-}$.

iii) Organic acids *e.g.* (oxalic and adipic acid).[21-23]

iv) Layered compounds *e.g.* (mineral chlorite).[19]

Table 2.1: Different M(II) and M(III) and their ionic radii.[4]

Cation	**Type**	**Ionic radii /Å**
Be	M(II)	0.30
Ca	M(II)	0.98
Co	M(II)	0.74
Cu	M(II)	0.69
Mg	M(II)	0.65
Mn	M(II)	0.80
Zn	M(II)	0.74
Al	M(III)	0.50
Co	M(III)	0.63
Cr	M(III)	0.69
Fe	M(III)	0.64
Mn	M(III)	0.66
Ti	M(III)	0.76

The interlayer spacing between the hydroxide layers in the HTlc is determined by:

i) The size of the anion (the HTlc's using halogens, beside I⁻, as anions have a similar thickness to that using carbonates as anions).[24]

ii) The number of the anions.

iii) The orientation of the anions.

iv) The strength of the bond between the anions and the hydroxide group.[4]

2.3.4 The value of m

The interlayer spacing between the brucite-like sheets is filled with anions and water molecules. In Formula 2.1 the m value corresponds to the amount of water that is present in the interlayer. This can be determined by thermogravimetric analysis, or by calculating the maximum amount of water that can be present in the assumed close packed configuration of oxygen atoms and subtracting the amount of sites that will already be occupied by the anion molecule.

2.4 Structural properties of HT and HTlc

The most extensive investigation of the structure of layered double hydroxide (LDH) was carried out on a sjőgrenite and pyroaurite structure, with the approximate composition of $Mg_6Fe_2(OH)_{16}CO_3.H_2O$. These studies were carried out on monocrystals.[15-20] To understand the structure of HT and HTlc's one can use the $Mg(OH)_2$ brucite-like structure. In pyroaurite the Mg^{2+} is substituted by trivalent Fe, whilst the Mg^{2+} in the HT is replaced by the Al^{3+} in the hydroxyl layer (brucite-like layer). This creates a net positive charge in the brucite-like sheet that is balanced by the presence of anions (carbonates) in the

interlayer space between the brucite-like sheets. In the interlayer, among the carbonate anions, water molecules are also found.[1,4]

The main structure of the HTlc's are determined by:

i) The nature of the brucite-like sheet, which contain the cations.
ii) The position of the anions and water molecules in the interlayer space (anions and water molecules can move randomly in the interlayer space due to H-bonding).
iii) The type of stacking in the brucite-like sheets (the carbonates are tied to the hydroxyl group through intermolecular bonding or via water molecules).[1,4,19]

HTlc can have the hydroxyl groups packed into two different stacking symmetries. These are of rhombohedral or hexagonal symmetry. HT and HTlc's with rhombohedral symmetry are commonly found in nature with a unit cell parameter of a and c = 2c'. The synthetic HTlc's have a hexagonal symmetry (Fig. 2.2), where the unit cell parameter is a, c = 3c'. Some minerals can consist of both rhombohedral and hexagonal symmetry, with the hexagonal symmetry being the internal part and the rhombohedral symmetry on the external part.[4]

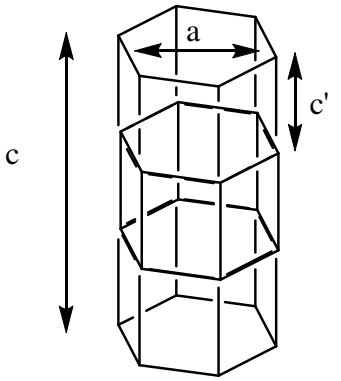

Fig. 2.2: Graphic presentation of the unit cell with hexagonal symmetry.

2.5 Characterisation techniques

There are many different techniques that have been used in the characterisation of HT's and HTlc's. These techniques include: XRD (the diagnostic technique), ICP-OES, IR

spectroscopy, electron microscopy, TGA and solid state NMR spectroscopy. Techniques specific to HTlc's include UV-Vis, ESR and EXAFS and XANES. These techniques differ in the information they provide about HT's and HTlc's and the principle of operation. Powder XRD is the most routinely used technique for HT's and HTlc's.

2.5.1 X-ray diffraction (XRD)

XRD analysis is the most powerful technique in the identification of a HTlc structure. The powder XRD of a HTlc shows a number of important features (pattern). The general powder XRD pattern for HTlc's is characterized by high intensity and sharp peaks at low 2θ value. The intensities of the peaks decrease and they become asymmetrical as the 2θ values increase. The layered packing in the HTlc is indicated by the equally spaced intense peaks at low 2θ value. At high 2θ values, overlapping peaks indicate the hexagonal plane of the HTlc. Powder XRD also provides information about the dimension of the unit cell of the HTlc. The distance between the cations in the brucite-like sheet is indicated by the *a* parameter. This is determined using the 110 plane (hexagonal axes).[7, 26-28] This plane is independent of the layer stacking, hence it is used to calculate the a parameter ($a = 2d_{110}$). The c' parameter depends on two factors:

i) The anion size.

ii) The value of x (Formula 2.1).[9,29-31]

2.5.2 Infrared analysis (IR)

IR analysis cannot be used to confirm the formation of the HTlc structure, but does give important information, such as;

i) The presence of different anions in the interlayer space between the brucite-like sheets.

ii) The anion's orientation.

iii) The different types of bonds that the anions form.

The OH in the brucite-like sheet is indicated by absorption bands around 3500-3600 cm^{-1}. This band is most often broad due to water molecules and hydroxyl groups within the brucite-like sheets.[32-34] The presence of water is indicated by the absorption band around 1600 cm^{-1} corresponding to water bending vibration(s). The adsorption band for most anions is around 1000-1800 cm^{-1}. The bands associated with carbonates (the most used anion) can be divided into: 670-690 cm^{-1} (υ1), 850-880 cm^{-1} (υ2) and 1350-1380 cm^{-1} (υ3).

2.5.3 Inductively Coupled Plasma-Optical Emission Spectroscopy (ICP-OES).

This technique is used to determine the amount of different metals and the respective ratios at which they are present in the catalyst. ICP-OES measures the emission of the different metals after they are excited by means of plasma. The amount of emission energy released at specific wavelengths is related to the concentration of that specific metal in the sample.[35]

2.5.4 Brunauer-Emmett Teller (BET) surface area measurment

BET is a technique used to determine the surface area and the pore size distribution of porous, finally divided materials, by a gas adsorption method. The most commonly used gas in the BET surface area method is nitrogen.[36]

2.5.5 Solid State-Nuclear Magnetic Resonance (SS-NMR)

This technique is used to investigate the geometry around the Al in the HTlc catalyst. In HTlc, Al has an octahedral geometry around it. If the geometry around Al is octahedral then the peak will be around 0 ppm, if the geometry around Al is tetrahedral then the peak in the SS-NMR will be around 55-80 ppm. However, It is important to use the magic-angle spinning (MAS) methodology in order to reduce quadrupole effects and dipole interaction.[4,37]

2.5.6 Thermal Gravimetric Analysis (TGA)

The thermal-gravimetric technique is used to detect the presence of any impurities in the HTlc. The thermal-gravimetric analysis does not give information about the characteristic structure of the hydrotalcite in question. However, TGA of the hydrotalcite shows two characteristic weight losses:

i) At low temperatures (endothermic), which corresponds to the loss of water from the interlayer. This does not affect the structure of the hydrotalcite and is a reversible process.

ii) At high temperatures (endothermic), which corresponds to the loss of the brucite-like layer hydroxyl group and the anion.[4]

Those two characteristic transitions depend on many factors, such as:

i) The type of anion present in the hydrotalcite-like structure.

ii) The treatment of the hydrotalcite prior to the analysis (drying temperature, heat treatment).

iii) The ratio of M(II)/M(III).[4]

2.5.7 Electron microscopy imaging

This technique is used to study the structural characteristics of HTlc, preferably by using a Cryo-transmission electron microscope (Cryo-TEM). The surface morphology of the HTlc, using a scanning electron microscope, can also be investigated. The difference between TEM and Cryo-TEM is that in the former the sample is viewed at room temperature, whilst the latter deals with viewing the sample at the temperature of liquid nitrogen. In this study Cryo-TEM was used because Os could sublime around 100 °C, making the sample sensitive to heat that will be generated by the electron beam. In SEM the electron beam does not generate as much heat, because SEM is only used to investigate the surface morphology.

2.6 Application of HTlc's

HT and HTlc's have gained a lot of attention due to their extensive applications. HTlc's are utilised as molecular sieves, anti-acid, flame-retardants and in ion exchange. Furthermore, HTlc's have gained more attention because they can be tailored to be used as catalysts, catalyst precursors or catalyst supports. HTlc's are used to carry out many different reactions. However, the following discussion will be focused on their application as catalysts in oxidation reactions.

2.6.1 HTlc's in oxidation catalysis

HTlc's can be tailored for specific catalytic application by changing the elements and the ratio in which they are present. Furthermore, the active cations can be isomorphically substituted with Mg^{2+} or Al^{3+} in the octahedral site.

Ru-Co-Al-CO_3 was used in the heterogenous oxidation of alcohols and aromatic compounds with molecular oxygen to produce aldehydes. This method produced aldehydes in yields ranging from 82 to 100% with a conversion ranging from 86 to

100%.[38] However, no leaching test was conducted to confirm if the reaction occurred heterogeneously.[38] In another study, Ru-Cu-Al HTlc was used to oxidise alcohols to aldehydes or ketones. The replacement of Co by Cu in the HTlc structure, resulted in the catalyst being more stable and recyclable. This method showed high selectivity for the oxidation of allylic, aromatic and aliphatic alcohols to their corresponding aldehydes or ketones, in yields ranging from 47 to 100%.[39]

Baeyer-Villiger oxidation is a reaction utilised in the production of lactones and esters from their respective ketones, using oxidants such as hydrogen peroxides. Heterogenisation of the Baeyer-Villiger oxidation was carried out using Mg-Al hydrotalcite with H_2O_2/nitrile as the oxidant. The yields of lactones produced from the corresponding ketones ranged from 26 to 100% with a conversion of 64 to 100%. There were no leaching tests reported in this study, to confirm the heterogeneity of the reaction.[40]

HT is also used as a basic catalyst to form epoxides, through epoxidation with hydrogen peroxide. This method results in epoxide yields ranging from 50 to 97%.[41] There have been attempts to improve on this by using different bases along with the hydrogen peroxide. Bases that have been used are nitriles[42] and amides.[43] However, the use of these bases did not improve the yield of epoxides significantly. Another approach to epoxidation using HT was taken by supporting organotungstic complexes on the HT. This method resulted in high selectivity (100%) but rather low conversion (< 40%). When organotungstate was used as the catalyst there was formation of other oxidation products such as diols, ketones and alcohols.[44]

Diols can be produced homogeneously by the Sharpless dihydroxylation reaction using Os containing catalysts. The Os-Zn-Al HTlc was used to heterogenise the dihydroxylation reaction.[8] The use of Os-Zn-Al HTlc by Friedrich *et al.*[8] results in diol yields ranging from 96 to 100%. Furthermore, HTlc's with Zn as the divalent metal showed greater catalytic activity, when compared to Co, Mg and Cu.[9] Both studies conducted leaching tests and the results showed no leaching of Os.

For more examples on the use of HTlc's in non-oxidative catalysis refer to reference 1, 4, 45, 46, 47, 48 and 49.

2.7 Project aim

There were several aims in this project. First, the synthesis and characterisation of Os-Zn-Al-HTlc for the heterogeneous aminohydroxylation reaction. The preference of using HTlc's was based on the fact that HTlc's were successfully employed to heterogenise reactions, and HTlc containing Os-Zn-Al was successfully used in the heterogenisation of the dihydroxylation reaction (a sister reaction to the aminhydroxylation reaction).

Second, investigating the effect of different reaction temperatures and solvent systems on the rate of the reaction and the effect of the catalyst crystallinity on the rate of the reaction and the yield of the β-amino alcohols obtained. The temperatures investigated were 25, 40 and 60 ^{o}C, while the solvents investigated were dry toluene, *t*-butanol/water (1:1 v/v) and acetonitrile/water (1:1 v/v). These latter two solvents are applied in the homogeneously catalysed reaction in literature.

Third, using the optimum catalytic conditions to be determined above in testing the catalyst activity against different classes (aliphatic, aromatic, aliphatic and functionalised) of olefins.

Fourth, the structure of the spent catalyst will be investigated.

Fifth, to investigate if Os leaches into the reaction mixture. If so, to determine whether the leached Os is catalytically active or not. This will enable one to determine if the reaction is truly heterogeneous or not. Recycling of the catalyst will also be investigated.

2.8 References

1) A. Vaccari, *Catal. Today*, **41** (1998) 53.

2) M. R. Othman, Z. Helwani, Martuns, W. J. N. Fernando, *Appl. Organometal. Chem.*, **23** (2009) 335

3) H. R. Oswald, R. Asper, in: R. M. A. Lieth (Ed.), *Physics and Chemistry of Materials with Layered Structures,* Vol. **1**, Reidel, Dordrecht (1977) 73.

4) F. Cavani, F. Trifiro, A. Vaccari, *Catal. Today*, **11** (1991) 173.

5) W. Feitknech, *Helv. Chim. Acta.,* **25** (1942) 131.

6) W. Feitknech, *Helv. Chim. Acta.,* **25** (1942) 555.

7) M. C. Gastuche, G. Brown, M. Mortland, *Clay Miner.,* **7** (1967) 177.

8) H. B. Friedrich, M. Govender, X. Makhoba, T. D. Ngcobo, M. O. Onani, *Chem. Commun.*, (2003) 2922.

9) T. Naicker, A. K. Datye, H. B. Friedrich, *Appl Catal A*, **350** (2008) 96.

10) A. J. Marchi, A. G. Sedran, C. R. Apesteguia, *In Prepr.IV th Int. Symp. On Scientific Bases For The Preparation Of Heterogeneous Catalyst*, Louvain-la-Neuve (**B**) 1986, H7.

11) A. J. Marchi, J. I. Di Cosimo, C. R. Apesteguia, *In F. Cossio, O. Bermudez, G. del Angel and R. Gomez (Editors), Proc. XI IberoAmer. Symp. on Catalysis, IMP*; Mexica D. F., 1988 Vol. 1-25.

12) W. F. Lee, Y. C. Chen, *Eur. Polym. J.,* **42** (2006) 1634.

13) Ph. Courty, D. Durand, E.Freund, A. Sugier, *J. Mol. Catal.,* **17** (1982) 241.

14) French patent 2,091,785 (1971), to BASF AG.

15) R. Allmann, *Acta Cryst.*, **B24** (1968) 972.

16) R. Allmann, H. H. Lohse, *N. Jhb. Miner. Mh.,* **6** (1966) 161.

17) L. Ingram, H. F. W. Taylor, *Miner. Mag.,* **36** (1967) 465.

18) R. Allmann, H. P. Jepsen, *N. Jhb. Miner. Mh.,* **12** (1969) 544.

19) R. Allmann, *Chimia*, **24** (1970) 99.

20) H. F. W. Taylor, *Miner. Mag.,* **39** (1973) 377.

21) S. Miyata, T. Kumura. *Chem. Lett.,* (1973) 843.

22) K. Chibwe, J. B. Valim, W. Jones, in proc. *Symp. On new catalytic materials and techniques. ASC meeting, Div. of petroleum chem.*, Miami (USA), 34 (3) (1989) 507.

23) M. A. Drezdzon, *Inorg. Chem.,* **27** (1988) 4628.

24) D. L. Bish, *Bull. Miner.,* **103** (1980) 170.

25) A. Schutz, P. Biloen, *J. Solid State Chem.*, **68** (1987) 360.

26) G. Brown, M. C. Gastuche*, Clay Miner.,* **23** (1975) 377.

27) S. Miyata, *Clays Clay Miner.,* **23** (1975) 369.

28) G. W. Brindley and S. Kikkawa, *Am. Miner.,* **64** (1979) 836.

29) T. Sato, T. Wakabayashi, M. Shimada, *Ind. Eng. Chem., Prod. Res. Dev.,* **25** (1986) 89.

30) H. P. Boenm, J. Stenile, C. Viewegar, *Angew. Chem. Int. Ed.*, **16** (1977) 265.

31) A. Deroy, J. P. Besse, P. Bondot, *Mat. Rev. Bull.,* **20** (1985) 1091.

32) M. J. H. Hermandez-Moreno, M. A. Ulibarri, J. L. Rendon and C. J. Serna, *Phys. Chem. Miner.*, **12** (1985) 34.

33) E. C. Kruissink, L. L. Van Reijen, J. R. H. Ross, *J. Chem. Soc., Faraday Trans.1,* **77** (1981) 649.

34) D. L. Bish and G. W. Brindley, *Amer. Miner.,* **56** (1971) 1007.

35) D. Skoog, D. West and F. Holler, *Fundamentals of Analytical Chemistry*, 4th edition (1993) Saundary College Publishing, Philadelphia, USA.

36) I. Chorkendorff, J. Niemantsverdriet, *Concepts of Modern Catalysis and Kinetics*, Wiely-VCH Verlag, Weinham, 2003.

37) D. Müller, W. Gessner, H. J. Behrens, G. Scheler, *Chem. Phys. Lett.,* **79** (1981) 59.

38) T. Matsushita, K. Ebitani, K. Kaneda, *Chem. Commun.,* (1999) 265.

39) H. B. Friedrich, F. Khan, N. Singh, M. Staden, *Synlett.*, **6** (2001) 869.

40) R. Llamas, C. Jiménez-Sanchidrián, J. R. Ruiz, *Tetrahedron*. **63** (2007) 1435.

41) C. Cativiela, F. Figueras, J. M. Fraile, J. I. Garcia, J. A. Mayoral. *Tetrahedron Lett.,* **36** (1995) 4125.

42) S. Ueno, K. Yamaguchi, K. Yoshida, K. Ebitani, K. Kaneda, *Chem. Commun.*, (1998) 295.

43) K. Yamaguchi, K. Ebitani, K. Kaneda, *J. Org. Chem*., **64** (1999) 2966.

44) J. Palomeque, F. Figueras, G. Gelbard, *Appl. Catal. A*, **300** (2006) 100.

45) M. Marquevich, X. Farriol, F. Medina, D. Montané, *Catal. Lett*., **85** (2003) 41.

46) Q. Jiao, H. Liu, Y. Zhao. Z. Zhang, *J. Mater. Sci*., **44** (2009) 4422.

47) E. R. van Selow, P. D. Cobden, P. A. Verbraeken, J. R. Hufton, R. W. van den Brink, *Ind. Eng. Chem. Res*., **48** (2009) 4184.

48) Z. Baán, A. Potor, A. Cwik, Z. Hell, G. Keglevich, Z. Finta, I. Hermecz, *Synth. Commun.*, **38** (2008) 1601.

49) K. Yan, X. Xie, J. Li, X. Wang, Z. Wang, *J. Natur. Gas Chem.*, **16** (2007) 317

Chapter Three

Experimental

3.1 Catalyst preparation

Reagents used in the synthesis of the catalyst:

i) Aluminium chloride hexahydrate ($AlCl_3.6H_2O$), Associated Chemical Enterprises.

ii) Osmium trichloride hydrate ($OsCl_3.nH_2O$), Heraeus.

iii) Sodium bicarbonate (Na_2CO_3), Merck.

iv) Sodium hydroxide (NaOH), Merck.

v) Zinc chloride ($ZnCl_2$), Merck.

The preparation of the catalyst was carried out using the low supersaturation technique following the literature method.[1,2] A number of catalyst were prepared using this technique. $OsCl_3.nH_2O$ (0.53 g, 1.53 mmol), $ZnCl_2$ (2.12 g, 15.3 mmol) and $AlCl_3.6H_2O$ (1.23 g, 5.10 mmol) were dissolved in 10 mL of de-ionized water. Sodium hydroxide solution 1M (46 mL), was used to dissolve 1.41 g (13.3 mmol) of sodium bicarbonate. The two solutions (i.e. metals solution and base solution) were added simultaneously and drop-wise into a 500 mL three necked round bottom flask, while the pH was maintained between 8-10. The pH was monitored by pH indicator paper. After complete addition of the solutions, the resulting mixture was heated to 65 ± 5 ^{o}C for 18 h. The resulting precipitate was allowed to cool to room temperature, after which it was filtered and washed to neutrality by large amounts of de-ionized water. Thereafter, the precipitate was dried in the oven for 12 h at 110 ^{o}C.

3.2 Catalyst characterisation

3.2.1 X-Ray diffraction (XRD)

XRD is the diagnostic technique for confirming the formation of HTlc's, since HTlc's exhibit a characteristic pattern (Section 2.5.1). The diffractograms presented in this study were obtained using (unless otherwise mentioned) a Bruker D8 Advance with diffracplus XRD commander software, and a Brucker VENTEC detector. The radiation source used was Cu Kα (wavelength of 0.1540 nm), operating on a long focus line with a voltage and amperage of 40 kV and 40 mA respectively. The samples (catalysts) were scanned in a 2 θ range from 2^o to 90^o at 0.5 degree per minute. The spent catalyst powder XRD was obtained using a Philips PW 1050 diffractometer equipped with a graphite monochromater and operated at 40 kV and 40 mA. The source of the radiation used was Co Kα, detector used was Sietronic 122 D automated microprocessor. The spend catalyst sample was scanned in a 2 θ range from 2^o to 90^o at 0.5 degree per minute.

3.2.2 Inductively Coupled Plasma-Optical Emission Spectroscopy (ICP- OES)

Reagents:

1) Aluminium standard, 1000 ppm, Polychem supplies cc.
2) Hydrochloric acid 32% (HCl), Associated Chemical Enterprises.
3) Osmium standard, 1000 ppm, Spectrascan.
4) Zinc standard, 1000 ppm, Spectracer.

This technique was used for two reasons; to confirm the presence of the three metals (i.e. Os, Zn and Al) in the catalyst and to determine the molar ratio in which the three metals are present in the catalyst relative to each other. The target ratio for the three metals Os: Zn: Al is 0.3: 3: 1. To obtain the metals ratio, standard solutions with different metal

concentrations were prepared and used to obtain a set of calibration curves. Two sets of standards (Table 3.1) were prepared from two independent multi-element standards, in a 100 mL plastic volumetric flask (it is preferred to use glass volumetric flasks and glass tubing for the ICP-OES, if available) using a 1000 ppm standard of each metal. The two independent multi-element standards contained 10 mL, 40 mL and 4 mL of Os, Zn and Al, respectively, yielding a final concentration of the metals in the solution of 100 ppm, 400 ppm and 40 ppm of Os, Zn and Al, respectively.

The sample (catalyst) for the ICP-OES analysis was prepared by accurately weighing 0.02 g of the catalyst, to which 5 mL of 32% HCl was added (HCl was used because it is not a strong oxidising acid, hence osmium tetraoxide will not be formed. Osmium tetraoxide is a volatile form of Os, and that could result in Os leaving the sample during the digestion process). The mixture was heated until the sample was fully dissolved and the volume of the acid was reduced to approximately 2 mL by further heating. After this the solution was filtered by gravity into a 100 mL volumetric flask and made to the mark with de-ionized water. The ICP-OES analysis was carried out using a Perkin Elmer Precisely Optical Emission Spectrometer, Optima 5300 DV. The plasma was in the radial position and three lines were used for each metal.

3.2.3 Fourier Transform Infra-Red Spectroscopy (FT-IR)

FT-IR was used to detect the presence of the carbonate ions. The spectra for the different catalysts were recorded in the range of 4000 – 400 cm^{-1} using a Perkin Elmer Precisely, Universal Attenuated Total Reflection (ATR) spectrum 100 series. The catalyst was crushed finely and a small amount was placed on the diamond window and pressurized.

Table 3.1: Preparation of ICP-OES standards used to obtain the molar ratio of the three metals (Os, Zn and Al) in the catalyst.

Standard	**1**	**2**	**3**	**4**	**5**
Concentration of Os/ ppm	10	20	30	40	50
Concentration of Zn/ ppm	40	80	120	160	200
Concentration of Al/ ppm	4	8	12	16	20
* volume taken from the multi-element standard/ mL	2.5	5	7.5	10	12.5

* The respective volume was pipeted into a 25 mL plastic volumetric flask and made to the mark with de-ionized water.

3.2.4 Brunauer-Emmett and Teller (BET) surface area measurements

This technique was used to determine the surface area of the catalyst. Approximately 0.05 g of the catalyst was accurately weighed and degassed under nitrogen flow overnight at 200 ^{o}C. After degassing, the mass was recorded and the sample was analysed at -196 ^{o}C, using nitrogen gas as the adsorbant. The BET surface area measurement was recorded using a Micromeritics Gemini instrument.

3.2.5 Scanning Electron Microscopy (SEM) and Energy Dispersion Spectroscopy (EDS)

SEM and EDS were used to study the surface morphology and to map the dispersion of the three metals (i.e. Os, Zn and Al) in the catalyst respectively. The images were obtained using a Jeol JSM-6100 scanning microscope with a Brucker signal processing unit detector.

3.2.6 Cryo-Transmission Electron Microscopy (TEM)

This technique was used to investigate the catalyst structure. HTlc's have characteristic rod shapes and beta like sheet in their structure.[2] The catalyst was placed in an agar grid, held in the sample holder, which was cooled using liquid nitrogen. The viewing of the catalyst was carried out at the temperature of liquid nitrogen to prevent the heat generated by the electron beam from destroying the compounds structure by subliming Os. The viewing of the sample was carried out using a Jeol-1010 electron microscope, with a megaview soft imaging system.

3.2.7 ^{27}Al Solid State-Nuclear Magnetic Resonance (SS-NMR)

The coordination around Al in HTlc's has a specific geometry. SS-NMR was used to determine the geometry around Al. The catalyst was packed into the solid probe and a semi circle was made at the base of the probe, to balance it during the spinning. The SS-NMR spectrum was obtained using a Brucker 600 MHz ultrashield instrument. The experimental conditions are outlined in Table 3.2.

Table 3.2: Experimental conditions for ^{27}Al SS-NMR.

Parameter	Conditions
Probe	4 mm MAS BB/ IH
Gas	Air/ nitrogen separator
Probe spin speed	12 kHz
^{27}AL	0.5 μs
Recycling delay	1 s

3.2.8 Thermal Gravimetric Analysis – Differential Scanning Calorimetry (TGA-DSC)

This technique was used to confirm the presence of both carbonate and water in the interlayer of the catalyst. HTlc's show two characteristic endothermic transitions that occur at low temperature.[3] The sample was placed on an aluminium pan, and the results were obtained using a TA instrument, SDTQ 600, under a nitrogen flow rate of 100 mL/ min. The ramping rate was 10 ^{o}C/ min, from 25 to 600 ^{o}C or 25 to 1000 ^{o}C, depending on the experiment.

3.3 Thermal treatment of catalyst under nitrogen

The thermal treatment of the catalyst (part of HTlca-2 was used) under nitrogen was carried out using Pyro therm furnaces. The temperature was increased at 30 ^{o}C at 30 min intervals from room temperature until it reached the final temperature of 300 ^{o}C. The

thermally treated catalyst was characterised by XRD, ICP-OES, IR, BET surface area, SEM-EDS and Cryo-TEM as described in Sections 3.2.1, to 3.2.6.

3.4 Product isolation and characterisation

The final products (i.e. the β-amino alcohols) were purified and isolated using different techniques in order to confirm the identity of the product and obtain the (isolated) percentage yield of the target product. Since there are no samples of the products commercially available for use as reference materials, chromatographic techniques were unsuitable for product confirmation and quantification. All solvents were used without further purification, unless otherwise mentioned. Centrifugation of the reaction mixture was done using a Heraeus Sepatech, Labofuge 200. Thin layer chromatography (TLC) was carried out using precoated silica gel on alumina plates (Merck silica gel 60 F_{254}, 20 cm x 20 cm). Column chromatography was carried out using Fluka silica gel 60 F_{254}, particle size 0.63-0.20 mm. The proton NMR spectra were recorded using a Bruker ultrashield 400 MHz spectrometer at 25 ^{o}C and the ^{13}C NMR spectra were recorded at 100 MHz on the same instrument under equivalent conditions. The chemical shits were recorded in ppm relative to $CDCl_3$ and d_6-DMSO. The FT-IR spectra were recorded using a Perkin Elmer Universal Attenuated Total Reflection (ATR) Sampling Accessory, attached to FT-IR Series 100. The reaction was monitored using a Perkin Elmer Autosystem XL gas chromatograph (GC). The GC method and the starting material retention time(s) are shown in Tables 3.3 and 3.4 respectively. Mass spectra were recorded using an Agilent 1100 series LC/MSD Trap. Preparative high performance liquid chromatography (HPLC) was carried out using a Shimadzu, LC-8A, equipped with a C8 column with a flow rate of 15 mL/min using water and methanol (0.1% formic acid v/v was added to both solvents). Detection was carried out using a UV detector with three channels (190, 215 and 254 nm). The method used is outlined in Table 3.5.

Table 3.3: GC temperature program and column specification, used to monitor the aminohydroxylation reaction.

Injector temperature	240 ^{o}C
Split Flow rate	On 25 mL/min
Attenuation Range	1 1
Column	Varian, CB Sil5 (25 m x 0.15 mm x 2 µm)
Oven initial temperature Ramp 1 Ramp 2 Ramp 3	50 10 ^{o}C /min to 80 ^{o}C /min held for 1 min 20 ^{o}C /min to 180 ^{o}C /min held for 1 min 40 ^{o}C /min to 240 ^{o}C /min held for 4 min
Detector temperature	280 ^{o}C

Table 3.4: Starting material retention times, obtained by GC, utilizing the method in Table 3.3.

Starting material (olefin)	**Retention time /min**	**Appendix A**
Cyclohexene	6.80	1
Hexene	4.86	3
Styrene	9.89	2
cis-Stilbene	17.4	4
Methylcinnamate	15.00	5
Dimethylfumarate	11.19	6
t-Butylcrotonate	10.04	7

Table 3.5: Method parameter used in preparative HPLC, equipped with a Hichrom 5 C8 (150 mm x 21.2 mm) column and flow rate of 15 mL/min.

Time /min	% Methanol
5	5
10	60
40	95
45	95

3.5 Catalytic activity in the aminohydroxylation reaction

3.5.1 Standard method

The aminohydroxylation reaction was carried out by adding 6 mL of solvent to a N_2 filled Schlenk tube, followed by the addition of the olefin (0.478 mmol), nitrogen source (chloramine-T) (2 eq, 0.2173 g) and the catalyst (0.03 g) in this respective order. The reactions were stirred and monitored by GC until complete conversion of the starting material (olefin) was observed.

3.5.2 Investigation into the effect of the solvent on the reaction

This investigation was carried out using three different solvents with different polarities. The solvents used were dry toluene, *t*-butanol/water (1:1 v/v) and acetonitrile/water (1:1 v/v). The olefin used in this study was cyclohexene and a partially polycrystalline HTlca-1 was utilised. The catalytic testing was carried out as described in Section 3.5.1.

3.5.3 Investigation into the effect of the temperature on the reaction

This investigation was carried out using three different temperatures (unless otherwise mentioned). The temperatures were 25 ^{o}C, 40 ^{o}C and 60 ^{o}C. The olefin used in this part of the study was styrene, and a partially polycrystalline HTlca-1 was utilised. The catalytic testing was carried out as described in Section 3.5.1.

3.5.4 Investigation into the effect of the catalyst structure on the reaction

This investigation was carried out using three different catalysts: partially polycrystalline catalyst (HTlca-1), crystalline catalyst (HTlca-2) and thermally treated catalyst (HTlca-3). The olefins used in this study were cyclohexene and *t*-butyl crotonate. The solvent used was acetonitrile/water (1:1 v/v). The catalytic testing was carried out as described in Section 3.5.1.

3.5.5 Screening of different olefins

List of olefins:

i) Cyclohexene (C_6H_{10}), Riedel-de Haën.

ii) Hexene (C_6H_{12}), Acros.

iii) Styrene (C_8H_8), uniLAB.

iv) *cis*-Stilbene ($C_{14}H_{12}$), Aldrich Chemistry.

v) Methylcinnamate ($C_{10}H_{10}O_2$), Aldrich Chemistry

vi) Dimethyl fumarate ($C_6H_8O_4$), Aldrich Chemistry.

vii) *t*-Butylcrotonate ($C_8H_{14}O_2$), Aldrich Chemistry.

List of solvents:

i) Acetonitrile (C_2H_3N), Merck.

ii) Toluene (C_7H_8), Merck.

iii) *t*-Butanol ($C_4H_{10}O$), Fluka.

Reagents

i) Chloramine-T ($C_7H_7ClNNaO_2S$), Aldrich Chemistry.

This investigation was carried out as described in Section 3.5.1, using HTlca-1 and acetonitrile/water or *t*-butanol/water (1:1 v/v). The olefins used in this study are shown in Table 3.6 along with their respective class.

Table 3.6: Olefins used in the aminohydroxylation reaction.

Olefin	**Class**
Cyclohexene	Aliphatic
Hexene	Aliphatic
Styrene	Aromatic
cis-Stilbene	Aromatic
Methylcinnamate	Functionalised aromatic
Dimethyl fumarate	Functionalised
t-Butyl crotonate	Functionalised

3.6 General procedure for product identification and purification

At the end of each reaction (disappearance of the starting material peak, determined by GC) the catalyst was removed by gravity filtration. The solvent was then removed under reduced pressure to yield the crude product, which contained mainly unreacted chloramine-T, *p*-toluenesulfonamide and the β-amino alcohol. The crude product was washed with a 15 mL sodium sulfite solution (1 g of sodium sulfite in 15 mL of de-ionized water) and 20 mL of ethyl acetate. The aqueous layer was separated and extracted with 2 x 20 mL ethyl acetate. The combined organic layer was then washed with 15 mL of 5% bleach solution. The aqueous layer was again separated and the organic layer was washed with 2 x 15 mL de-ionized water. After this the organic layer was dried over anhydrous magnesium sulfate and the solvent was removed under reduced pressure to yield the crude product. The β-amino alcohol was purified by silica gel column chromatography. The column was eluted by gradient elution, starting with hexane containing 5% ethyl acetate and the polarity was increased in 5% intervals until 30% ethyl acetate was reached.

3.6.1 Product isolation of cyclohexene β-amino alcohol

The corresponding β-amino alcohol of cyclohexene was crystallized from the reaction solvent at low temperature. Another method for the isolation of cyclohexene β-amino alcohol is by using prepative HPLC following the method outline in Table 3.5.

3.6.2 Product isolation of *cis*-stilbene β-amino alcohol

The corresponding β-amino alcohol of *cis*-stilbene is not soluble in the reaction solvent. Therefore, it precipitated out of the solvent once formed. At the end of the reaction, the catalyst and the pure product were filtered off using Büchner funnel and washed with cold *t*-butanol/water (1:1 v/v). Thereafter, dimethyl sulfoxide (DMSO) was added to the catalyst and the pure product. The product was soluble in DMSO but not the catalyst. The

solution was filtered and the DMSO solution was then centrifuged to separate any fine catalyst particles which pass through the filter paper. Upon addition of ice to the solution, the product precipitated out from DMSO.

3.6.3 Product isolation of hexene β-amino alcohol

The corresponding β-amino alcohol of hexene was purified and isolated using semi-preparative HPLC. The method used and the column description is outlined in Table 3.5.

3.7 Product characterisation

The NMR shifts presented were obtained using $SiMe_4$ as the reference point (0.00 ppm). The solvent indicated in Sections 3.7.1 to 3.7.7 is the solvent that was used to dissolve the respective product to allow solution NMR analysis.

3.7.1 *N*-(2-hydroxycyclohexyl)-4-methylbenzenesulfonamide (β-amino alcohol of cyclohexene)[3]

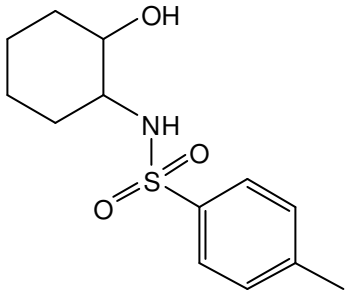

^{1}H NMR (400 MHz, $CDCl_3$): δ 1.5-1.72 (m, 8H), 2.44 (s, 3H), 3.21 (m, 1H), 3.78 (d, J = 2.48 Hz, 1H), 4.80 (d, J = 7.48 Hz, 1H), 7.32 (d, J = 8.04 Hz, 2H), 7.79 (d, J = 8.24 Hz, 2H). ^{13} C NMR (100 MHz, $CDCl_3$) δ 19.7 (s, 1C), 21.5 (s, 1C), 23.3 (s, 1C), 27.9 (s, 1C), 31.4 (s, 1C), 55.1 (s, 1C), 68.7 (s, 1C), 126.9 (s, 2C), 129.7 (s, 2C), 137.9 (s, 1C), 143.3 (s, 1C). IR (cm^{-1}) = 3414 (*m*), (OH), 3137 (*m*), (NH), 2938 (*w*), (CH_2), 2849 (*w*), (CH_3), 1598 (*m*), (Ar), 1029 (*m*), (S=O). Mass calculated = 269, MS = 291 *m/z* (*M* + Na).

3.7.2 *N*-(hydroxyhexan-2-yl)-4-methylbenzenesulfonamide (β-amino alcohol of hexene)[4]

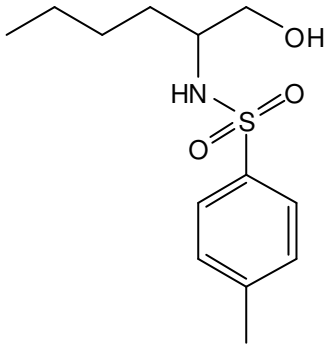

^{1}H NMR (400 MHz, $CDCl_3$) δ 0.87 (t, J = 6.86 Hz, 3H), 1.2-1.40 (m, 6H), 2.42 (s, 3H), 2.7-2.80 (m, 1H), 3.0-3.01 (m, 1H), 3.6-3.70 (m, 1H), 7.31 (d, J = 8.04 Hz, 2H), 7.74 (d, J = 8.20 Hz, 2H). ^{13} C NMR (100 MHz, $CDCl_3$) δ 13.9 (s, 1C), 21.5 (s, 1C), 22.5 (s, 1C), 27.4 (s, 1C), 34.3 (s, 1C), 48.6 (s, 1C), 70.4 (s, 1C), 127.1 (s, 2C), 129.7 (s, 2C), 136.7 (s, 1C), 143.5 (s, 1C). Mass calculated = 271.1, MS = 293.1 *m/z* (*M* + Na).

3.7.3 *N*-(-2hydroxyl-1-phenylethyl)-4-methylbenzenesulfonamide (β-amino alcohol of styrene)[5]

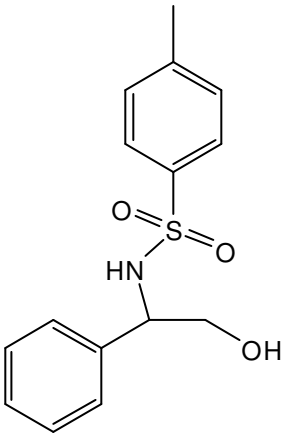

^{1}H NMR (400 MHz, $CDCl_3$) δ 2.42 (s, 3H), 3.0-3.03 (m, 1H), 3.2-3.29 (m, 1H), 4.79 (d, J = 4.40 Hz, 1H), 4.89 (d, J = 4.40 Hz, 1H), 7.2-7.34 (m, 7H), 7.72 (d, J = 8.28 Hz, 2H). ^{13} C NMR (100 MHz, $CDCl_3$) δ 21.5 (s, 1C), 30.9 (s, 1C),50.1 (s, 1C), 125.8 (s, 2C), 127.1 (s, 2C), 128.3 (s, 1C), 128.7 (s, 2C), 129.8 (s, 2C), 136.7 (s, 1C), 140.7 (s, 1C), 143.6 (s, 1C). IR (cm^{-1}) :=3399 (*m*), (OH), 3149 (*m*), (NH), 2926 (*w*), (CH_2), 2862 (*w*), (CH_3), 1599 (*w*), (Ar), 1086 (*m*), (S=O). Mass calculated = 291, MS = 313 *m/z* (*M* + Na).

3.7.4 *N*-(2-hydroxyl-1,2-diphenylethyl)-4-methylbenzenesulfonamide (β-amino alcohol *cis*-stilbene)[6]

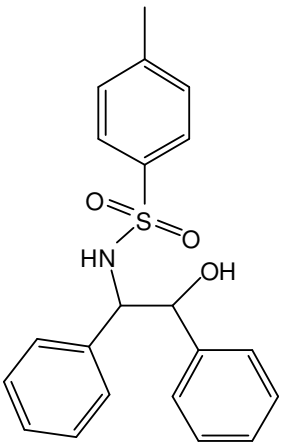

^{1}H NMR (400 MHz, DMSO) δ 2.21 (s, 3H), 4.28 (dd, J = 6.80, 9.20 Hz, 1H), 4.62 (dd, J = 6.80, 9.20 Hz, 1H), 5.37 (d, J = 4.80 Hz, 1H), 7.0-7.29 (m, 14H), 8.08 (d, J = 4.80 Hz, 1H). ^{13} C NMR (100 MHz, DMSO) δ 20.8 (s, 1C), 63.3 (s, 1C), 75.3 (s, 1C), 126.1 (s, 2C), 126.3 (s, 1C), 126.7 (s, 2C), 126.9 (s, 1C), 127.0 (s, 2C), 127.5 (s, 2C), 128.2 (s, 2C), 128.8 (s, 2C), 138.5 (s, 1C), 138.8 (s, 1C), 141.6 (s, 1C), 142.6 (s, 1C). IR (cm^{-1}) =3461 (*m*), (OH), 3323 (*m*), (NH), 3031 (*w*), 1598 (*w*), (Ar), 1055 (*m*), (S=O). Mass calculated = 367.1, MS = 389.12 *m/z* (*M* + Na).

3.7.5 Methyl-2-hydroxy-3-(4- methylbenzenesulfonamide)-3-phenylpropanoate (β-amino alcohol of methylcinnamate)[7]

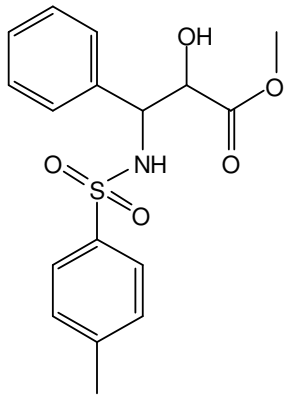

^{1}H NMR (400 MHz, $CDCl_3$) δ 2.32 (s, 3H), 3.18 (d, J= 4.16 Hz, 1H), 3.75 (s, 3H), 4.34 (dd, J = 2.36, 4.04 Hz, 1H), 4.85 (dd, J = 2.22, 9.70 Hz, 1H), 5.52 (d, J = 9.72 Hz, 1H), 7.0-7.18 (m, 7H), 7.53 (d, J = 8.20 Hz, 2H). ^{13} C NMR (100 MHz, $CDCl_3$) δ 21.4 (s, 1C), 53.2 (s, 1C), 58.9 (s, 1C), 74.2 (s, 1C), 126.8 (s, 2C), 126.9 (s, 2C), 127.8 (s, 2C), 128.4 (s, 2C), 129.2 (s, 1C), 137.4 (s, 1C), 137.5 (s, 1C), 143.1 (s, 1C), 172.4 (s, 1C). IR (cm^{-1}) = 3477 (*m*), (OH), 3139 (*m*), (NH), 2967 (*w*), (CH_3), 2882 (*w*), (CH_3), 1598(*w*), (Ar), 1738 (*m*), (C=O), 1056 (*m*), (S=O). Mass calculated = 349.3, MS = 372 *m/z* (*M* + Na).

3.7.6 Dimethyl-2-hydroxy-3-(4-methylbenzenesulfonamide)succinate (β-amino alcohol of dimethylfumarate)[3]

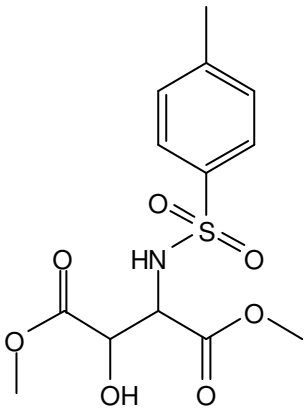

^{1}H NMR (400 MHz, $CDCl_3$) δ 2.41 (s, 3H), 3.23 (d, J = 5.20 Hz, 1H), 3.60 (s, 3H), 3.76 (s, 3H), 4.39 (dd, J = 1.92, 9.80 Hz, 1H), 4.59 (dd, J = 1.78, 5.02 Hz, 1H), 5.37 (d, J = 9.88 Hz, 1H), 7.29 (d, J = 8.20 Hz, 2H), 7.70 (d, J = 8.28 Hz, 2H). ^{13} C NMR (100 MHz, $CDCl_3$) δ 21.5 (s, 1C), 53.1 (s, 1C), 53.4 (s, 1C), 57.9 (s, 1C), 71.5 (s, 1C), 127.2 (s, 2C), 129.6 (s, 2C), 136.5 (s, 1C), 143.8 (s, 1C), 168.7 (s, 1C), 171.3 (s, 1C). IR (cm^{-1}) = 3503 (*m*), (OH), 3260 (*m*), (NH), 2923 (*w*), 1598 (*w*), (Ar), 1738 (*m*), 1730 (*m*), (C=O), 1056 (*m*), (S=O). Mass calculated = 331, MS = 353 *m/z* (*M* + Na).

3.7.7 *tert*-Butyl-2-hydroxy-3-(4-methylbenzenesulfonamide)butanoate (β-amino alcohol of *tert*-butylcrotonate)

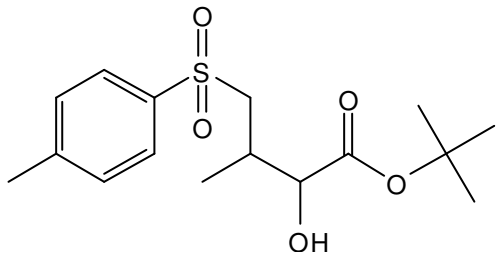

^{1}H NMR (400 MHz, $CDCl_3$) δ 0.98 (d, J = 6.72 Hz, 3H), 1.51 (s, 9H), 2.41 (s, 3H), 3.22 (d, J = 3.64 Hz, 1H), 3.8-3.86 (m, 2H), 4.75 (d, J = 10.08 Hz, 1H),7.29 (d, J = 7.96 Hz, 2H), 7.75 (d, J = 8.32 Hz, 2H). ^{13} C NMR (100 MHz, $CDCl_3$) δ 17.9 (s, 1C), 21.5 (s, 1C), 27.9 (s, 3C), 51.5 (s, 1C), 73.6 (s, 1C), 84.1 (s, 1C), 126.9 (s, 2C), 129.7 (s, 2C), 138.6 (s, 1C),143.3 (s, 1C), 171.6 (s, 1C). IR (cm^{-1}) = 3446 (*m*), (OH), 3260 (*m*), (NH), 2985 (*w*), (Ar), 2919 (*w*), (CH_3), 1598 (*w*), (ar), 1716 (*m*), (C=O), 1048 (*m*), (S=O). Mass calculated = 329, MS = 351 *m/z* (*M* + Na).

3.8 Single crystal analysis

Single crystals of the β-amino alcohols of cyclohexene and methylcinnamate were grown in MeCN/water by slow evaporation after the compounds was purified. The crystals of the β-amino alcohol of *t*-butylcrotonate was grown in dichloromethane layered with hexane followed by slow evaporation, after the compound was purified. Data collection for the β-amino alcohol of cyclohexene, methylcinnamate and *t*-butylcrotonate was carried out on an *APEX2*,[8] data reduction for β-amino alcohol of cyclohexene obtained by *SAINT* and the software utilised to solve and refine all three structure was *SHELXS97* and *SHELXL97*.[9] Data reduction for β-amino alcohol of methylcinnamate and *t*-butylcrotonate by *SAINT-Plus* and *XPREP*.

3.9 Spent catalyst characterisation

The reaction was carried out using three fold quantities of the reagents, solvent and catalyst (HTlca-1) (Section 3.5.1). Cyclohexene was used as the olefin, acetonitrile/water (1:1 v/v) as the solvent system and HTlca-1 as the catalyst. The characterisation techniques used were XRD, ICP-OES, BET surface area measurements, TEM and SEM as described in Sections 3.2.1, 3.2.2, 3.2.4, 3.2.5 and 3.2.7, respectively.

3.10 Leaching test

This study was carried out using two solvent systems, MeCN/water (1:1 v/v) and *t*-BuOH/water (1:1 v/v) (Section 3.5.1). The catalyst used was HTlca-1 and cyclohexene as the olefin. However, the reaction was stopped after approximately 20% conversion of cyclohexene. Thereafter, the catalyst was removed by gravity filtration and the reaction mixture was centrifuged at 3000 rpm for 15 min, for the removal of any suspended fine catalyst particles in the reaction mixture. The reaction mixture was then stirred until the end of the normal duration that the reaction takes in the presence of the catalyst. At the end of the period, GC analysis was undertaken to investigate if any further conversion of

the starting material had taken place in the absence of the catalyst, to determine if any Os that may have leached was catalytically active or not. Furthermore, to determine if any Os leached from the catalyst to the reaction solution, ICP-OES was undertaken. The standards (Table 3.7) were prepared from a multi-element standard, in a 100 mL plastic volumetric flask using a 1000 ppm standard of each metal. The multi-element standard contained 5 mL, 20 mL and 2 mL of Os, Zn and Al, respectively, yielding a final metal concentration in the standard solution of 50 ppm, 200 ppm and 20 ppm of Os, Zn and Al, respectively. Since the matrix is different between the standards (aqueous) and the samples (organic/aqueous), standards of Os (10 ppm and 5 ppm) (Table 3.8) were prepared in the different matrices to investigate the effect of the matrix on the analysis. Different matrices affect the ICP-OES analysis due to different uptake to the nebuliser, change in the excitation conditions in the plasma and droplet size going to the plasma.[10,11]

3.11 Recycling test

For the determination of the recyclability of the catalyst, the catalyst was recycled twice. The reaction was carried out as described in Section 3.5.1. At the end of the reaction, the catalyst was filtered by Buchner funnel filtration and reused with fresh starting material i.e. olefin (cyclohexene), nitrogen source (chloramine-T) (2 eq) and solvent system (i.e. MeCN/water (1:1 v/v).

Table 3.7: Preparation of ICP-OES standards for the leaching test.

Standard	**1**	**2**	**3**	**4**	**5**
Concentration of Os/ ppm	5	10	15	20	25
Concentration of Zn/ ppm	20	40	60	80	100
Concentration of Al/ ppm	2	4	6	8	10
* volume taken from the multi-element standard/ mL	2.5	5	7.5	10	12.5

* The respective volume was pipeted into a 25 mL plastic volumetric flask and made to the mark with de-ionized water.

Table 3.8: Investigation into the effect of the matrix on the ICP-OES analysis using two standards and three different matrices.

Standard / Os [a]	Matrix	Concentration / ppm [b]	Ratio
5 ppm	Aqueous	5.07	1
5 ppm	MeCN/water (5%)	7.46	1.47
5 ppm	*t*-BuOH/water (5%)	9.30	1.83
10 ppm	Aqueous	10.16	1
10 ppm	MeCN/water (5%)	14.54	1.43
10 ppm	*t*-BuOH/water (5%)	17.90	1.76

[a] standards were prepared from a 1000 ppm Os standard (for 5 ppm and 10 ppm, 0.5 mL and 1 mL of the 1000 ppm standard were placed into a 100 mL glass volumetric flask and made to the mark with de-ionised water, respectively). [b] obtained using two point calibration using the aqueous 5 and 10 ppm standards.

The ratio obtained was used to give a rough estimation of the amount leached, if any, of Os into the two reaction solvent systems (*i.e.* MeCN/water and *t*-BuOH/water).

3.12 References

1) H. B. Friedrich, M. Govender, X. Makhoba, T. D. Ngcobo, M. O. Onani, *Chem. Commun.*, (2003) 2922.

2) T. Naicker, A. K. Datye, H. B. Friedrich, *Appl. Catal. A*, **350** (2008) 96.

3) B. M. Choudray, N. S. Chowdari, K. Jyothi, M. L. Kantam*, J. Mol. Catal. A*, **196** (2003) 151.

4) Z. Wang, Y-T. Cui, Z-B. Xu, J. Qu, *J. Org. Chem*., **73** (2008) 2270.

5) K-I Yamada, M. Nakano, M. Maekawa, T. Akindele, K.Tomioka, *Org. Lett*., **10** (2008) 3805.

6) G. Li, H-T Chang, K. B. Sharpless, *Angew. Chem. Int. Ed. Engl*., **35** (1996) 451.

7) E. Nandanan, P. Phukan, G. C. G. Pais, A. Sudalai, *Indian J. Chem.*, **38B** (1999) 287.

8) Bruker. *APEX2 and SAINT*. Bruker AXS Inc., (2005), Madison, Wisconsin, USA.

9) G. M. Sheldrick. Acta Cryst. **A64**, (2008), 112.

10) P. Masson, *Spectrochim. Acta Part B*. **54** (1999) 603.

11) J. W. Olesik, *Anal. Chem.*, **15** (1996) 469A.

Chapter Four

Results and discussion

4.1 Catalyst characterisation

4.1.1 X-ray Diffraction (XRD)

HTlc's have similar XRD patterns which act as a finger-prints for identification of HTlca. The XRD results were used in this study to confirm the formation of the hydrotalcite-like catalysts (HTlca-1 and HTlca-2). The pattern for the HTlc's is characterised by the high intense peaks at a low 2θ values. As the values for the 2θ increase, the intensity of the peaks decrease, in the plane order 003 to 110. The equal spacing between planes, 003 and 006, and 006 and 012, indicate the stacking order of the HTlc's. HT and HTlca's have a hexagonal plane, which is the 110 plane, shown by a doublet peak at high 2θ value and low intensity. The presence of a hydroxide in the material is indicated by a peak with a d-spacing of 11.1 Å. The sharpness of the peaks is indicative of the crystallinity of the catalyst. The XRD diffractograms for HTlca-1 and HTlca-2 (Fig. 4.1 and Fig. 4.2) showed the characteristic XRD patterns for HTlc as mentioned above. Furthermore, the results obtained also agree with those reported in literature.[1] The peaks in the XRD diffractogram for HTlca-1 (Fig. 4.1) are less sharp than those observed in the XRD diffractogram for HTlca-2 (Fig. 4.2). This is probably related to the crystallite size, as determined by the Scherrer equation (Appendix 1B) of HTlca-1 and HTlca-2 (Table 4.1).

The average distance between the cations (in the brucite-like structure) can be represented by the *a* parameter. The *a* parameter can be calculated using the d-spacing of the first peak in the HT and HTlc's doublet peak (the 110 plane). For both HTlca-1 and HTlca-2 the *a* parameter was calculated (Table 4.1, Appendix 2B), which is in agreement with that presented in the literature,[1] and was found to be 3.06 Å for Os Zn Al. The *c* dimension corresponds to thrice the 003 plane d-spacing (Table 4.1) and is also in agreement with that in literature.[1]

Table 4.1: Crystallite size and unit cell parameters for HTlca-1 and HTlca-2.

HTlca	Crystallite size / Å	*a* Parameter / Å	*c* Parameter / Å
1	233	3.06	22.90
2	196	3.06	23.09

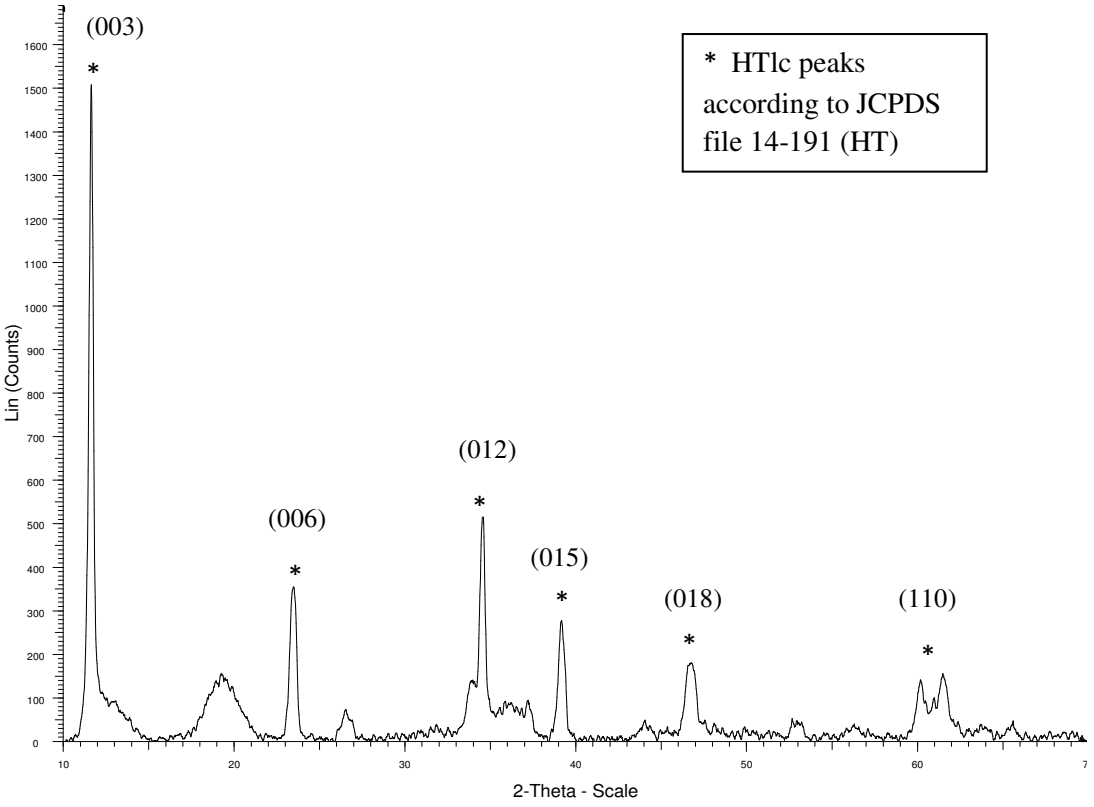

Fig. 4.1: XRD diffractogram of HTlca-1.

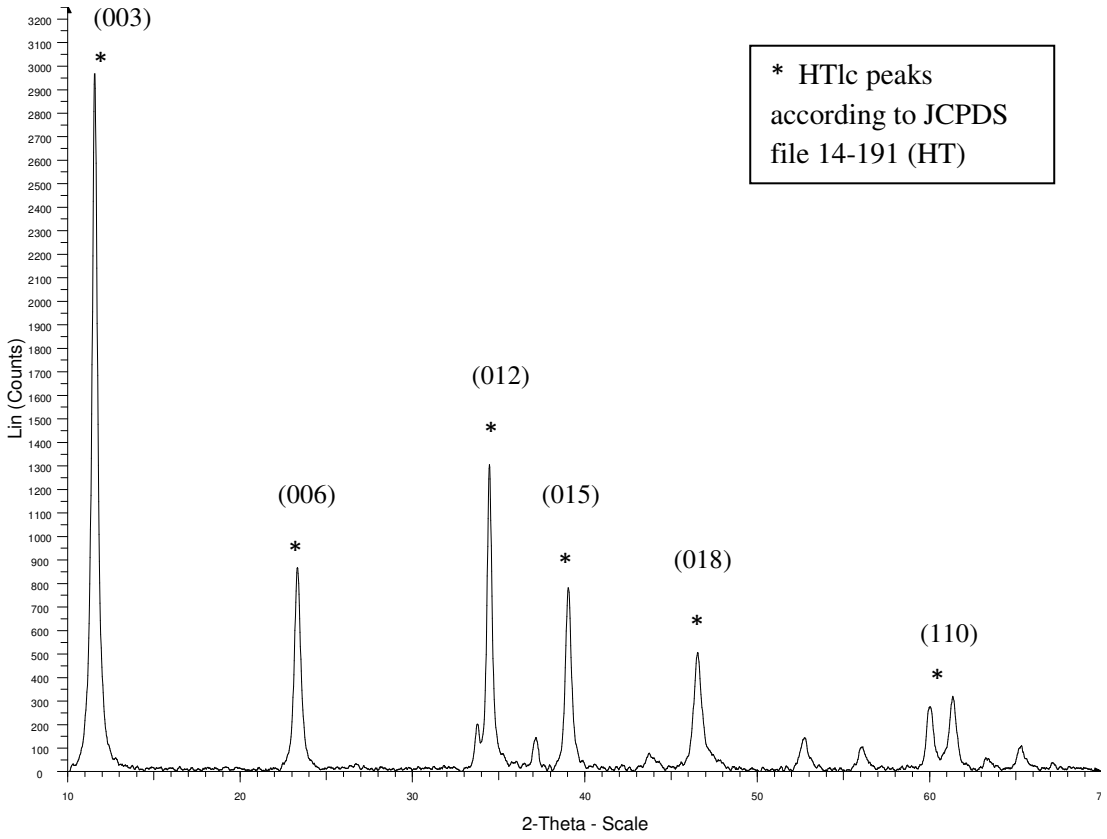

Fig. 4.2: XRD diffractogram of HTlca-2.

4.1.2 Inductive Coupling Plasma-Optical Emission Spectroscopy (ICP-OES)

The presence of the three metals (Os, Zn and Al) in the HTlca's was quantitatively determined by means of ICP-OES (Table 4.2). This technique is a bulk technique, and provides information about the total ratio of the three metals present in the catalyst. In HTlca-1 and HTlca-2 the ratio of Os to Al was close to the target of 0.3. This figure is reported to give the HTlc structure,[1] which also demonstrates good activity in the dihydroxylation reaction.[2] However, the ratio of Zn to Al was slightly higher than the target value of 3.

Table 4.2: Average ICP-OES metal content ratio for HTlca-1 and HTlca-2, determined using two independent multi-elemental standards.

HTlca	Os/Zn/Al [a]	Os/Zn/Al ICP-OES[b]
1	0.3/3/1	0.31/3.70/1
2	0.3/3/1	0.29/3.56/1

[a] target ratio of the three metals in the catalyst.

[b] calculations shown in Appendix 3B

4.1.3 Fourier Transform Infra-Red Spectroscopy (FT-IR)

Infrared spectroscopy does not provide structural information about HT and HTlc's. However, IR analysis can be used to detect the presence of the carbonate ions and water molecules in the interlayer and the hydroxide groups that make up the brucite-like sheets. The detection of these molecules occurs through the presence of their characteristic vibration and stretching bands. The IR spectra for both HTlca-1 and HTlca-2 (Appendix 4B and 5B respectively) showed similar bands. The hydration (*i.e*. presence of water) of the HTlca's was observed by the broad band around 3400 cm^{-1} (indicating the O-H stretch in the water molecule) and the shoulder band around 1600 cm^{-1} (indicating hydrogen bonds between the water molecules).[3-5] Carbonate stretching was indicated in both HTlca's by the band around 1350 cm^{-1}. The out of plane and in plane bending of the carbonate ions was shown by the bands around 800 cm^{-1} and 700 cm^{-1} respectively. The presence of the metal oxide was indicated by the band around 550 cm^{-1}.

4.1.4 Brunauer-Emmett and Teller (BET) surface area measurements

The small surface areas of HTlc's are attributed to the external surface, since N_2 cannot or can only slowly penetrate into the interlayer space.[5] Due to that, the surface areas for both HTlc's were expected to be small. The sharp peaks in the XRD diffractogram indicate that the catalysts are more phase pure as well as more crystalline (with HTlca-2 being more

crystalline that HTlca-1). Usually, the more crystalline the catalyst, the lower the surface area. A large crystallite size also indicates that the surface area should be small. Thus, HTlca-2 would be expected to have a larger surface area than HTlca-1. This was not observed as shown in Table 4.3. This could be because HTlca-1 has slightly larger pores, resulting in the higher surface area.

Table 4.3: Surface area measurement-BET and crystallite size for HTlca-1 and 2.

Catalyst	**Surface area measurement-BET / m^2/g**	**Crystallite size/ Å**
1	87	233
2	59	196

4.1.5 Scanning Electron Microscopy (SEM) and Electron Dispersion Spectroscopy (EDS)

The surface morphology of the two HTlca's, and the distribution of the three metals in the HTlca's, was investigated by means of SEM and EDS, respectively. However, both techniques are surface and near surface techniques, unlike ICP-OES, thus SEM and EDS provide qualitative analysis. The comparison between the SEM images of HTlca-1 and HTlca-2 (Fig. 4.3 and Fig. 4.4, respectively) shows that HTlca-2 is more crystalline than HTlca-1.

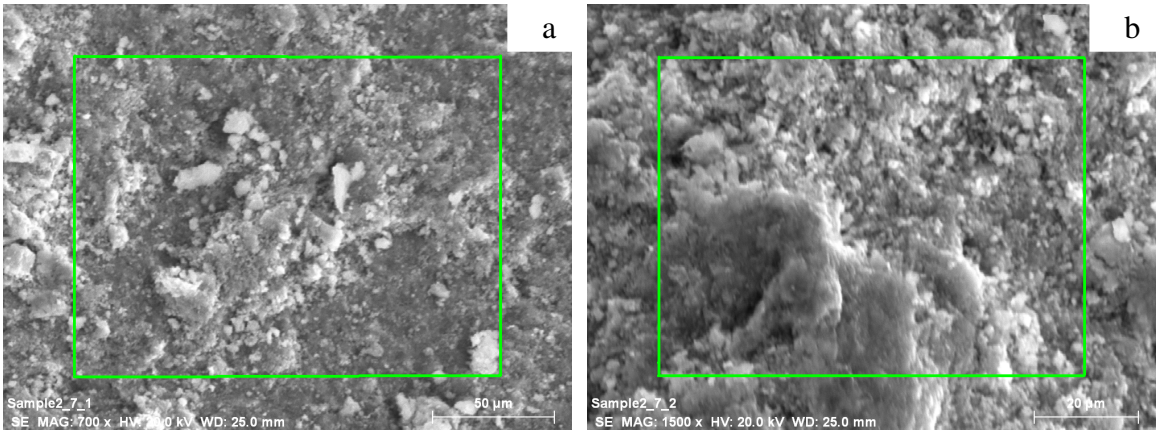

Fig. 4.3: SEM images of two regions (a and b) in HTlca-1.

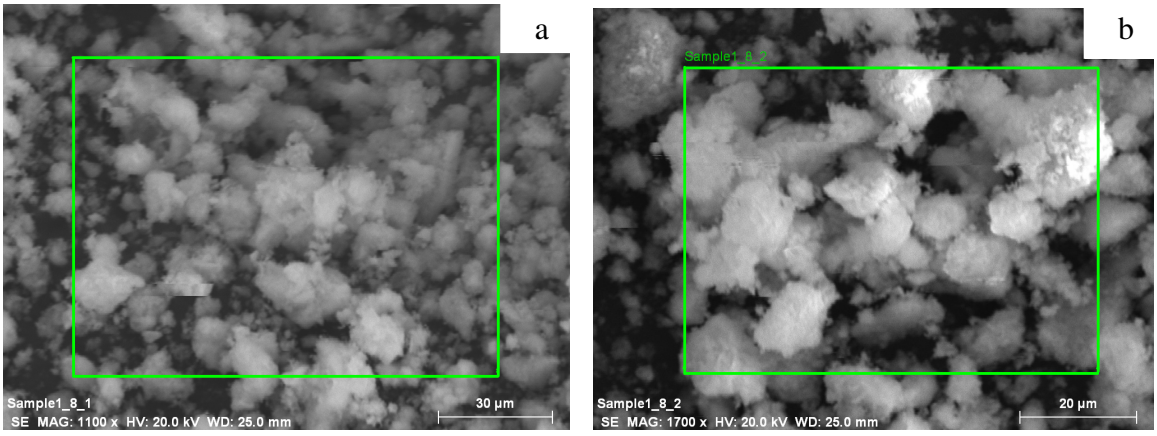

Fig. 4.4: SEM images of two regions (a and b) in HTlca-2.

These results correlate with the XRD results mentioned previously, by the sharper peaks observed for HTlca-2 than those of HTlca-1 in the XRD diffractogram. Since the sample was ground and selected randomly for the EDS analysis, one can assume that the sample is homogeneous. The results from EDS analysis of two selected regions in HTlca-1 and HTlca-2 are shown in Tables 4.4 and 4.5, respectively. More importantly, EDS images show that Os is homogeneously distributed in the HTlca's (Fig. 4.5 and 4.6 for HTlca-1 and HTlca-2, respectively), with no agglomeration detected. Furthermore, these results indicate that Os is most likely part of the catalyst structure and not just supported on the HTlc. If Os was supported on the HTlc, it is unlikely to be homogeneously distributed, rather, agglomerations would be observed in different regions.

Table 4.4: The different elemental content in HTlca-1, in two selected regions, as determined by SEM-EDS.

Element	**Element % in region a**	**Element % in region b**
Zinc K	33.49	33.46
Osmium L	2.59	2.40
Aluminium K	12.17	13.07
Oxygen K	51.75	52.07
Total	100	100

Table 4.5: The different elemental content in HTlca-2, in two selected regions, as determined by SEM-EDS.

Element	**Element % in region a**	**Element % in region b**
Zinc K	33.85	33.45
Osmium L	2.47	2.43
Aluminium K	11.93	12.27
Oxygen K	51.75	51.85
Total	100	100

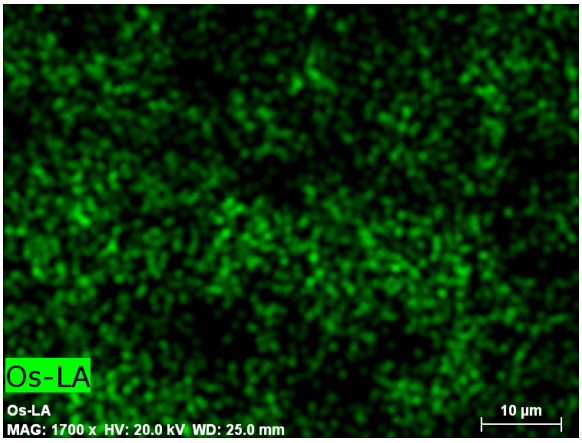

Fig. 4.5: EDS of region a (Fig. 4.3) in HTlca-1.

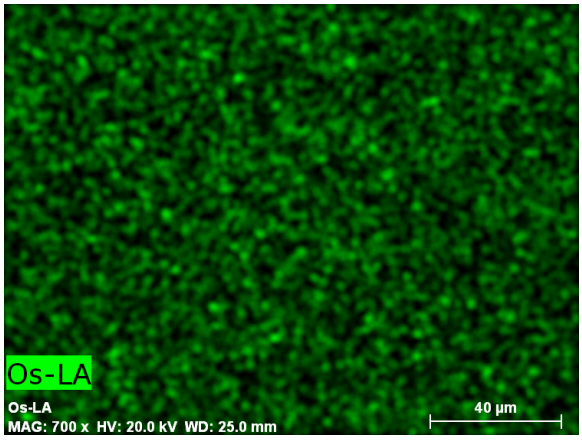

Fig. 4.6: EDS of region b (Fig. 4.4) in HTlca-2.

The mapping image for HTlca-1 (Appendix 6B) shows a homogeneous distribution of the three elements (Os, Zn and Al) in that region. This can be confirmed as there is no particular colour (Os is shown in green, Zn in red and Al in blue) agglomerating at a specific region in the catalyst. Similar observations were noted for HTlca-2 (Appendix 7B). The black regions seen in both images are due to the lack of sample material in those regions.

4.1.6 Cryo-Transmission Electron Microscopy (TEM)

The structural characteristics of HTlc's in the TEM images are indicated by the rod-like, beta-like sheet structures[1,5] and hexagonal plates.[6] These structures were observed for HTlca-1 and HTlca-2 (Fig. 4.7 and Fig. 4.8, respectively). However, it may be that the rod like structures are hexagonal plates aligned on their side rather than flat to the camera. These images show similar structures to those found in literature for HTlc's that contain Os.[1]

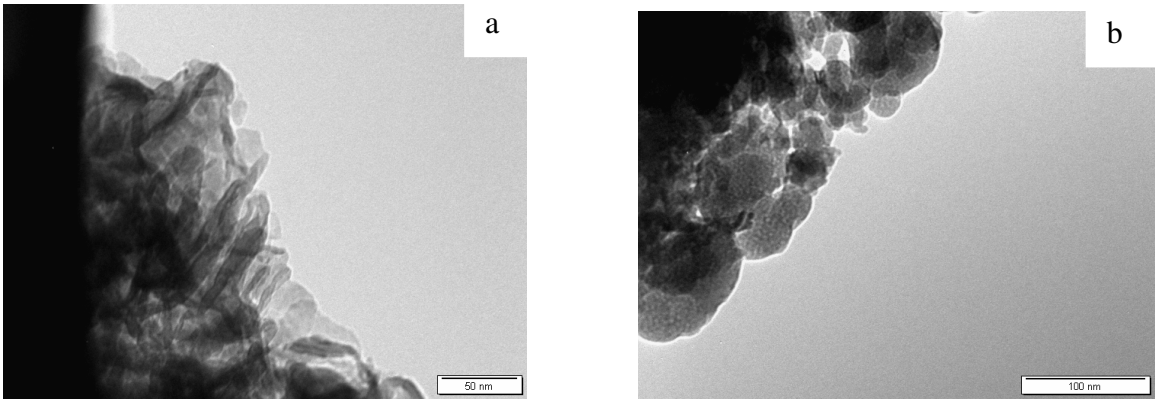

Fig. 4.7: Shows the rod structure (a and b) in HTlca-1.

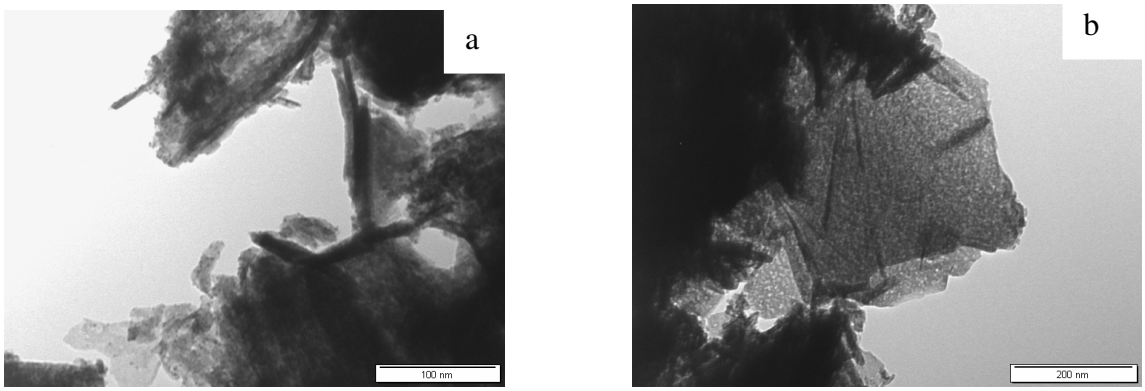

Fig. 4.8: Shows the rod structure (a) and the sheet-like structure (b) in HTlca-2.

The electron diffraction pattern of HTca-2 demonstrates great similarity to that reported in literature (Fig. 4.9).[7] Hence, this can be utilised as further proof of the formation of the HTlc. The absence of rings around the spots (Fig. 4.9) indicates that the HTlc is crystalline, confirming the powder XRD results.

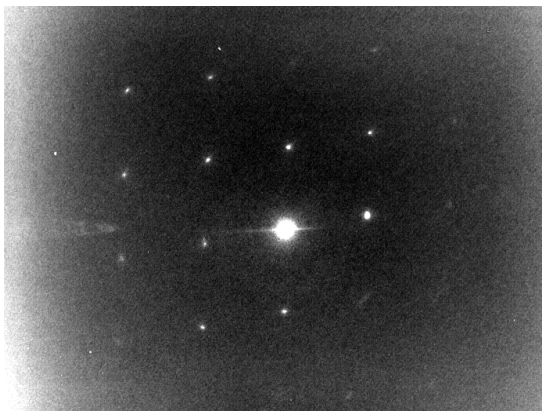

Fig. 4.9: Electron diffraction of HTlca-2.

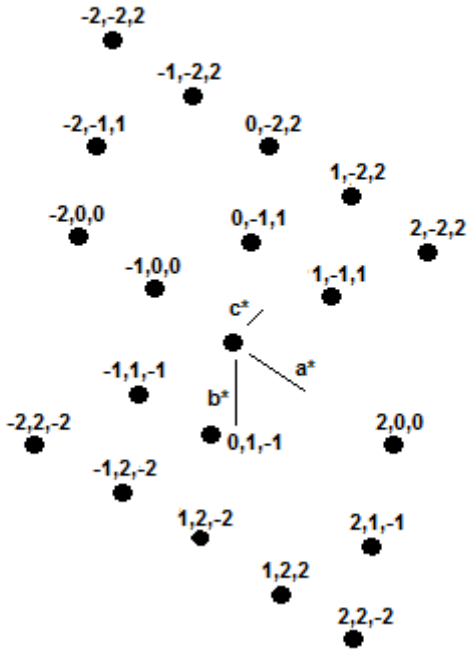

Fig. 4.10: Computerised TEM electron diffraction and index of a HTlc.[5]

4.1.7 ^{27}Al Solid State Nuclear Magnetic Resonance

The ^{27}Al Solid State NMR spectra for HTlca-1 and HTlca-2 are shown in Fig. 4.11 and Appendix 8B respectively. Magic angle spinning was used in order to reduce both the dipole interaction and the quadrupole effect. The position of the peak indicates the type of geometry around Al. A peak at around 0 ppm is indicative of an octahedral geometry. If a peak is present around 55-80 ppm then the geometry around Al is tetrahedral.[8] Al in HT and HTlc's exhibits octahedral geometry,[8] which is observed in the spectra for HTlca-1 and HTlca-2 by the peak at 0 ppm. This correlates with the XRD results. If Al doesn't exhibit an octahedral geometry around it, the HTlc will not form, hence the XRD pattern of HTlc will not be obtained.

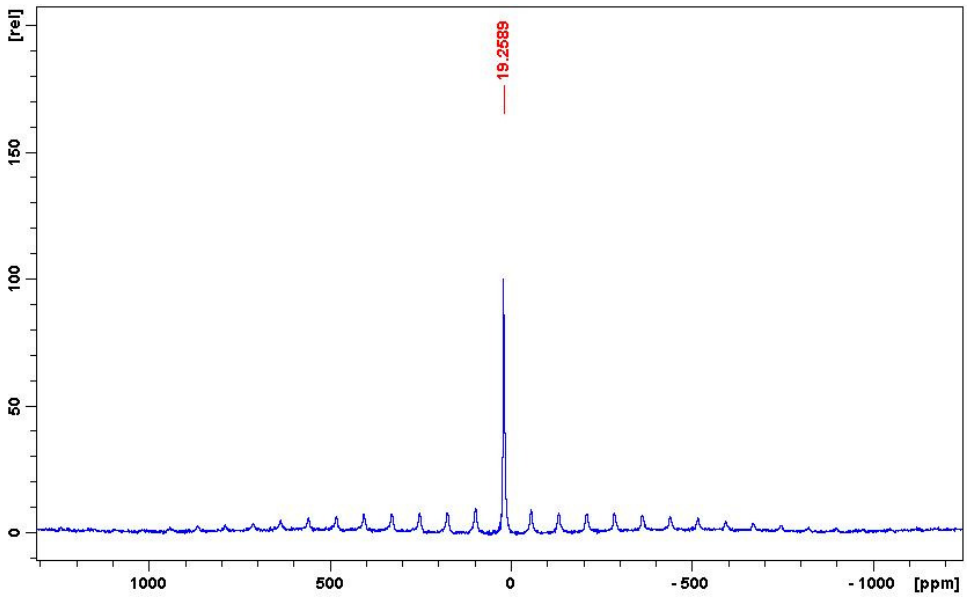

Fig. 4.11: The ^{27}Al Solid State NMR spectra for HTlca-1.

4.1.8 Thermal Gravimetric analysis - Differential Scanning Calorimetry (TGA-DSC)

The thermal behavior of both HTlca-1 and 2 are similar, in that there are two characteristic endothermic losses at low temperatures (Fig. 4.12, Appendix 9B, respectively). However, the DSC shows two endothermic peaks (a and b in Fig. 4.12) which are not within the

range that is stated in literature (first peak 370 to 570 K, and the second peak 620 to 740 K).[9] It has also been observed that there are different factors that can affect the temperature range. One of the factors is the low temperature treatment (hydration and drying).[9] The reason for the temperature range for HTlca-1 and HTlca-2 being below that indicated in literature remains unclear.

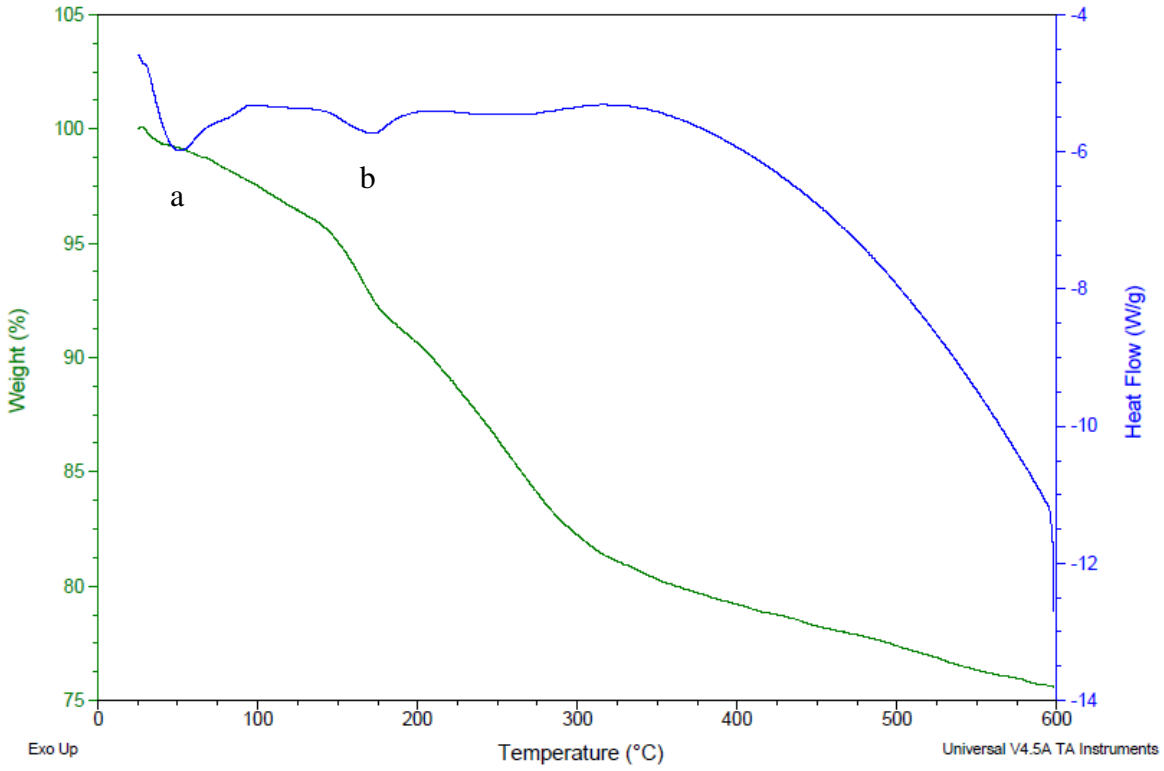

Fig. 4.12: TGA-DSC analysis of HTlca-1.

4.2 Heat treated catalyst (HTlca-3) characterisation

The heat treatment under nitrogen was carried out up to 300 ^{o}C as performed in literature,[1] in an attempt to prevent Os sublimation (as OsO_4 which would form in air) as well as to maintain the HTlc structure. The TGA-DSC results indicated that there was no loss of material after 300 ^{o}C, while below that temperature there are two endothermic losses (Section 4.1.8). It has been reported that HTlc's catalytic activity increases upon heat treatment under nitrogen or calcinations.[9] In this study, characterisation of the treated

catalyst is important in order to make sure the structure of the HTlc does not collapse upon thermal stress.

4.2.1 X-ray Diffraction (XRD)

The XRD of HTlca-3 showed that the catalyst did not maintain the HTlc structure after heating. This is indicated by the absence of all the characteristic features in the pattern (Section 4.1.1) expected of the HTlc. The XRD (Fig. 4.13) shows that there is no crystalline HTlc phase present. However, according to literature,[1] Os can migrate to the surface upon heating, which was proved by HRTEM. Furthermore, calcination of HT at 300 °C resulted in the presence of both the HT phase and the metal oxide phase,[10] possibly, in part, due to the low crystallinity of the heat treated catalyst this was not observed for HTlca-3.

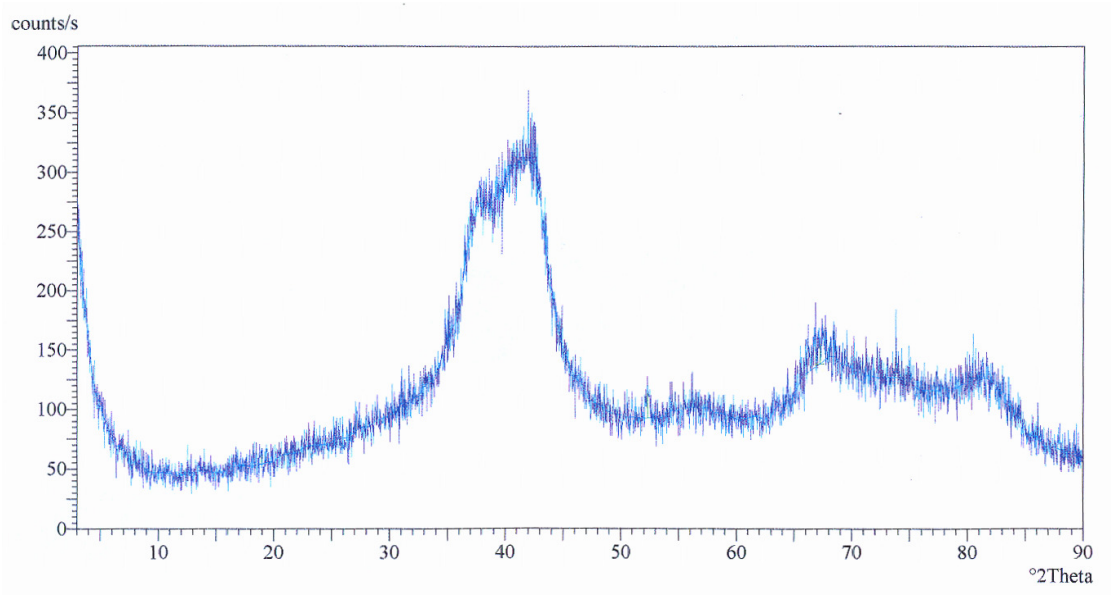

Fig. 4.13: XRD diffractogram of HTlca-3.

4.2.2 Inductive Coupling Plasma-Optical Emission Spectroscopy (ICP-OES)

To determine the effect of heat treatment under nitrogen on the ratio in which the three metals in the HTlca-2 are present, ICP-OES was undertaken (Table 4.6). However, the ICP-OES results show that the concentration of Os decreased by 42%. This could be due to Os sublimation.

Table 4.6: ICP-OES metal content ratio for heat treated HTlca-1.

Heat treatment	Os/ Zn/ Al ICP-OES ratio
Before treatment	0.29/ 3.56/ 1
After treatment (HTlca-3)	0.17/ 3.56/ 1

4.2.3 Fourier Transform-Inra-Red (FT-IR)

The IR analysis of the heat treated catalyst, showed a broad band around 3390 cm^{-1} indicating the presence of water in the catalyst. This is expected, because, for the complete removal of water, higher temperatures (> 300 ^{o}C) are required.[7] For complete removal of carbonate ions, the temperature for the heat treatment must be increased.

4.2.4 Brunauer-Emmett and Teller (BET) surface area measurements

The heat treatment also had a significant effect on the surface area of the catalyst. The surface area before the heat treatment was 59 m^2/g, after the heat treatment the surface area increased to 150 m^2/g. This is a further indication of the change that occurred in the catalyst structure. Furthermore, the high surface area is in agreement with the results from the XRD diffractogram, which indicates that the catalyst is not very crystalline (partially amorphous).

4.3 Catalyst activity testing

The investigation of the catalyst activity in the aminohydroxylation reaction was initiated by testing the effect of the reaction solvent and temperature on the catalyst activity determined by the time of the reaction until 100% depletion of the starting material, as determined by GC. Furthermore, the effect of catalyst crystallinity and structure on the reaction time and selectivity (depletion of starting material and yield of β-amino alcohols), under the optimum reaction conditions was investigated.

4.3.1 Solvent effect on the reaction time

The solvents that were chosen for this study display a wide range of polarity (*i.e.* toluene, MeCN/water (1:1 v/v) and *t*-BuOH/water (1:1 v/v).[11] In terms of the reaction time (the time required to achieve 100% depletion of the starting material) toluene showed the longest reaction time for all the olefins tested, excluding styrene, due to the fact that chloramine-T is not completely soluble in toluene. Styrene demonstrated the shortest reaction time in toluene, however, the reason for this is unclear. For complete solubility of chloramine-T in toluene, an equivalent amount of water could be added. However, this would result in a biphasic system since toluene and water are immiscible. When MeCN/water (1:1 v/v) and *t*-BuOH/water (1:1 v/v) were used as the solvent system the reaction gave a shorter reaction time than when toluene was used and a comparable reaction time to each other (Fig. 4.14). This could be due to the fact that chloramine-T is completely soluble in these two solvent systems, pushing the reaction to completion in a shorter period of time.

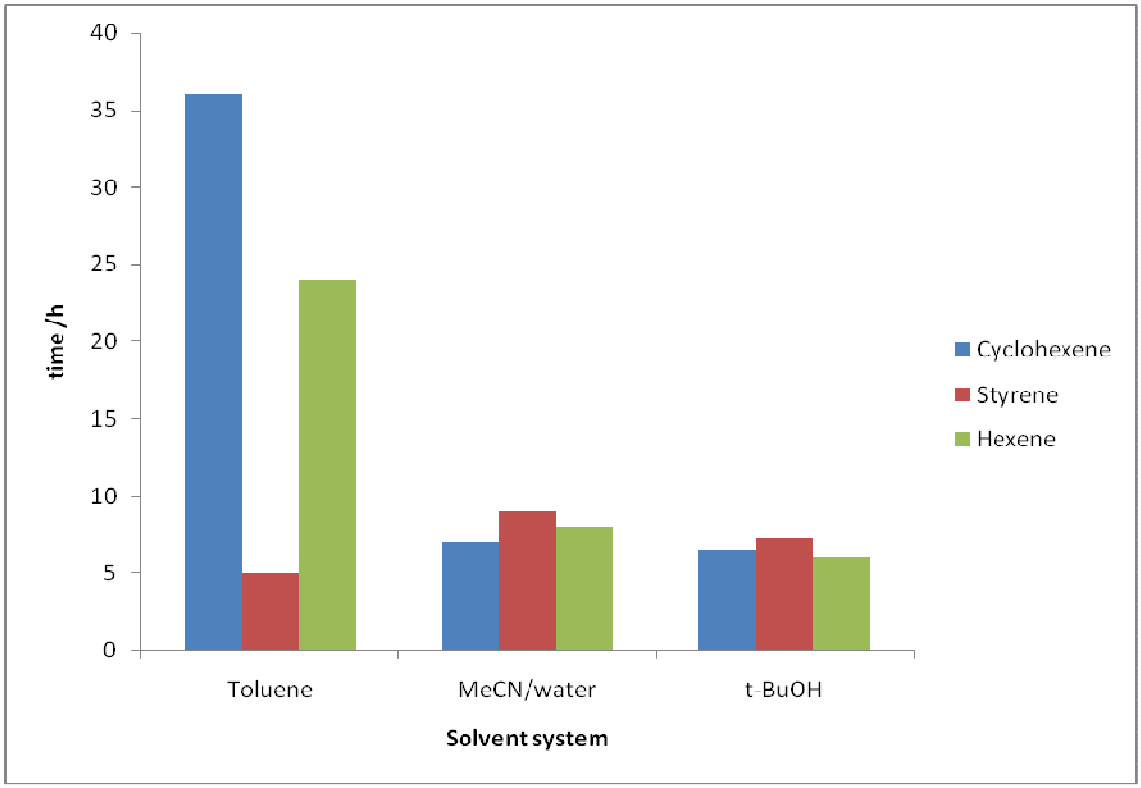

Fig. 4.14: Effect of the solvent system on the reaction time for 100% conversion of the olefin determined by GC, using chloramine-T as the nitrogen source, HTlca-1 as the catalyst at 60 °C.

The above can also be explained using the dielectric constants of the solvent systems used. Dielectric constant is defined as " the measure of how well the solvent can insulate opposite charges from one another".[12] Solvents achieve this by clustering the negative charges at the positive poles and the positive charges at the negative poles. In terms of the solvents used in this study, the dielectric constant for toluene is 2.38 (at 25 °C), for MeCN it is 38 (at 25 °C) and it is 11 (at 25 °C, which was also the reaction temperature) for *t*-BuOH.[10] However, in this study, mixtures of MeCN/water (1:1 v/v) and *t*-BuOH/water (1:1 v/v) were used; the dielectric constants for these mixtures are 55.69[13] and 36.59,[14] respectively. A clear relationship is observed between the solvent systems, dielectric constant and the time required for 100% depletion of the starting material in the aminohydroxylation reaction. To explain, the reaction time increases in the following order; MeCN/water (1:1 v/v) ≈ *t*-BuOH/water (1:1 v/v) < toluene, and the dielectric constants for these solvents decrease in the same order. In other words, the aminohydroxylation reaction is best carried

out in a solvent system that exhibits a high dielectric constant. Taking into consideration the dielectric constants of the amino alcohols, *e.g.* diethanol amine, 24.64,[15] it is evidently why both MeCN/water (1:1 v/v) and *t*-BuOH/water (1:1 v/v) exhibit a shorter reaction time than toluene (because both solvents have higher dielectric constant than toluene). The dielectric constant for MeCN/water (1:1 v/v) is 55.69 at 25 °C and 47.94 at 60 °C,[13] for *t*-BuOH/water (1:1 v/v) the dielectric constant is 36.59 at 20 °C and 27.80 at 60 °C. The dielectric constant always remains higher in the solvent system than that for the amino alcohol. In the homogeneous aminohydroxylation reaction, water hydrolysis enhances the formation of the amino alcohol. Thus, the long reaction time in toluene can be attributed to this phenomenon. Unlike MeCN and *t*-BuOH, water is immiscible with toluene, which also gives rise to the longer reaction time.

4.3.2 Effect of temperature on the reaction time

This investigation was carried out at temperatures of 25, 40 and 60 ^{o}C using the three solvent systems mentioned in Section 4.3.1. Styrene was selected for this study, since it demonstrated comparable reaction times in all three solvent systems. When toluene was used as the solvent system, the reaction time decreased with an increase in reaction temperature up to 60 ^{o}C (Fig. 4.15). However, at that temperature diol formation occurred (approximately 40%), (detected by a GC peak at 11.1 min, Appendix 10B). This increase could be due to the fact that more chloramine-T is available to force the reaction forward. Temperature did not have a significant effect on both reaction time and product distribution when MeCN/water and *t*-BuOH/water (1:1 v/v) were used as the solvent systems. Only trace amounts of diol were detected in MeCN/water and *t*-BuOH/water (1:1 v/v). The suppression of diol formations could be due to the fact that chloramine-T is completely soluble in these two solvent systems, hence it forces the reaction towards the aminohydroxylation route. In addition, water increases the rate of hydrolysis, which yields the β-amino alcohol.[16] The reaction was not carried out at 40 ^{o}C in MeCN/water and *t*-BuOH/water because no significant difference in terms of the reaction time and product distribution was detected between the experiments carried out at 25 ^{o}C and 60 ^{o}C. The dielectric constant can also be used to explain why temperature does not have a significant

effect on the reaction time when MeCN/water (1:1 v/v) and *t*-BuOH/water (1:1 v/v) are used, since the constant is higher at both temperatures than that for toluene.

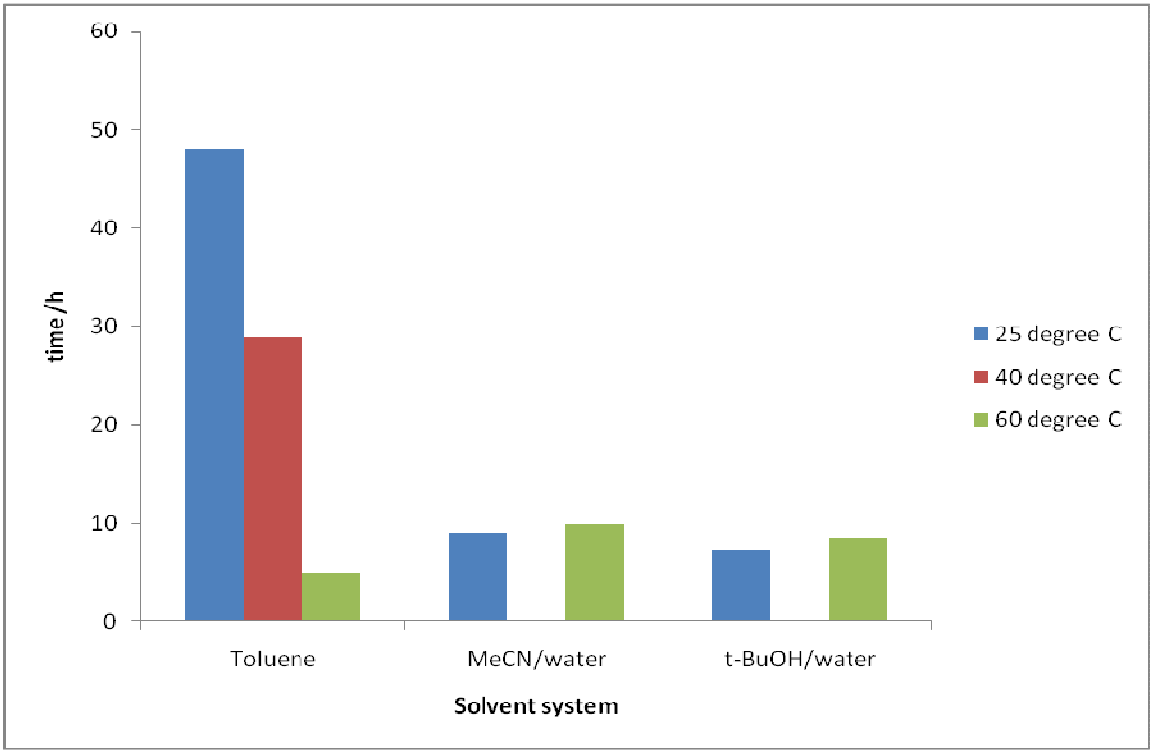

Fig. 4.15: Effect of temperature on reaction time (complete depletion of starting material), using chloramine-T as nitrogen source, HTlca-1 as catalyst.

4.3.3 Effect of the catalyst structure on the reaction

Three different catalysts (with structural differences) were used in this investigation, HTlca-1, HTlca-2 and HTlca-3. In a structural comparison between HTlca-1 and HTlca-2, the latter is more pure and crystalline HTlc than the former. The comparison between these two HTlca's (in the aminohydroxylation reaction) will aid in understanding to what extent the structure of the HTlc is important to catalytic activity (in terms of reaction time and isolated product yield). HTlca-3 was studied to investigate if the heat treatment would increase the catalytic activity. However, since it destroyed the HTlc structure, this allowed for the investigation of the HTlc *vs* a non-HTlc structure on the catalytic activity. These studies were carried out utilizing cyclohexene and *t*-butylcrotonate as the olefins with

MeCN/water (1:1 v/v) as the solvent system. The results obtained demonstrated a significant level of similarity between HTlca-1 and HTlca-2 in terms of the reaction time (Fig. 4.16) and the isolated yield of the β-amino alcohol (Fig. 4.17). This could be due to the fact that HTlca-1 and HTlca-2 are comparable in terms of HTlc structure, the Os content (Section 4.1.2) (which is the active species) and surface areas (Section 4.1.4) (allowing comparable accessability of olefins to the active sites).[17] When HTlca-3 was utilised in the reaction, the reaction time (100% depletion of starting material) decreased, especially with cyclohexene as the respective olefin (Fig. 4.16). However the lowest isolated yields of the β-amino alcohols, with rise in diol formation were observed (Fig. 4.17). This could be attributed to the loss of the HTlc structure. Literature has shown that the HTlc structure is important for a number of reactions (Section 2.6.1).[1,2]

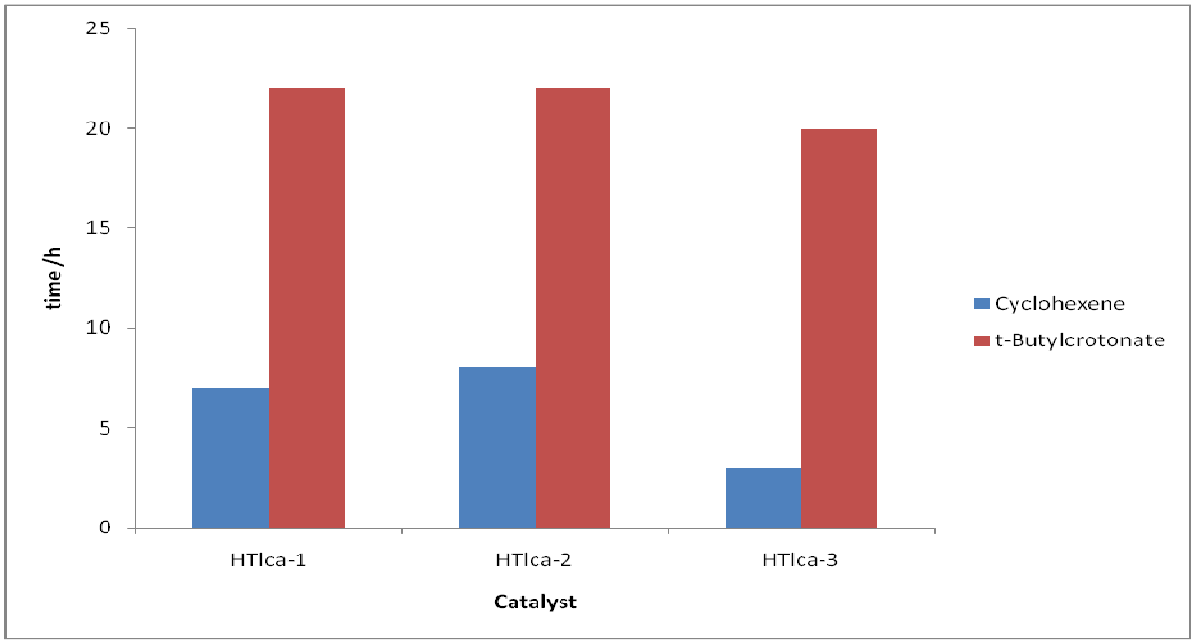

Fig. 4.16: Effect of the catalyst structure on the reaction time (100% conversion of the olefin), using chloramine-T as the nitrogen source, MeCN/water (1:1 v/v) as the solvent system, at 25 °C.

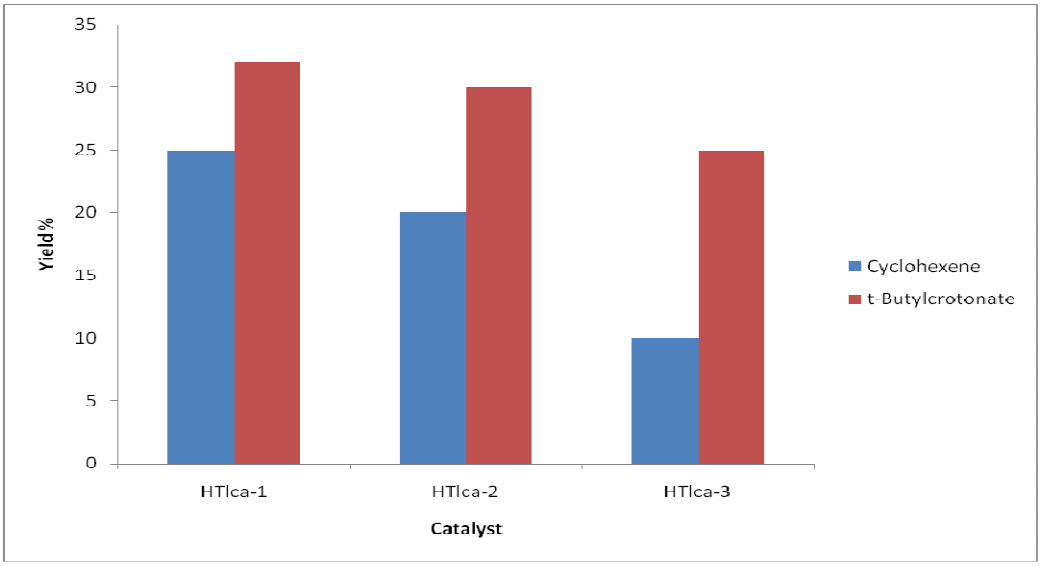

Fig. 4.17: Effect of the catalyst structure on the isolated yield of β-amino alcohol, using chloramine-T as the nitrogen source, MeCN/water (1:1 v/v) as the solvent system at 25 °C.

4.3.4 Screening the activity of the system using different olefins

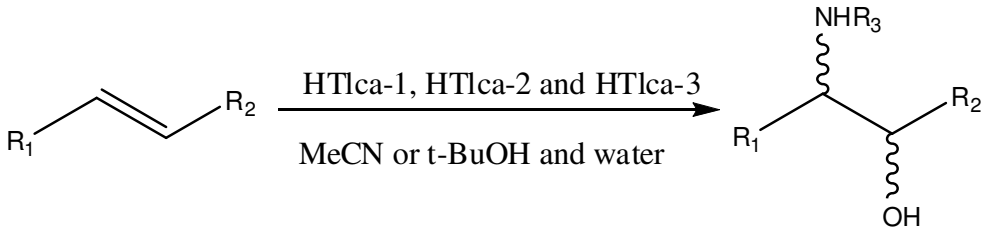

1) $R_1 = CH_2$, $R_2 = CH_2$.
2) $R_1 = C_4H_9$, $R_2 = H_2$
3) $R_1 = Ar$, $R_2 = H_2$
4) $R_1 = Ar$, $R_2 = Ar$
5) $R_1 = Ar$, $R_2 = COOCH_3$
6) $R_1 = COOCH_3$, $R_2 = COOCH_3$
7) $R_1 = CH_3$, $R_2 = COOC(CH_3)$

1) $R_1 = CH_2$, $R_2 = CH_2$, $R_3 = TsO$
2) $R_1 = C_4H_9$, $R_2 = H_2$, $R_3 = TsO$
3) $R_1 = Ar$, $R_2 = H_2$, $R_3 = TsO$
4) $R_1 = Ar$, $R_2 = Ar$, $R_3 = TsO$
5) $R_1 = Ar$, $R_2 = COOCH_3$, $R_3 = TsO$
6) $R_1 = COOCH_3$, $R_2 = COOCH_3$, $R_3 = TsO$
7) $R_1 = CH_3$, $R_2 = COOC(CH_3)$, $R_3 = TsO$

Scheme 4.1**:** The catalytic aminohydroxylation reaction of seven olefins and their corresponding amino alcohols products, using HTlca-1 as catalyst.

The olefins utilized in this study allow the investigation of electronic and steric effects on the reaction time (100% depletion of starting material) (Fig. 4.18) and the isolated yield (Fig. 4.19 and Table 4.7). The substrates can be divided into aliphatic, aromatic and functionalised olefins. All the screening reactions were carried out at 25 °C.

The reaction time (100% depletion of starting material) is observed to be shorter for the aliphatic olefins than for the functionalised ones, with hexene having the shortest reaction time and *cis*-stilbene, methylcinnamate and dimethylfumarate not reaching complete depletion of starting material within 24 h (Fig. 4.18). Furthermore, the two solvent systems show comparable reaction times for the same substrate. Similar observations were also reported in literature.[18,19]

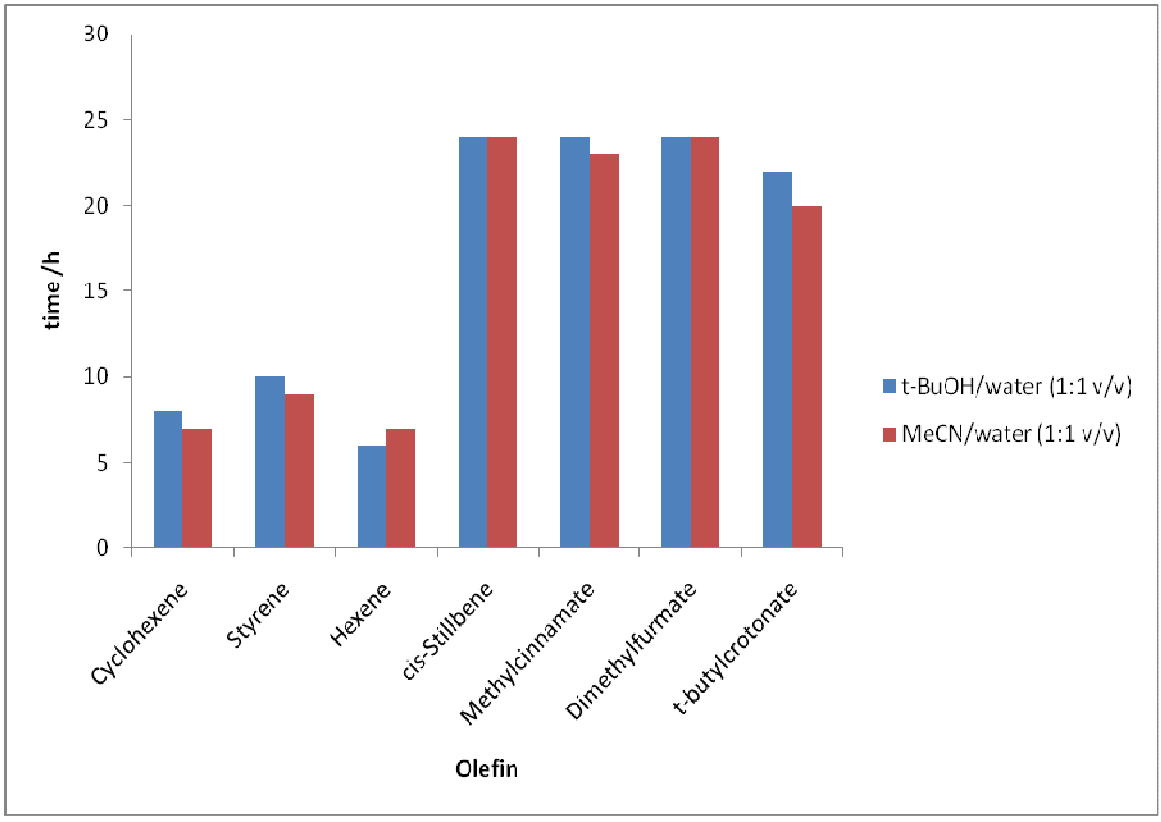

Fig. 4.18: Reaction time (99.99% to 100% depletion of starting material) for the different olefins using chloramine-T as the nitrogen source and HTlca-2 as the catalyst, at 25 °C.

In homogeneous aminohydroxylation the isolation of the β-amino alcohol is especially difficult when chloramine-T is used as the nitrogen source.[16] This difficulty was also encountered in the heterogeneous aminohydroxylation. This results in the low isolated yields obtained in this study. The solvent systems do not significantly affect the isolated yield of the β-amino alcohol obtained. However, the products obtained from functionalised olefins show the highest isolated yields (up to 35%) of β-amino alcohols obtained (Fig. 4.18) (Table 4.7), whilst the products from unfunctionalised olefins (*e.g*. hexene) demonstrate the lowest yield (8%). However, the results obtained by high performance liquid chromatography-mass spectrometry (HPLC-MS), suggest that a yield of > 99% was obtained, since only three peaks are observed (Appendix 12B), implying major product loss during the work up of the reaction. The first peak elutes with a less polar solvent system and the other two with a more polar solvent system. The first peak has a mass that corresponds to that of *p*-toluenesulfonamide (which is a byproduct from chloramine-T). The second and third peaks show masses that correspond to the mass of the target product (two peaks for the product due to the formation of the *cis* and *trans* isomers of the β-amino alcohol). As mentioned previously, the functionalised olefins (methylcinnamate, dimethylfumarate and *tert*-butylcrotonate) gave higher isolated yields and faster reaction times than the unfunctionalised olefins due to the strong polarisation effect of the double bond between osmium and the tosyl group (Os=Ts) in the postulated reaction intermediate,[18,19] and the double bond in these molecules being electron deficient, as they are adjacent to the electron withdrawing carbonyl group.

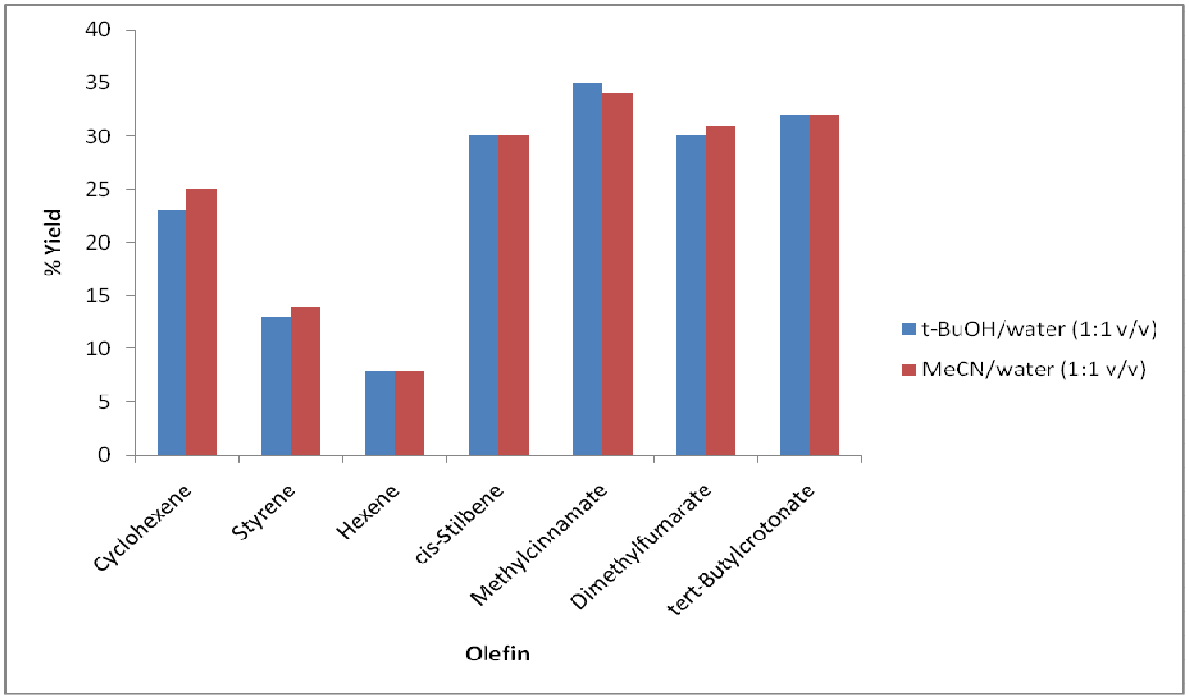

Fig. 4.19: Isolated % yield of β-amino alcohols of different olefins, using chloramine-T as the nitrogen source and HTlca-2 as the catalyst at 25 °C.

4.4 Crystal structures

4.4.1 *N*-(2-hydroxycyclohexyl)-4-methylbenzenesulfonamide[20]

The isolated product of the aminohydroxylation reaction of cyclohexene was obtained by means of preparative HPLC (Section 3.6.1). The product was dissolved in a MeCN/water mixture (1:1 v/v) and the solvent was left to slowly evaporate. The crystals grown were needle-like in shape and were transparent.

Table 4.7: Isolated percentage yield of the β-amino alcohol obtained from different olefins, using HTlca-1, in two different solvent systems.

Substrate	**Structure**	**% Yield** [a]	
		b	c
Cyclohexene	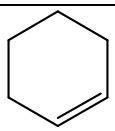	23	25
Hexene	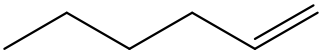	8	8
Styrene	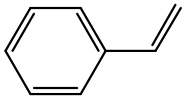	13	14
cis-Stilbene *	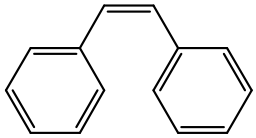	30	30
Methylcinnamate *	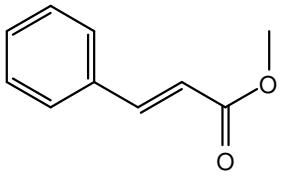	35	34
Dimethylfumarate *	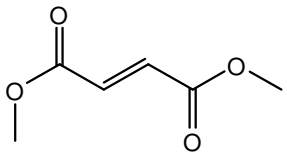	30	31
tert-Butylcrotonate	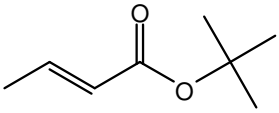	32	32

[a] isolated yield by chromatography.(b) *t*-BuOH/water (1:1 v/v).(c) MeCN/water (1:1 v/v). *depletion of starting material obtained by calibration curve determined to be 99.99% (Appendix 11B).

The crystal structure of this compound packs in a triclinic $P\hat{I}$ unit cell. The packing shows that the cell unit consists of two molecules (Z = 4). The asymmetric unit of the compound consist of two symmetrically independent molecules (Fig. 4.20). The cyclohexene ring in the molecule adopts a chair conformation (Fig. 4.20) and with respect to the plane of the ring, the tosylamino and hydroxyl groups occupy the equatorial and axial positions respectively. Furthermore, the crystal packing is stabilized by hydrogen bonds (N-H---O and O-H---N) between the two independent molecules (Table 4.8). For a more comprehensive discussion, Tables for unit cell parameters, bond length and angles refer to Appendix 13B.

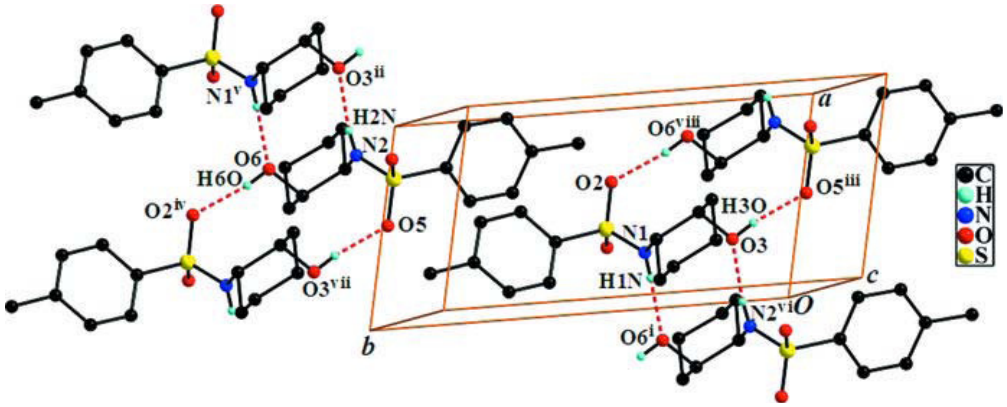

Fig. 4.20: Crystal structure of N-(2-hydroxycyclohexyl)-4-methylbenzenesulfonamide, showing hydrogen bonds.

Table 4.8: Hydrogen bonds geometry (Å, °) in *N*-(2-hydroxycyclohexyl)-4-methylbenzenesulfonamide.[20]

D – H---*A*	*D* – H	H---*A*	*D*---*A*	*D* – H---*A*
N1 – H1*N*---O6^{i}	0.83 (2)	2.00 (2)	2.8255 (17)	175.0 (18)
N2 – H2*N*---O3^{ii}	0.82 (2)	2.00 (2)	2.8155 (18)	173.1 (19)
O3 – H3*O*---O5^{iii}	0.83 (2)	1.93 (2)	2.7489 (15)	171 (2)
O6 – H4*O*---O2^{iv}	0.83 (2)	1.98 (2)	2.8001 (15)	169 (2)

Symmetry codes: (i) –*x* + 1 , -*y* + 1, -*z* + 1,: (ii) *x* + 1, *y* + 1, *z*,: (iii) *x*, *y* - 1, z,: (iv) *x*, *y*+ 1,*z*.

4.4.2 Methyl-2-hydroxy-3-(4- methylbenzenesulfonamide)-3-phenylpropanoate[21]

The crystal of the title compound was grown in a MeCN/water mixture (1:1 v/v), after isolation and purification using chromatography (Section 3.6). The crystals were needle-like and transparent.

The crystal structure of this compound packs in a monoclinic $P2_1/c$ unit cell. The packing shows that the unit cell consists of two molecules (Z = 4) similar to that observed in Fig. 4.20. The asymmetric unit of the compound consist of two symmetrically independent molecules (Fig. 4.21). The crystal structure is stabilized by intra- and inter-molecular interactions (Fig. 4.21). The intra-molecular forces are indicated by one O-H---O and three C-H---O bonds (Table 4.9) that formed hydrogen-bonded sheets running along the *b* axis and aligned along the crystallographic *ac* face. The *p*-tosyl and the phenyl rings are almost parallel to each other (dihedral angle = 17.2 (1)°), this close proximity giving rise to π-π interactions (centroid-centroid distance = 3.184 (10) Å). However, due to steric hindrance, the hydrogen on the NH group is not involved in any hydrogen bonding. For a more comprehensive discussion, Tables for unit cell parameters, bond length and angles refer to Appendix 14B.

Table 4.9: Hydrogen bonds geometry (Å, °) in *N*-(2-hydroxycyclohexyl)-4-methylbenzenesulfonamide.[21]

D – H---*A*	*D* – H	H---*A*	*D*---*A*	*D* – H---*A*
O3 – H3*A*---O2*i*	0.84	2.50	3.270 (2)	152
C1 – H1*C*---O1*ii*	0.98	2.52	3.392 (2)	149
C4 – H4---O3*iii*	1.00	2.50	3.484 (2)	166
C1 – H1*C*---O1*ii*	0.98	2.52	3.392 (2)	149

Symmetry codes: (i) $x + 1$, $y + 1$, z: (ii) $-x + 1$, $-y + 1$, $-z + 2$,: (iii) x, $y - 1$, z,: (iv) x, $y - 1$,z.

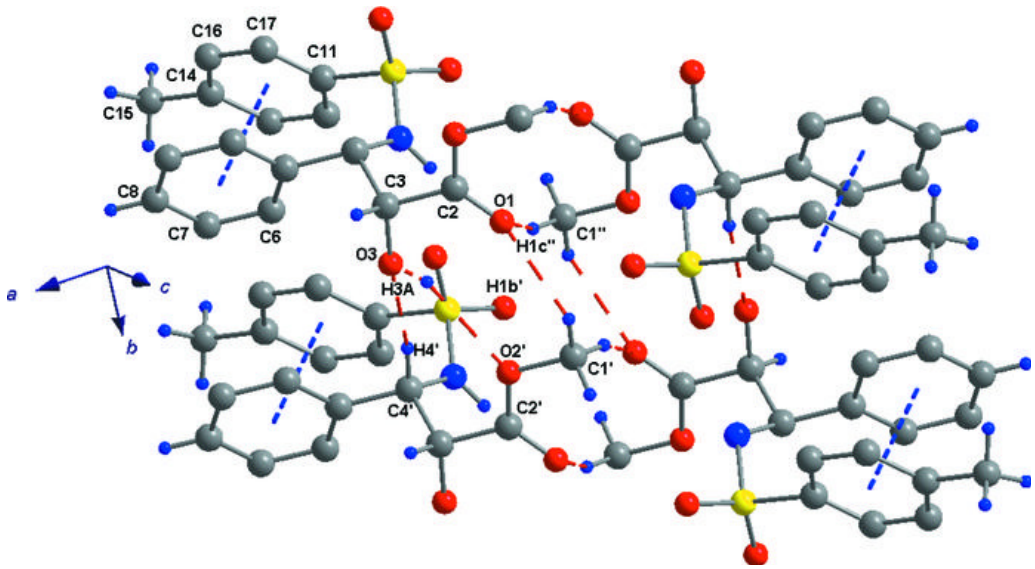

Fig. 4.21: Crystal structure of methyl-2-hydroxy-3-(4- methylbenzenesulfonamide)-3-phenylpropanoate.

4.4.3 *tert*-Butyl-2-hydroxy-3-(4-methylbenzenesulfonamide) butanoate[22]

The title product was purified using chromatography (Section 3.6). The isolated product was dissolved in dichloromethane and layered with hexane. The crystals were grown by slow evaporation, had cubic-like shapes and were transparent.

The crystal structure of this compound packs in a triclinic $P\hat{I}$ unit cell. The packing of the molecule shows that the unit cell consists of one molecule (Z = 2). The crystal structure is stabilised through hydrogen bonds (N – H---O and O – H---O). The hydrogen bonds (Table 4.10) in the crystal results in a centrosymmetric dimer generating R_2^2 (12) rings through the N – H---O interactions, and R_2^2 (14) rings through the O – H---O interactions (Fig. 4.22). The crystal lattice is further stabilised by a weak C – H---O interaction. For a more comprehensive discussion, Tables for unit cell parameters, bond length and angles refer to Appendix 15B.

Table 4.10: Hydrogen bonds geometry (Å, °) in *N*-(2-hydroxycyclohexyl)-4-methylbenzenesulfonamide.[22]

D – H---*A*	*D* – H	H---*A*	*D*---*A*	*D* – H---*A*
N1 – H1*D*---O1^{i}	0.84	2.50	3.270 (2)	152
O3 – H3---O4^{i}	0.98	2.52	3.392 (2)	149
C1 – H1*C*---O4^{ii}	1.00	2.50	3.484 (2)	166

Symmetry codes: (i) –*x* + 1 , -*y* + 1, -*z* + 1,: (ii) -*x* + 1, -*y* + 2, -*z* + 2.

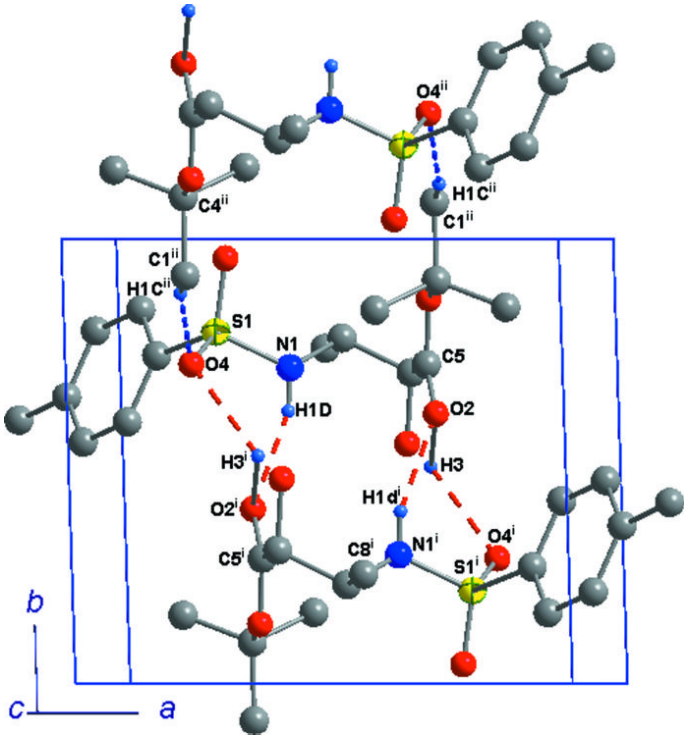

Fig. 4.22: Crystal structure of *tert*-butyl-2-hydroxy-3-(4-methylbenzenesulfonamide) butanoate.

The hydrogen bond (N – H---O) and (O – H---O) in all three structures are similar but the bond distances are different. This could be due to the difference in the bond angle (*D* – H--*A*)[23] reported in Tables 4.8, 4.9 and 4.10. For a more comprehensive discussion refer to Appendix 15B.

All crystal structures showed that, the nitrogen atom, attached to the β carbon, is far from the electron withdrawing group, and this results in the formation of the β-amino alcohol. This phenomenon is also reported for the homogeneous system.[17]

4.5 Leaching test

For the reaction to be strictly heterogeneous, the active species must not leach into the reaction mixture, or, if they leach, their homogeneous form must not be catalytically active.[24] To determine if the reaction is heterogeneous, the catalyst was removed after approximately 20% of the starting material had reacted (after 2h) (Section 3.10). The reaction mixture (without the catalyst) was allowed to stir for further 6 h to assess if Os had leached, since the reaction would proceed should catalytically active dissolved Os species be present. The leaching results showed that Os does leach, to a small degree (determined by ICP) but not in an active form (determined by GC analysis to observe if there was any further starting material depletion after removal of the catalyst).

The estimate of the amount of Os leached was calculated (Appendix 16B) for the solvent systems, MeCN/water (v/v 1:1) and *t*-BuOH/water (v/v 1:1), and was found to be 3.0 % and 2.9 %, respectively. However, the leached Os is not catalytically active, because no further conversion of the starting material (cyclohexene) was observed upon removal of the catalyst. The same leaching test was carried out with HTlca-2, using solvent systems MeCN/water (v/v 1:1) and *t*-BuOH/water (v/v 1:1), and 2.9% and 3.4% of Os leached respectively. These results thus indicated that HTlca-1 and HTlca-2 are comparable in terms of the amount of Os lost in the reaction solution.

An important result of this work over that previously reported,[18,19,25-27] is that the lowest level of inactive Os leaching to the reaction mixture was observed. Previous attempts at heterogenisation the aminohydroxylation reaction had shown leaching of up to 50 %.[26]

4.6 Recycling test

One of the main advantages of heterogeneous over homogeneous catalysis, is that the catalyst can be (easily) recycled a number of times.[17] The results for the recycling test showed that the reaction time increases with an increase in the number of recycles (Fig. 4.22). The increase in the reaction time may be due to the leaching of Os or, more likely, a slow loss of HTlc structure (Section 4.7). However, the isolated yield of the β-amino alcohol of cyclohexene (Fig. 4.23) did not change significantly regardless of the number of cycles (25, 25 and 23%, respectively).

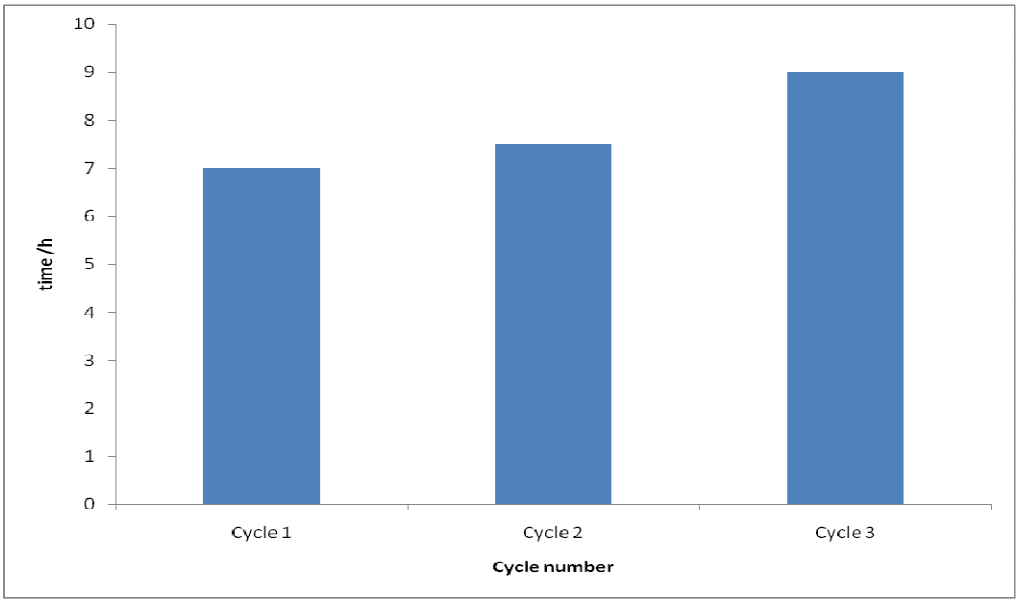

Fig. 4.23: Effect of catalyst recycling on the reaction time (100% conversion of cyclohexene) using chloramine-T as the nitrogen source, HTlca-2 as the catalyst, MeCN/water (1:1 v/v) as the solvent system at 25 °C.

4.7 Spent catalyst characterisation

To obtain a sufficient amount of the spent catalyst for characterisation, the reaction was scaled up three fold. After the reaction, the catalyst was filtered and dried under vacuum, for analysis.

4.7.1 X-ray Diffraction (XRD)

The XRD diffractogram of the spent catalyst (Fig. 4.24) shows that the catalyst is still indeed a hydrotalcite-like compound after the aminohydroxylation reaction. The low count in the XRD diffractogram could be due to the spent catalyst losing some of its crystallinity during the course of the reaction. The observed shift of the hexagonal peak from 60° 2θ to approximately 70° 2θ is due to the different radiation source that was used in the powder XRD instrument.

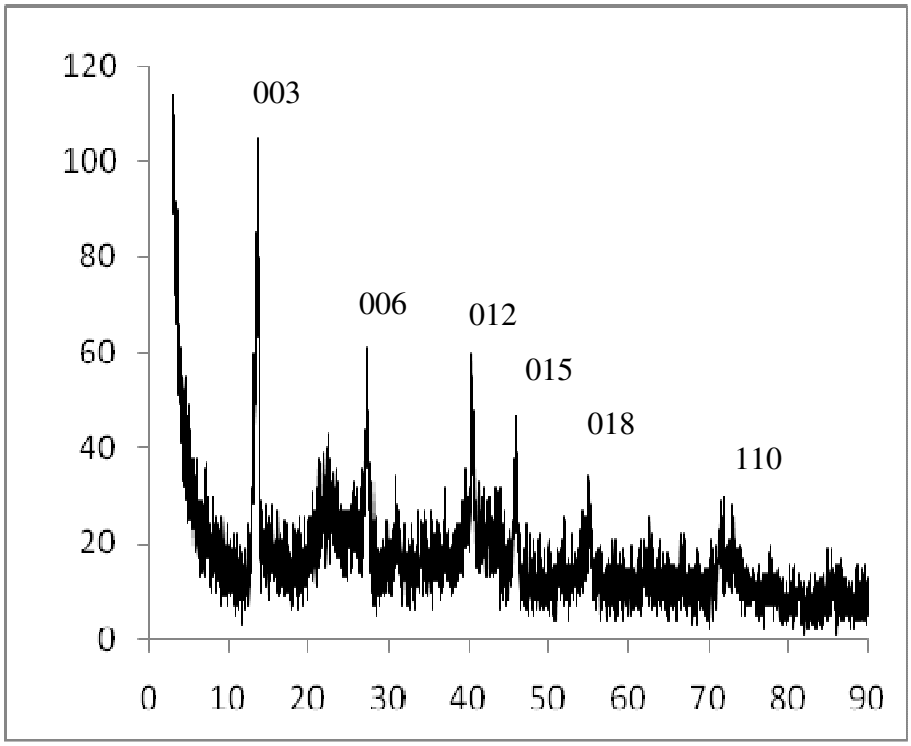

Fig. 4.24: XRD diffractogram of the spent catalyst.

4.7.2 Scanning Electron Microscope (SEM-EDS) of the spent catalyst.

Os is homogeneously distributed throughout the catalyst (Fig. 4.25). This confirms that the Os is still part of the catalyst and not simply supported on the hydrotalcite-like catalyst.

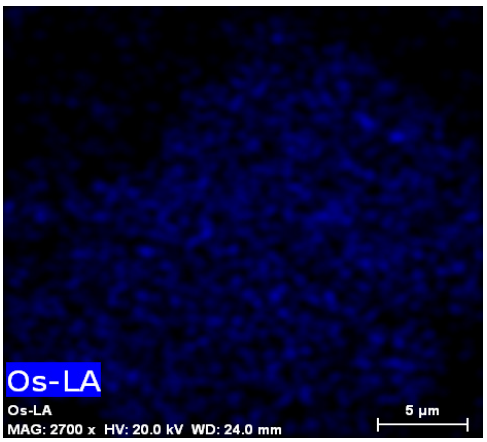

Fig. 4.25: Os distribution in the spent catalyst, obtained by EDS.

4.7.3 Cryo-Transmission Electron Microscopy (TEM) of the spent catalyst.

The charactristic shapes of the hydrotalcite-like catalyst (hexagonal plates) was not observed in the spent catalyst (Fig. 4.26). However, the rod-like structures observed could be the hexagonal plates alignend on their side rather than flat.

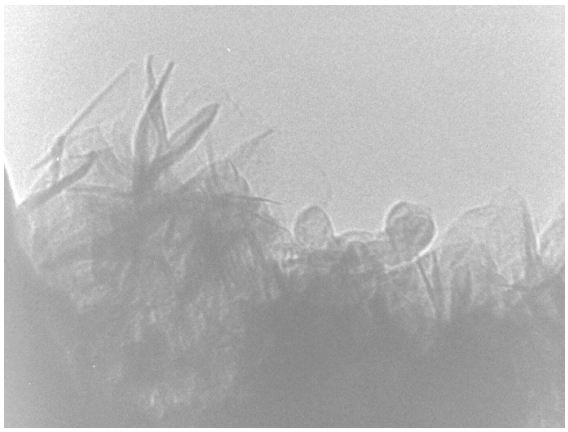

Fig. 4.26: The rod and the sheet-like structures of the spent catalyst.

The results from the electron diffraction analysis (Fig. 4.27), show that the catalyst is polycrystalline (or partially amorphous), which is indicated by the rings and the spots.[5] Hence, this could be the likely reason for the increase in the reaction time with increase in the recycle number.

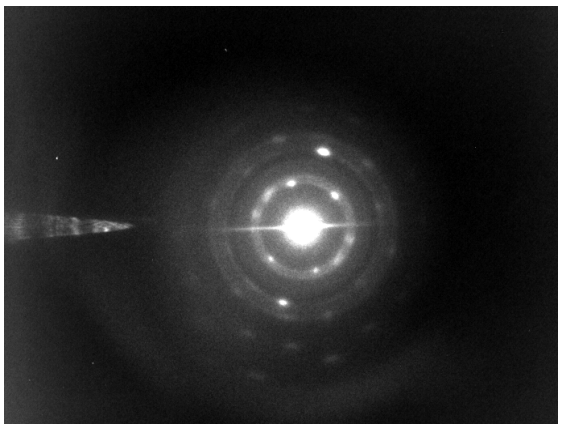

Fig. 4.27: Electron diffraction of the spent catalyst.

4.7.4 Inductive coupling plasma-optical emission spectroscopy (ICP-OES) of the spent catalyst.

To investigate the amount of the three metals present in the spent catalyst, ICP analysis was undertaken (Table 4.8). The amount of Os and Zn has decreased after the reaction, which indicates leaching from the catalyst structure to the reaction mixture.

Table 4.8: The metal ratio in the catalyst before the reaction and after the reaction.

Catalyst	Os	Zn	Al
Before reaction	0.31	3.70	1.00
After reaction	0.22	3.50	1.00

4.7.5 Brunauer-Emmett and Teller (BET) surface area measurements

The results from the XRD and the electron diffraction analyses indicate that the spent catalyst should have a larger surface area than that of the catalyst before the reaction. The surface area indeed increased to 107 m^2/g, from 87 m^2/g before the reaction. This change may be due to grinding of the catalyst to a fine powder by the magnetic stirrer bar during

the course of the reaction and/or redox processes on the catalyst's surface carrying a potential loss of HTlc structure.

4.8 References

1) T. Naicker, A. K. Datye, H. B. Friedrich, *Appl. Catal. A*, **350** (2008) 96.

2) H. B. Friedrich, M. Govender, X. Makhoba, T. D. Ngcobo, M. O. Onani, *Chem. Commun.*, (2003) 2922.

3) M. J. H. Hermandez-Moreno, M. A. Ulibarri, J. L. Rendon, C. J. Serna, *Phys. Chem. Miner.,* **12** (1985) 34.

4) E. C. Kruissink, L. L. van Reijen, J. R. H. Ross, *J. Chem. Soc., Faraday Trans. 1*, **77** (1981) 649.

5) F. M. Labajos, V. Rives, P. Malet, M. A. Centeno, M. A. Ulibarri, *Inorg. Chem.,* **35** (1996) 1154.

6) D-P. Qui, W-G. Hou, *Physicochem. Eng. Aspects*, **336** (2009) 12.

7) D. B. Williams, B. C. Carter, *Transmission Electron Microscopy: A text book for materials science*, Volume IV, Klumer Academic/Plenum, New York, 1996.

8) T-J. Park, S-S. Choi, Y. Kim, *Bull. Korean Chem.*, **30** (2009) 149.

9) A. Vaccari, *Catal. Today*, **41** (1998) 53.

10) S. Miyata, *Clays Clay Miner.*, **28** (1980) 50.

11) E. M. Kosower, *J. Am. Chem. Soc.*, **80** (1958) 3253.

12) P. Y. Bruice, *Organic chemistry*, 4th ed., Pearson education, Inc. Upper Saddle River, 2004.

13) L. G. Gagliardi, C. B. Castells, C. Rafols, M. Roses, E. Bosch, *J. Chem. Eng. Data*, **52** (2007) 1103.

14) G. Akerlof. *J. Am. Chem. Soc.*, **54** (1932) 4125.

15) C-J. Hsieh, J-M. Chen, M-H. Li, *J. Chem. Eng. Data*, **52** (2007) 619.

16) B. B. Lohray, P. S. Thombare, V. Bhushan, *PINSA*, **68** (2002) 391.

17) J. Hagen, *Industrial Catalysis: A practical approach*, 2nd edition (2006), Weily-VCH. Weinheim.

18) B. M. Choudary, N. S. Chowdari, K. Jyothi, M. L. Kantam, *J. Mol. Catal. A*, **196** (2003) 151.

19) A. Mandoli. D. Pini, A. Agostini, P. Salvadori, *Tetrahedron Asymmetry*, **11** (2000) 4039.

20) M. I. Fadlalla. H. B. Friedrich. G. E. M. Maguire. M. D. Bala, *Acta. Cryst.*, **E66** (2010) o463.

21) M. I. Fadlalla. H. B. Friedrich. G. E. M. Maguire. B. Omondi, *Acta. Cryst.*, **E66** (2010) o3279.

22) M. I. Fadlalla. H. B. Friedrich. G. E. M. Maguire. B. Omondi, *Acta. Cryst.*, **E67** (2011) o648.

23) W. Fuller, *J. Phys. Chem.*,**63** (1959) 1705.

24) R. A. Sheldon, M. Wallau, I. W. C. E. Arends, U. Schuchardt, *Acc. Chem. Res*. **31** (1998) 485.

25) X. Yang, H. Liu, M. Xu, G. Lin, *Tetrahedron Asymmetry*, **15** (2004) 1915.

26) C. H. Jo, S. Han, J. W. Yang, E. J. Roh, U. Shin, C. E. Song, *Chem. Commun*, (2003) 1312.

27) C. E. Song, C. R. Oh, S. W. Lee, S. Lee, L. Canali, D. C. Sherrington, *Chem. Commun*, (1998) 2435.

Chapter 5

Conclusion and summary

Five major conclusions can be drawn from the results obtained. First, the synthesis of Os-Zn-Al HTlc was successfully carried out following the co-precipitation method. The success of the synthesis was determined by powder XRD (which showed the typical HTlc's characteristic features, Section 4.1.1). The ratio of the three metals (Os-Zn-Al) in the catalyst determined by ICP-OES was 0.31/ 3.6/ 1, respectively, which is close to the target ratio of 0.3/ 3/ 1 (Section 4.1.2). The SEM-EDS showed that Os is homogeneously distributed over the catalyst indicating that Os is part of the structure (Section 4.1.5).

Second, when toluene was used as the solvent system the time of the reaction generally increased significantly in comparison to MeCN/water (1:1 v/v) and *t*-BuOH/water (1:1 v/v) (Section 4.3.1). Temperature did have a significant effect on the reaction time (the reaction time is inversely proportional to the reaction temperature), when toluene was used as the solvent. However, this effect or relationship was not observed when MeCN/water (1:1 v/v) or *t*-BuOH/water (1:1 v/v) was used (Section 4.3.2). HTlca-1 and HTlca-2 showed acceptable reaction times and the highest isolated % yields of the β-amino alcohols. The heat treated catalyst (HTlca-3) was less selective and gave rise to diol formation. However, HTlca-1 and HTlca-2 showed comparable activity to each other in terms of reaction time (99.99% to 100% depletion of starting material) and % isolated yield of β-amino alcohol of the different olefins.

Third, the testing of the different olefins showed 99.99% reactant depletion, but due to the difficulties associated in the purification (in homogeneous AA) of the β-amino alcohol, the highest (35%) isolated yield of β-amino alcohol was obtained when methylcinnamate was used as the olefin and the lowest (8%) when hexene was used. The reaction time was shorter for the aliphatic olefins than that of the functionalised olefins (Section 4.3.4), due to the presence of the electron withdrawing group (carbonyl group) and the strong polarisation effect of Os=Ts, this is also reported in literature.

Fourth, the spent catalyst characterisation (Section 4.4) showed that the catalyst maintained the HTlc structure throughout the aminohydroxylation reaction, but lost some of its crystallinity.

Fifth, the leaching test showed that 3.0% and 2.9% Os leached when MeCN/water (1:1 v/v) and *t*-BuOH/water (1:1 v/v) were used, respectively. Furthermore, this method demonstrated a true heterogeneous approach to the aminohydroxylation reaction and resulted in the lowest level of inactive Os leaching reported to date. The catalyst was recycled three times with an increase in the reaction time but no significant change in the β-amino alcohol yield with increasing cycle numbers.

Future work

This work can be expanded by investigating the effect of different nitrogen sources on the reaction time and catalyst selectivity to the target product (β-amino alcohols). Moreover, the effect of using microwave irradiation to speed up the reaction time and to investigate the effect (if any) of microwave irradiation on the amount of leached Os could be investigated. Furthermore, the use of labelled chemicals to investigate the mechanism in which the reaction is carried out heterogeneously can be undertaken. In addition the ICP-OES can be carried out using glass tubing fittings, to eliminate any Os sticking to the plastic tubing.

Appendix B

List of tables

List of figures

Appendix A

List of figures

Appendix A

Appendix A

List of figures

Appendix: 1A

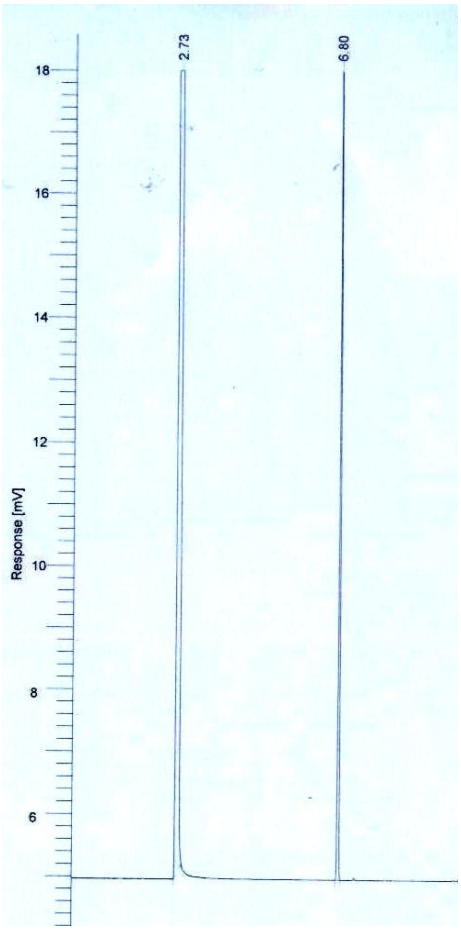

2.73 min : MeCN

6.80 min : Cyclohexene

Fig. 1A: GC chromatogram of cyclohexene in MeCN/water (1:1 v/v).

Appendix 2A

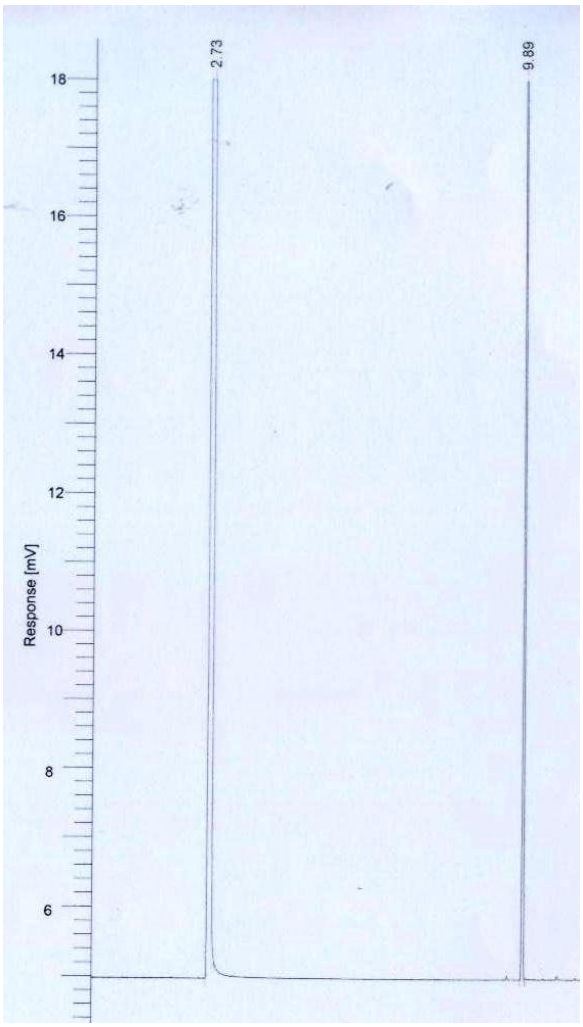

2.73 min : MeCN

9.89 min : Styrene

Fig. 2A: GC chromatogram of styrene in MeCN/water (1:1 v/v).

Appendix 3A

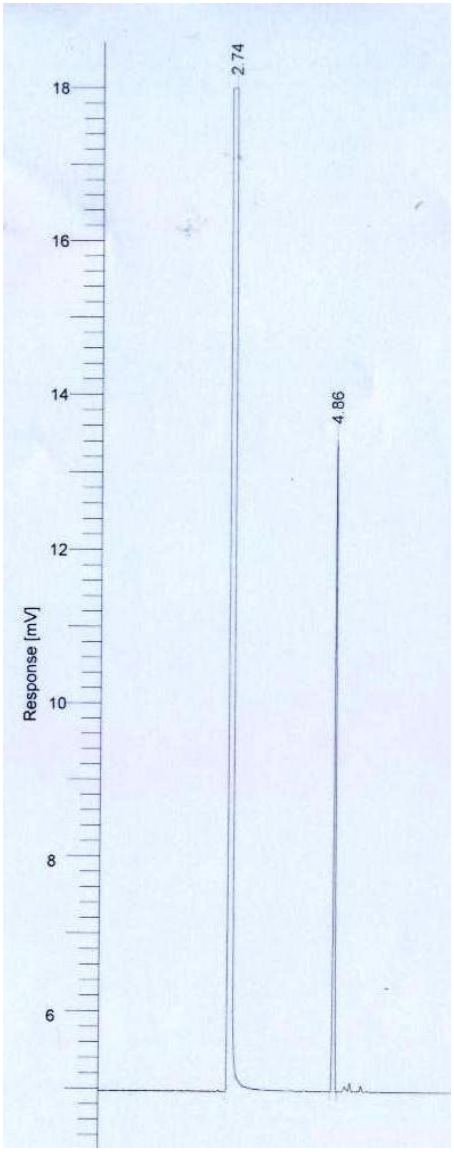

2.73 min : MeCN

4.86 min : Hexene

Fig. 3A: GC chromatogram of hexene in MeCN/water (1:1 v/v).

Appendix 4A

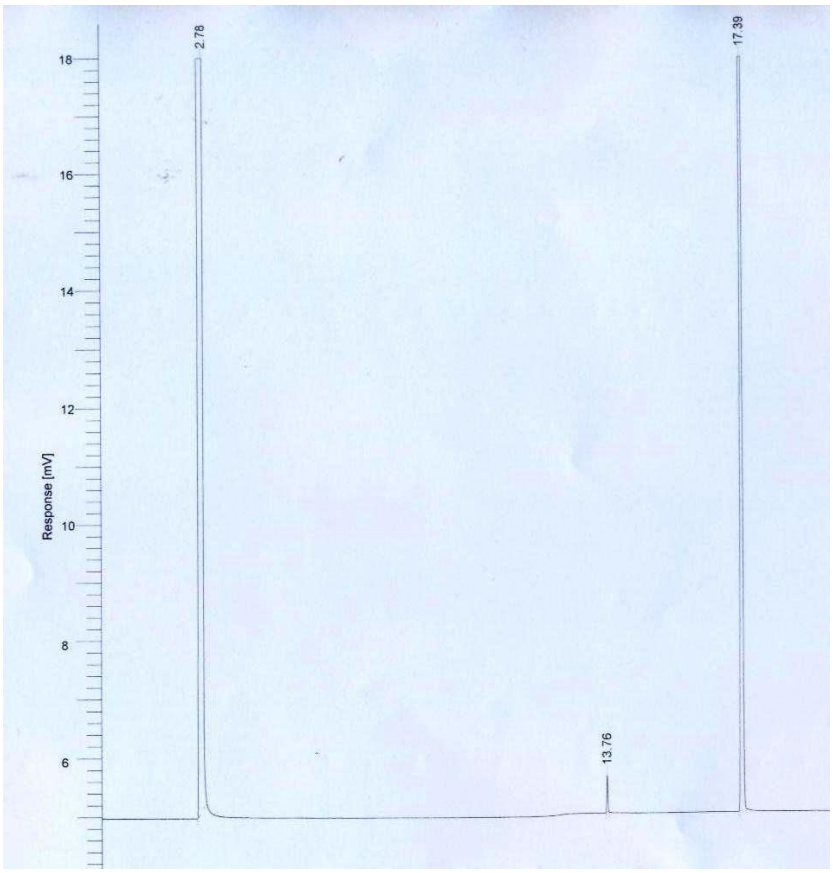

2.76 min : MeCN

17.39 min : *cis*-Stilbene

Fig. 4A: GC chromatogram of *cis*-stilbene in MeCN/water (1:1 v/v).

Appendix 5A

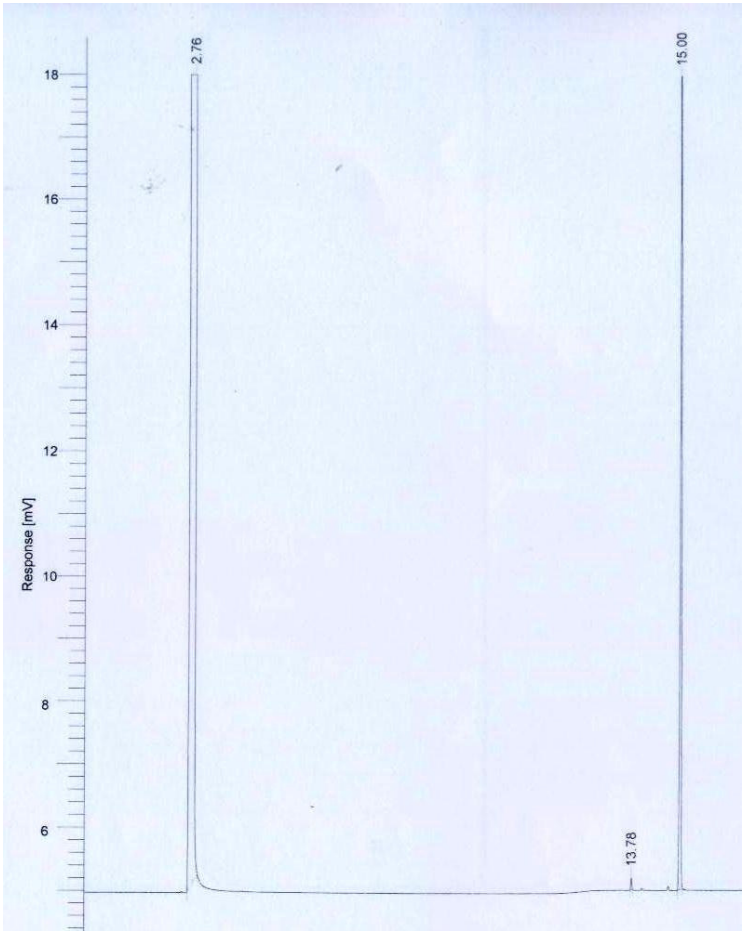

2.76 min : MeCN

15.00 min : Methylcinnamate

Fig. 5A: GC chromatogram of methylcinnamate in MeCN/water (1:1 v/v).

Appendix 6A

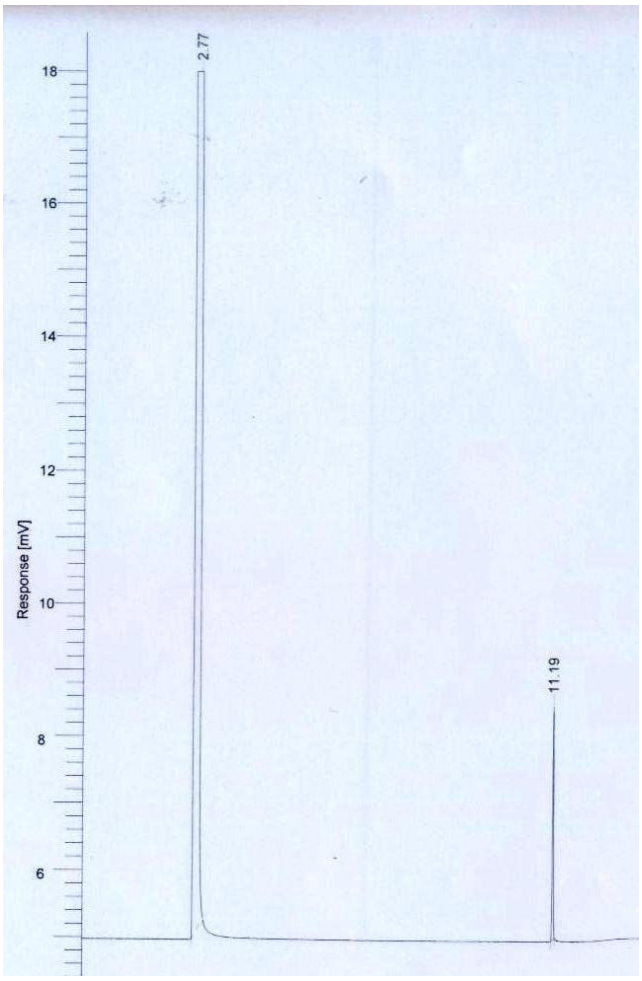

2.77 min : MeCN

11.19 min : Dimethylfumarate

Fig. 6A: GC chromatogram of dimethylfumarate in MeCN/water (1:1 v/v).

Appendix 7A

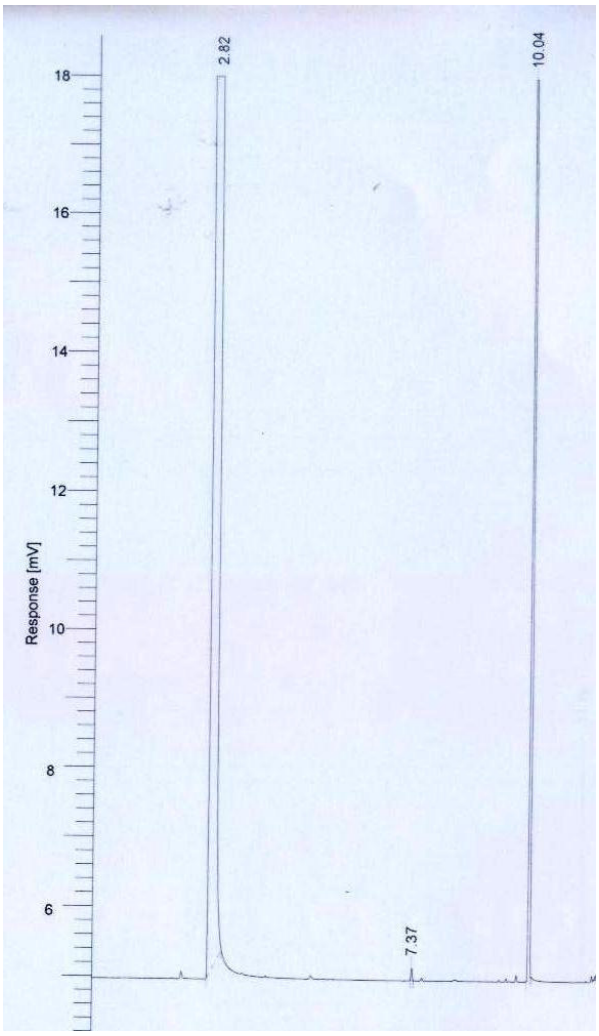

2.82 min : MeCN

10.04 min : *t*-butylcrotonate

Fig. 7A: GC chromatogram of *t*-butylcrotonate in MeCN/water (1:1 v/v).

Appendix B

Appendix B

List of tables

List of figures

Appendix: 1B

Calculation of the crystallite size

Crystallite size (L) = (k x λ) / (β x cos θ)

where k = shape factor (0.891)

λ = wavelength of the source (1.5406 Å for Cu kα radiation)

β = FWHM (Full Width Half Maximum)

θ = peak position

Catalyst HTlca-1:

L = (0.891 *x* 1.5406) / (0.00507 *x* cos 11.583)

= 233 Å

Catalyst HTlca-2:

L = (0.891 *x* 1.5406) / (0.00605 *x* cos 11.520)

= 196 Å

Appendix: 2B

Calculations of the *a* parameter

a parameter = $2d_{110}$

where d = d of the first peak in the 110 plane

Catalyst HTlca-1:

$a = 2 \times 1.53$

$= 3.06$

Catalyst HTlca-2:

$a = 2 \times 1.53$

$= 3.06$

Appendix: 3B

Calculation of the metal ratio using ICP-OES, utilizing two independent multi-elemental standards.

HTlca-1:

Multi-elemental standard A

Average concentration of osmium = 18.21 mg/L

$= 18.21 \times 10^{-3}$ g/L

Mass of osmium = 18.21×10^{-3} g/L x 0.1 L

$= 1.821 \times 10^{-3}$ g

Mass of osmium in the catalyst = 1.821×10^{-3} g/0.0214 g

$= 85.09 \times 10^{-3}$ g Os/g catalyst

Number of moles of Osmium = mass/molar mass

$= 85.09 \times 10^{-3}$ g/190.2 g/mol

$= 4.474 \times 10^{-4}$ mol

Average concentration of zinc = 74.69 mg/L

$= 74.69 \times 10^{-3}$ g/L

Mass of zinc = 74.69×10^{-3} g/L x 0.1 L

= 7.469×10^{-3} g

Mass of zinc in the catalyst = 7.469×10^{-3} g/0.0214 g

= 0.3490 g Zn/g catalyst

Number of moles of zinc = mass/molar mass

= 0.3490 g/65.39 g/mol

= 5.337×10^{-3} mol

Average concentration of aluminium = 8.286 mg/L

= 8.286×10^{-3} g/L

Mass of aluminium = 8.286×10^{-3} g/L x 0.1 L

= 0.8286×10^{-3} g

Mass of aluminium in the catalyst = 0.8286×10^{-3} g/0.0214 g

= 0.03872 g Al/g catalyst

Number of moles of aluminium = mass/molar mass

= 0.03872 g/26.98 g/mol

$= 1.435 \times 10^{-3}$ mol

The number of moles for each of the three metals was divided by the number of moles of aluminum, to obtain the ratio of the three metals (Os, Zn and Al) present in the catalyst, which is 0.31/3.71/1.

Tables 3.1B: Tabulated calculation results for the metal molar ratio in HTlca-2, following the calculations described on pg 111. The mass of HTlca-2 used for the ICP-OES was 0.0214 g. Multi-element standard A.

	Os (190.2 g/mol)	Zn (65.3 g/mol)	Al (26.9 g/mol)
Average concentration / g/L	19.87×10^{-3}	83.74×10^{-3}	9.539×10^{-3}
Mass of the metal /g	1.987×10^{-3}	8.374×10^{-3}	0.9539×10^{-3}
Mass of the metal / g metal/g catalyst	98.86×10^{-3}	416.6×10^{-3}	47.46×10^{-3}
Number of moles of metal / mol	5.198×10^{-4}	6.371×10^{-3}	1.759×10^{-3}
Ratio	0.29	3.62	1

Tables 3.2B: Tabulated calculation results for the metal molar ratio in HTlca-1, following the calculations described on pg 111. The mass of HTlca-1 used for the ICP-OES was 0.0236 g. Multi-element standard B.

	Os (190.2 g/mol)	Zn (65.3 g/mol)	Al (26.9 g/mol)
Average concentration / g/L	21.34×10^{-3}	85.52×10^{-3}	9.550×10^{-3}
Mass of the metal /g	2.134×10^{-3}	8.552×10^{-3}	0.9550×10^{-3}
Mass of the metal / g metal/g catalyst	90.42×10^{-3}	362.3×10^{-3}	40.40×10^{-3}
Number of moles of metal / mol	4.75×10^{-4}	5.541×10^{-3}	1.499×10^{-3}
Ratio	0.31	3.69	1

Tables 3.3B: Tabulated calculation results for the metal molar ratio in HTlca-2, following the calculations described on pg 111. The mass of HTlca-2 used for the ICP-OES was 0.0220 g. Multi-element standard B.

	Os (190.2 g/mol)	Zn (65.3 g/mol)	Al (26.9 g/mol)
Average concentration / g/L	23.18×10^{-3}	90.63×10^{-3}	10.68×10^{-3}
Mass of the metal /g	2.318×10^{-3}	9.063×10^{-3}	1.068×10^{-3}
Mass of the metal / g metal/g catalyst	105.36×10^{-3}	411.95×10^{-3}	48.54×10^{-3}
Number of moles of metal / mol	5.539×10^{-4}	6.299×10^{-3}	1.799×10^{-3}
Ratio	0.30	3.5	1

Appendix: 4B

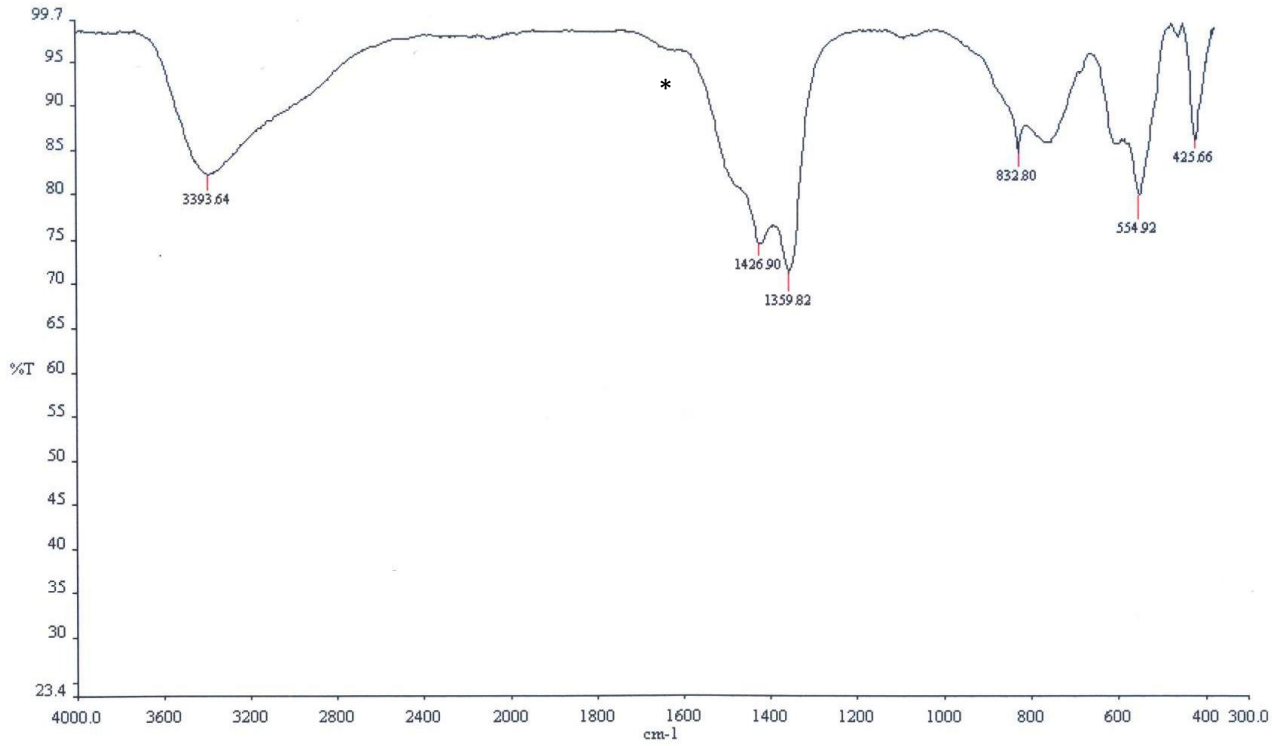

Fig. 4B: IR spectrum of HTlca-1

Band at 3393 cm $^{-1}$ corresponds to OH in brucite-like sheets and it is broad due to water present.

* (≈ 1600 cm^{-1}) This band (shoulder) corresponds to water.

Band at 832 cm $^{-1}$ (υ2) and 1350 cm^{-1} (υ3) correspond to carbonates.

Appendix: 5B

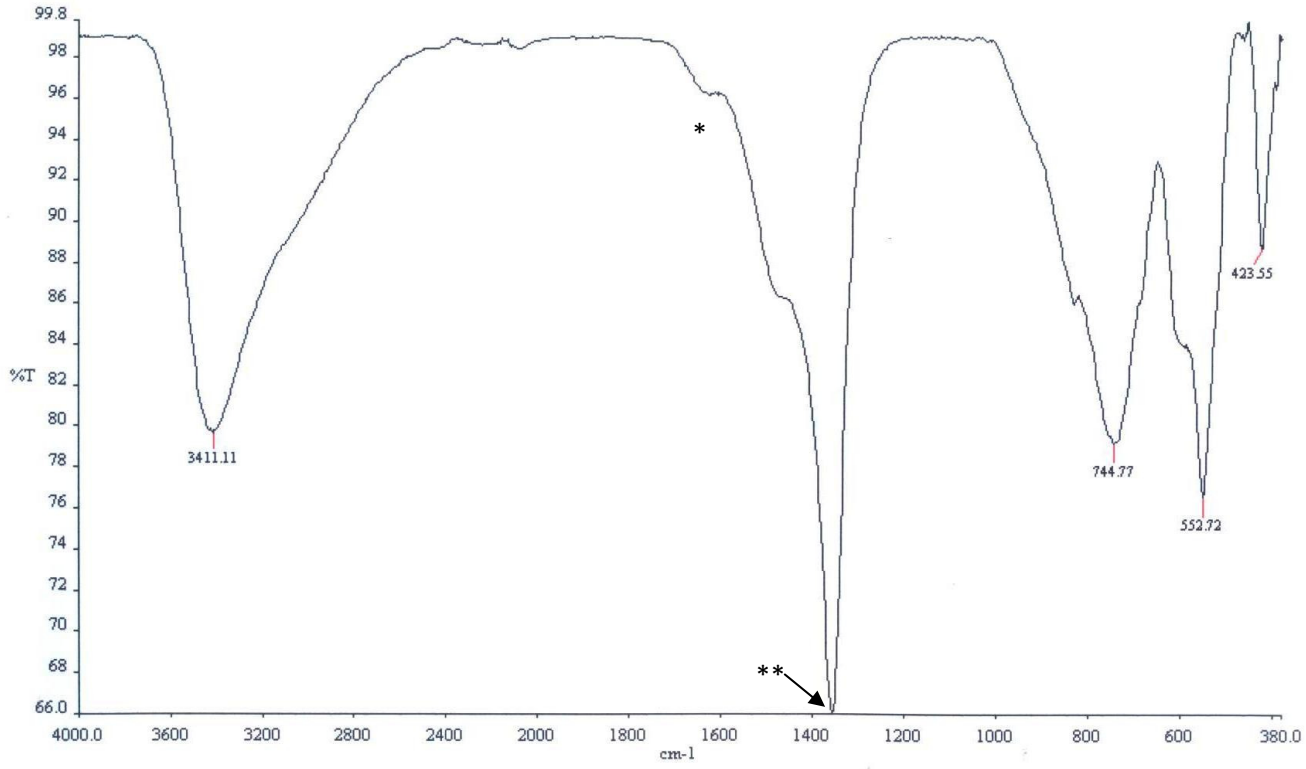

Fig. 5B: IR spectrum of HTlca-2

Band at 3411 cm $^{-1}$ correspond to OH in brucite-like sheets and its broad due to water present.

*(≈1600 cm^{-1}) This band (shoulder) correspond to water.

**Band correspond to carbonates (υ3).

Appendix: 6B

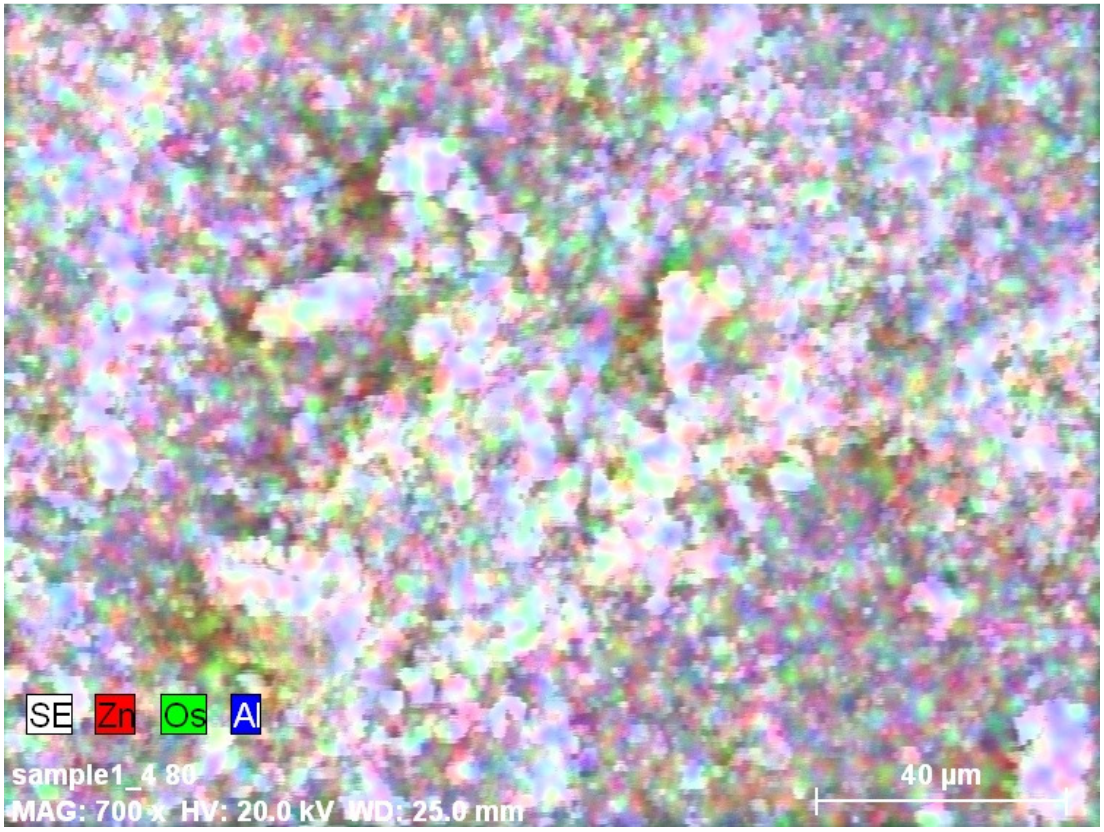

Fig. 6B: Elemental mapping of HTlca-1

Appendix: 7B

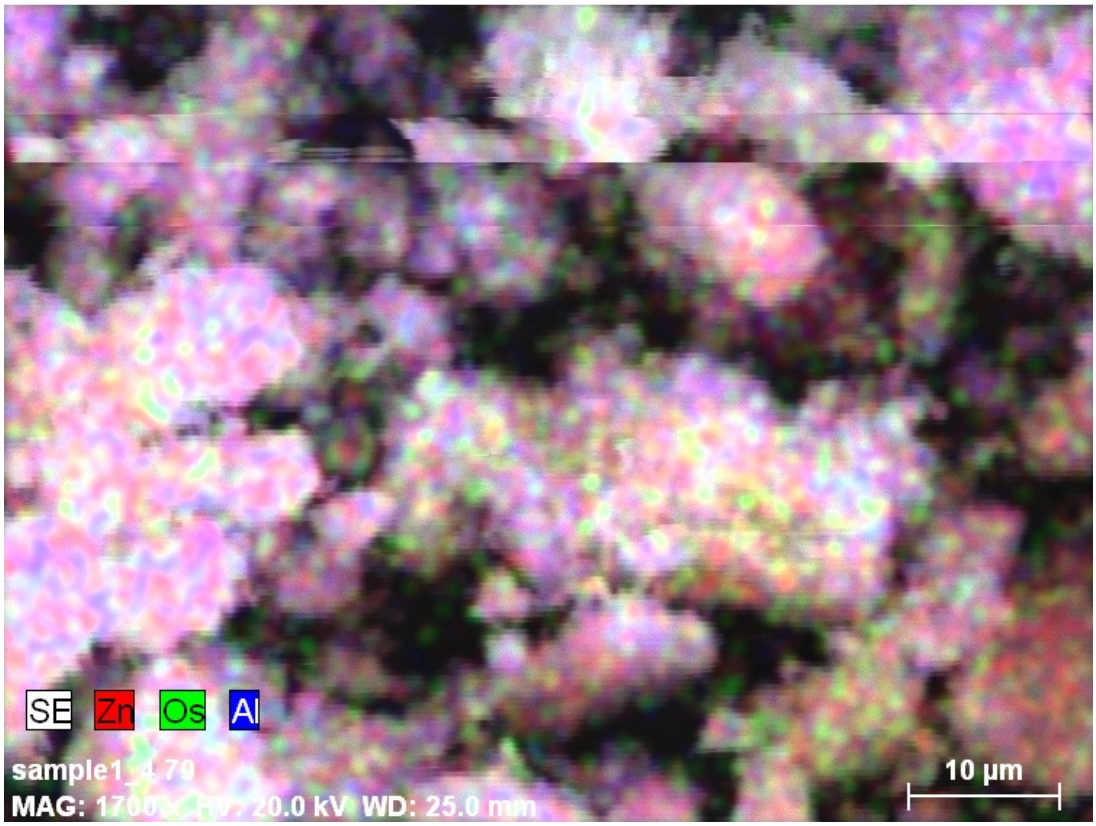

Fig. 7B: Elemental mapping of HTlca-2

Appendix: 8B

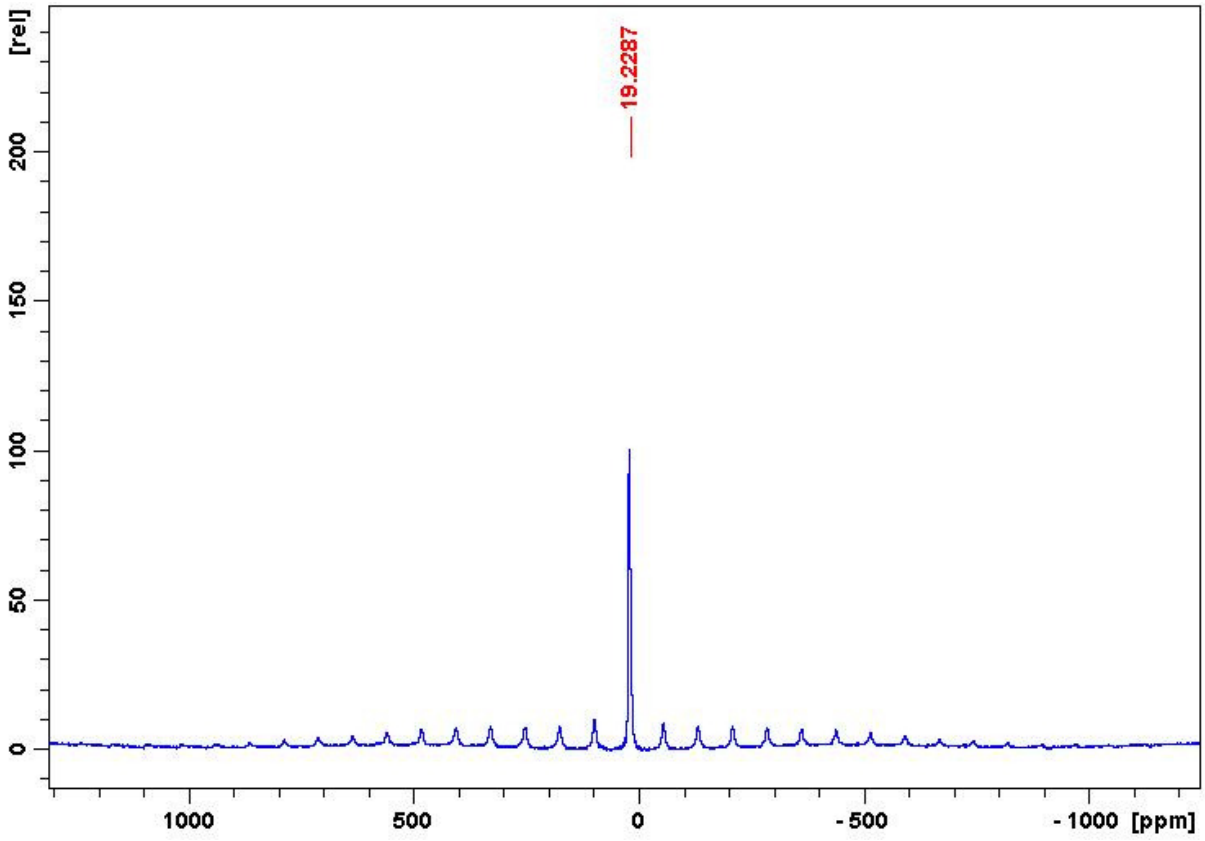

Fig. 8B: ^{27}Al SS-NMR spectrum of HTlca-2

Appendix: 9B

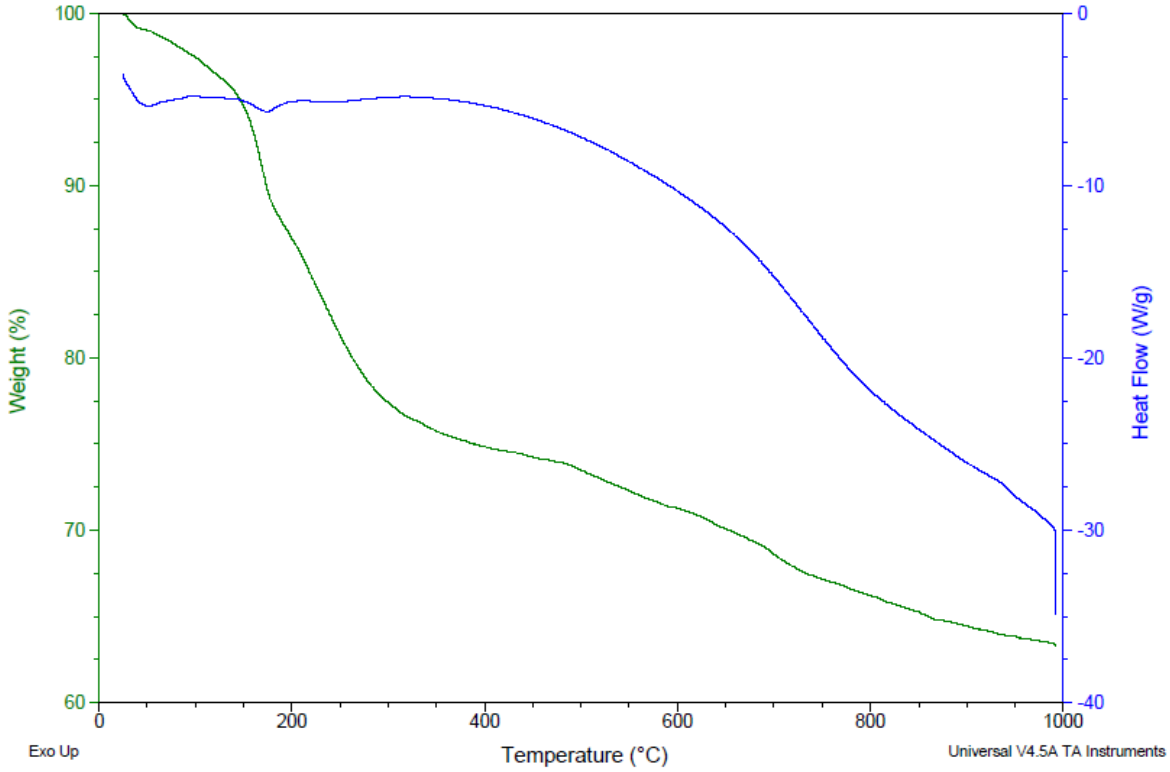

Fig. 9B: TGA-DSC plot of HTlca-2

Appendix: 10B

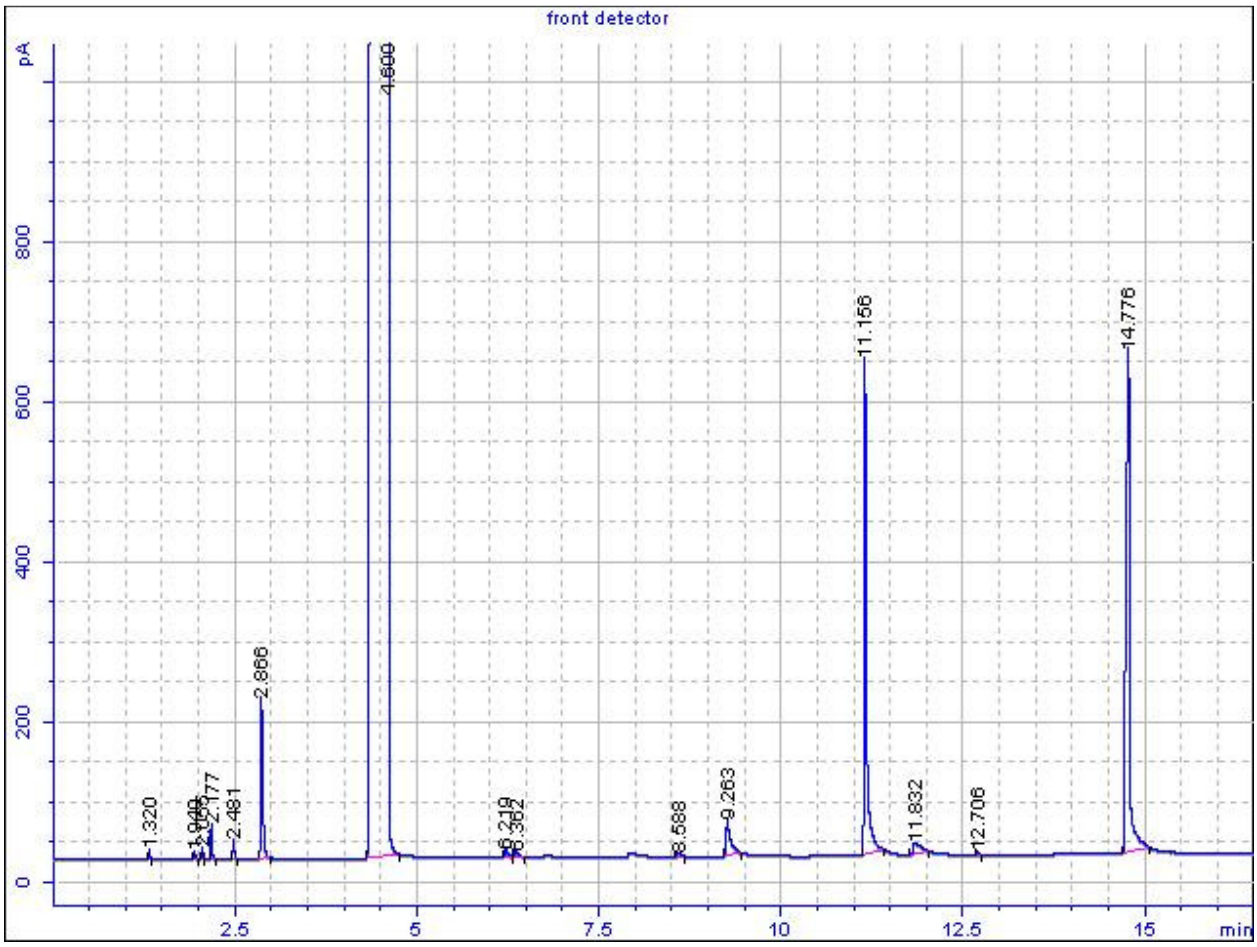

Fig. 10B: GC chromatogram of styrene used in the aminohydroxylation reaction at 60 ^{o}C with toluene as the solvent.

4.60 min : toluene

11.15 min : styrene oxide

14.77 min : *p*-toluenesulfonamide

All minor peaks are impurities in toluene.

Appendix: 11B

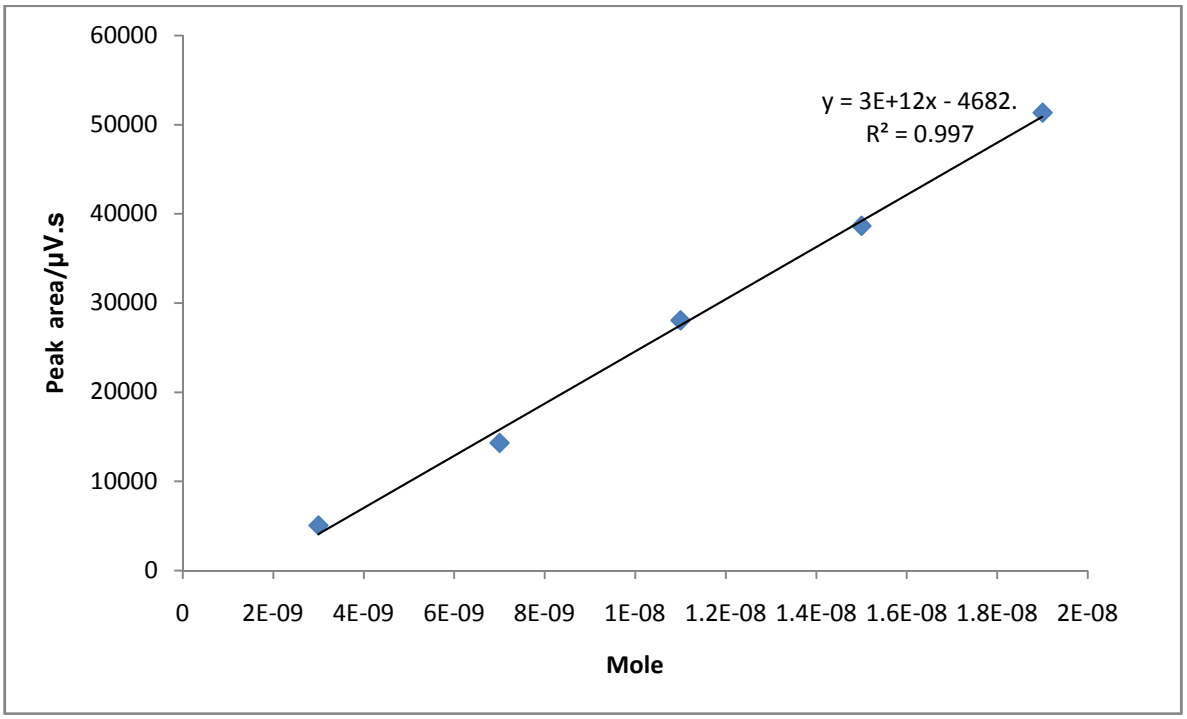

Fig. 11.1B: Calibration curve of *cis*-stilbene obtained by GC.

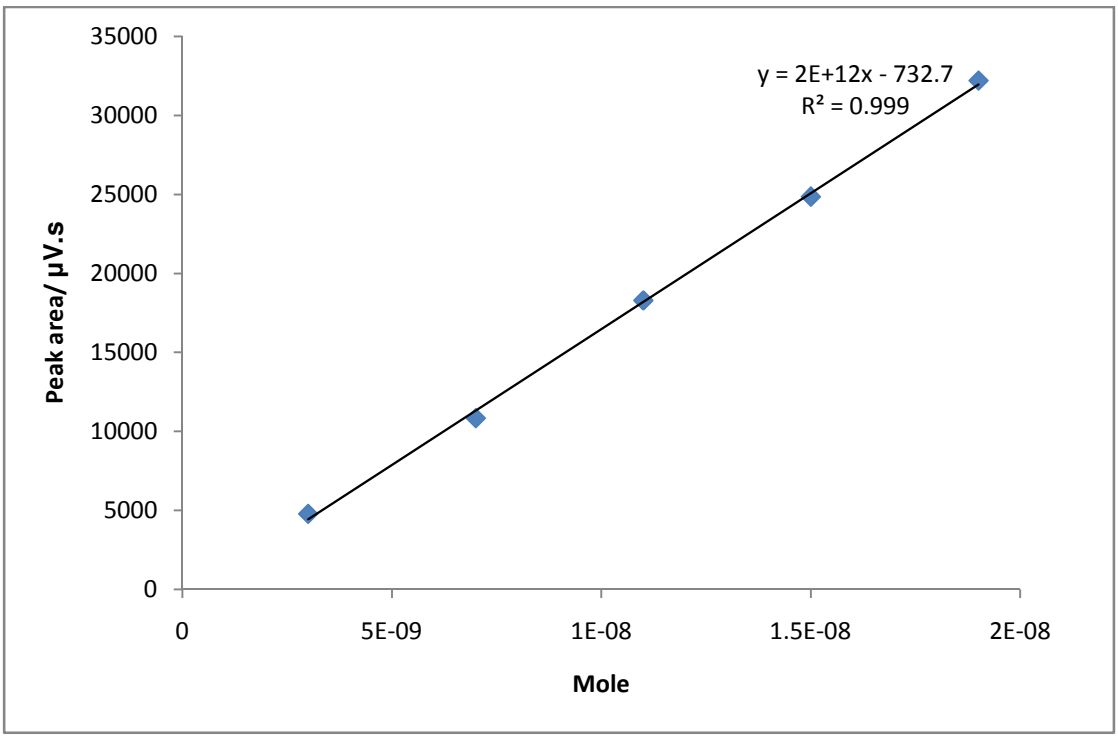

Fig. 11.2B : Calibration curve of methylcinnamate obtained by GC.

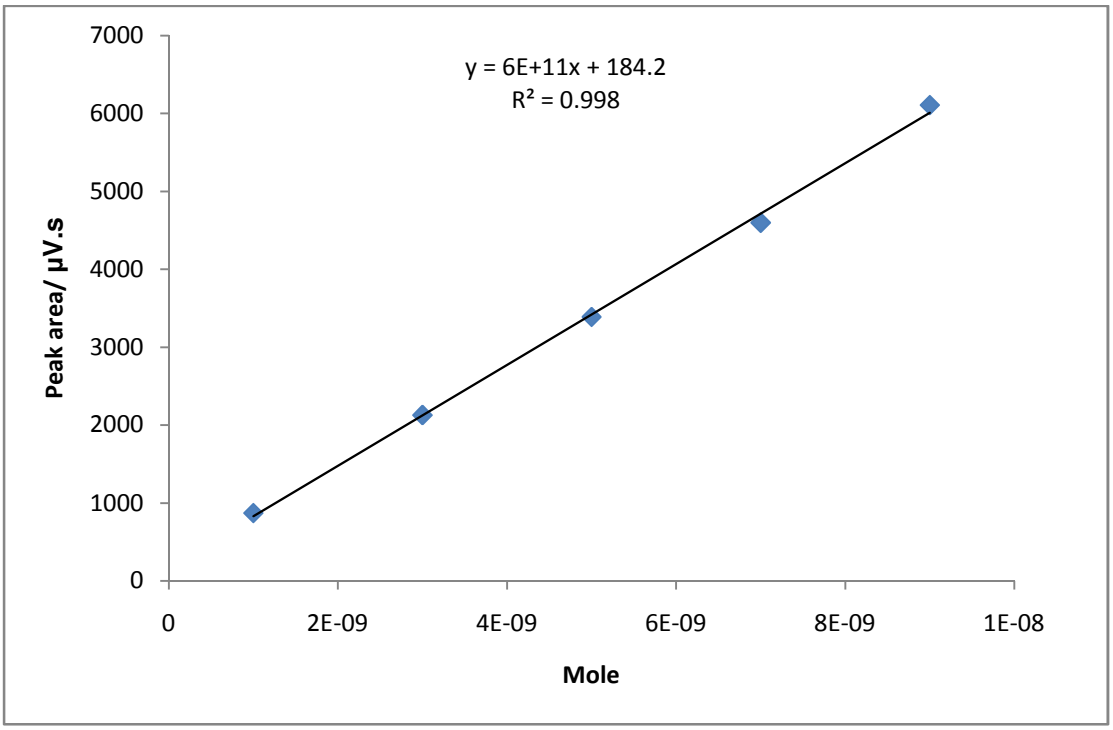

Fig. 11.3B : Calibration curve of dimethylfumarate obtained by GC.

Calculations for the starting material consumption in the aminohydroxylation reaction.

Starting material: *cis*-stilbene

Calibration line equation $y = 3 \times 10^{12} x - 4682.3$.

Peak area of *cis*-stilbene when MeCN/water (1:1 v/v) was used as the solvent system for the aminohydroxylation reaction after 24 h = 11905 μV.s.

Peak area of *cis*-stilbene when *t*-BuOH/water (1:1 v/v) was used as the solvent system for the aminohydroxylation reaction after 24 h = 7749 μV.s.

To obtain the conversion of *cis*-stilbene in MeCN/water (1:1 v/v), solving for x.

$x = (11905 - 4682.3)/ 3 \times 10^{12} = 0.2 \times 10^{-8}$ mol

Percentage mol conversion of *cis*-stilbene

$= (0.478 \times 10^{-3}$ mol $- 0.2 \times 10^{-8}$ mol$)/ 0.478 \times 10^{-3}$ mol

$= 0.9999 \times 100$

$= 99.99\%$

Similar calculations were carried out to obtain the conversion of *cis*-stilbene in *t*-BuOH/water (1:1 v/v)

All the calculations for methylcinnamate and dimethylfumarate, in the two solvent systems were carried out using the same calculations as for *cis*-stilbene, using the equation line from Figs.11.2B and 11.3B, respectively. The peak area obtained and used in the calculations for the two olefins in the two solvent systems is shown in Table 1B.

Table 11.1B: Peak area of the two olefins in the two solvent systems

Olefin	**Peak area /** μV.s	
	MeCN/water	***t*-BuOH/water**
Methylcinnamate	-[a]	18975
Dimethylfumarate	5033	2348

[a] 100 % conversion obtained.

Appendix: 12B

HPLC chromatogram of hexene

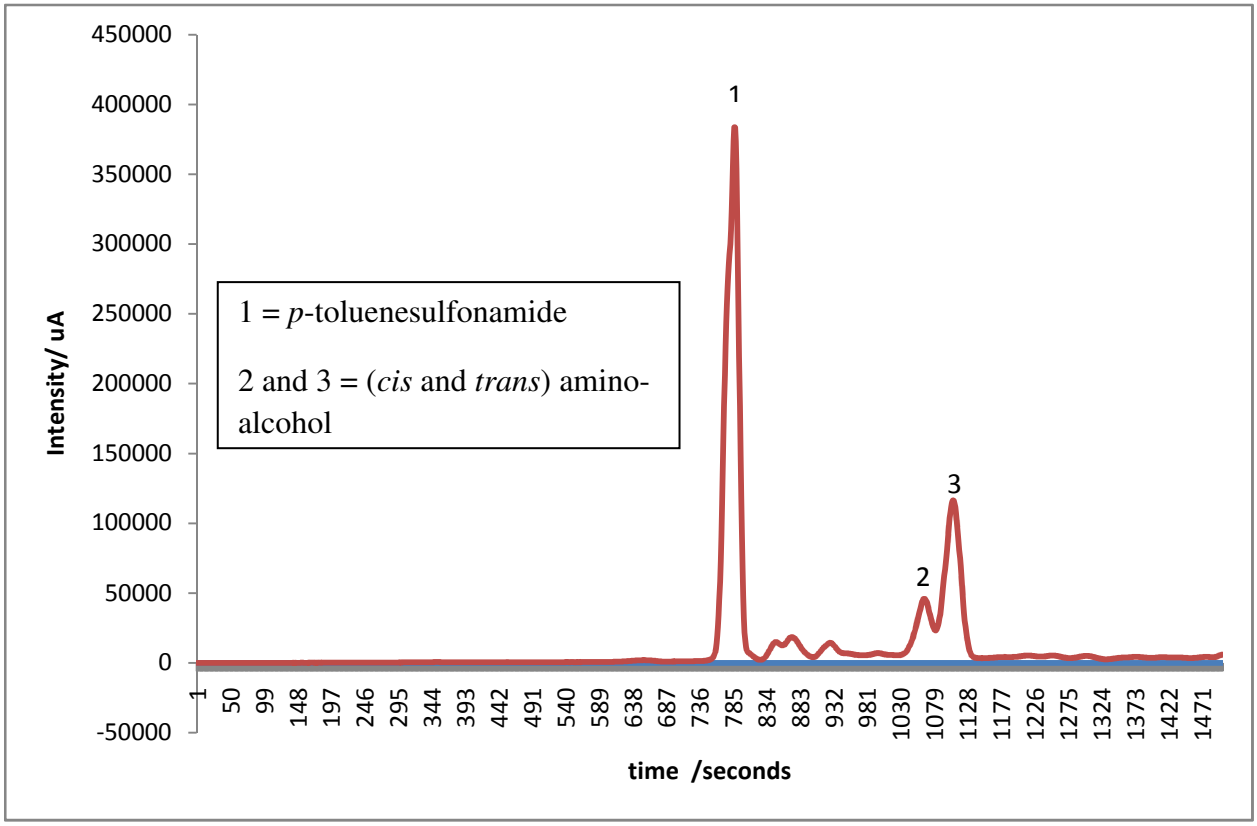

Fig. 12B: HPLC trace of the reaction mixture, hexene used as the olefin.

Appendix: 16B

Calculations for amount of Os leaching

Leaching test for HTlca-1

Butanol/water (1:1) solvent system

Calculation of the amount of osmium leached into the reaction mixture.

ICP-OES concentration = 5.07 mg/L

Volume of sample = 1 mL, diluted to 10 mL using de-ionized water

Amount of osmium leached = 5.07 mg/L *x* 0.01 L *x* 10

= 0.507 mg

To account for the different matrices:

The amount of Os leached / the average ratio obtained from Table 3.8 (Pg. 54)
= 0.507 mg/ 1.79 = 0.283 mg

Amount of osmium in the catalyst at the start of the reaction = 0.0305 g *x* 0.31 (ratio of Os in the catalyst) = 9.45×10^{-3}g

% of osmium leached = (0.283×10^{-3} g/9.45×10^{-3} g) *x* 100

= 2.9%

Acteonitrile/water (1:1) solvent system

Calculation of the amount of osmium leached into the reaction mixture.

ICP-OES concentration = 4.21 mg/L

Volume of sample = 1 mL, diluted to 10 mL using de-ionized water

Amount of osmium leached = 4.21 mg/L *x* 0.01 L *x* 10

= 0.421 mg

To account for the different matrices:

The amount of Os leached / the average ratio obtained from Table 3.8 (Pg. 54)
= 0.421 mg/ 1.45 = 0.290 mg

Amount of osmium in the catalyst in the reaction = 0.0306 g *x* 0.31 (ratio of Os in the catalyst) = 9.48×10^{-3}g

% of osmium leached = (0.290×10^{-3} g/9.48×10^{-3} g) *x* 100

= 3.0%

Leaching test for HTlca-2

Butanol/water (1:1) solvent system

Calculation of the amount of osmium leached into the reaction mixture.

ICP-OES concentration = 5.51 mg/L

Volume of sample = 1 mL, diluted to 10 mL using de-ionized water

Amount of osmium leached = 5.51 mg/L *x* 0.01 L *x* 10

= 0.551 mg

To account for the different matrices:

The amount of Os leached / the average ratio obtained from Table 3.8 (Pg. 54)
= 0.551 mg/ 1.79 = 0.307 mg

Amount of osmium in the catalyst in the reaction = 0.0304 *x* 0.29 (ratio of Os in the catalyst) = 8.81×10^{-3}g

% of osmium leached = (0.307 x 10^{-3} g/8.81 x 10^{-3} g) x 100

= 3.4 %

Acteonitrile/water (1:1) solvent system

Calculation of the amount of osmium leached into the reaction mixture.

ICP-OES concentration = 3.72 mg/L

Volume of sample = 1 mL, diluted to 10 mL using de-ionized water

Amount of osmium leached = 3.72 mg/L x 0.01 L x 10

= 0.372 mg

To account for the different matrices:

The amount of Os leached / the average ratio obtained from Table 3.8 (Pg. 54)
= 0.372 mg/ 1.45 = 0.256 mg

Amount of osmium in the catalyst in the reaction = 0.0303 g x 0.29 (ratio of Os in the catalyst) = 8.78 x 10^{-3}g

% of osmium leached = (0.256 x 10^{-3}g/8.78 x 10^{-3}g) x 100

= 2.9%